Cellular and Molecular Life Sciences (2022) 79:567
https://doi.org/10.1007/s00018-022-04596-5

ORIGINAL ARTICLE

Mycobacterium tuberculosis exploits MPT64 to generate myeloid-derived suppressor cells to evade the immune system

Sanpreet Singh[1] · Sudeep K. Maurya[1] · Mohammad Aqdas[1] · Hilal Bashir[1] · Ashish Arora[3] · Vijayender Bhalla[1,4] · Javed N. Agrewala[1,2]

Received: 30 June 2022 / Revised: 19 September 2022 / Accepted: 9 October 2022

Abstract

Mycobacterium tuberculosis (Mtb) is a smart and successful pathogen since it can persist in the intimidating environment of the host by taming and tuning the immune system. *Mtb* releases MPT64 (Rv1980c) protein in high amounts in patients with active tuberculosis (TB). Consequently, we were curious to decipher the role of MPT64 on the differentiating dendritic cells (DCs) and its relation to evading the immune system. We observed that pre-exposure of differentiating DCs to MPT64 (DC^{MPT64}) transformed them into a phenotype of myeloid-derived suppressor cells (MDSCs). DC^{MPT64} expressed a high level of immunosuppressive molecules PD-L1, TIM-3, nitric oxide (NO), arginase 1, IDO-1, IL-10 and TGF-β, but inhibited the production of pro-inflammatory cytokines TNF-α, IL-6 and IL-12. DC^{MPT64} chemotaxis function was diminished due to the reduced expression of CCR7. DC^{MPT64} promoted the generation of regulatory T cells (Tregs) but inhibited the differentiation of Th1 cells and Th17 cells. Further, high lipid and methylglyoxal content, and reduced glucose consumption by DC^{MPT64}, rendered them metabolically quiescent and consequently, reduced DC^{MPT64} ability to phagocytose *Mtb* and provided a safer shelter for the intracellular survival of the mycobacterium. The mechanism identified in impairing the function of DC^{MPT64} was through the increased production and accumulation of methylglyoxal. Hence, for the first time, we demonstrate the novel role of MPT64 in promoting the generation of MDSCs to favor *Mtb* survival and escape its destruction by the immune system.

Keywords *Mtb* · Dendritic cells · MDSCs · Tregs

Introduction

Mycobacterium tuberculosis (*Mtb)* persists skillfully by deceiving the host immune system. It adopts multiple contrivances, viz., disrupts the fusion of phagosome-lysosome [1], neutralizes the function of reactive nitrogen and oxygen-free radicals [2], induces necrosis of macrophages [3, 4], impairs the antigen processing and presentation [5, 6], hampers apoptosis of infected cells [7], inhibits autophagy and lysosomal functions [8] and impedes the production of interferons [9]. Suggesting that the pathogen is not only utilized by the host to generate protective immunity, but the bacterium too successfully subjugates the host immune system [10, 11].

The *Mtb* uses its proteins, like Acr1, to successfully inhibit the maturation of DCs [12, 13]; DCs exposed to ManLAM failed to fully mature and showed a decline in the level of MHCI and MHCII, CD83, CD86 and CCR7 [14], and LprA, LprG and LpgH too downregulates the MHCII expression [15–17]. Further, an encounter of DCs with *Mtb* secretory Ag (MTSA) during differentiation promotes the survival of the intracellular bacterium by inhibiting the production of ROS [18]. Moreover, ESAT-6 has been reported to inhibit the phagolysosome fusion [19]. Similarly, PtpA and SapM proteins inhibit phagosome maturation. PtpA suppresses the acidification of phagosomes [20] and Ndk interacts with the Rac1 protein of host cells and prevents the

✉ Javed N. Agrewala
jagrewala@gmail.com

1 Immunology Laboratory, CSIR-Institute of Microbial Technology, Chandigarh 160036, India

2 Immunology Laboratory, Department of Biomedical Engineering, Indian Institute of Technology Ropar, Rupnagar 140001, India

3 Department of Biochemistry and Structural Biology, CSIR-Central Drug Research Institute, Lucknow 226031, India

4 Biosensor Laboratory, CSIR-Institute of Microbial Technology, Chandigarh, India

Published online: 25 October 2022

assembly of the NOX2 [21]. Many proteins, such as PknE (protein kinaseE), Ndk, nuoG, SecA2 and PtpA, have been reported to induce necrosis and apoptosis of infected host cells [7, 22, 23]. Furthermore, *Mtb* elicits the generation of MDSCs that fail to activate T cells [24]. Along with Tregs, MDSCs presence is reported in TB granulomas to suppress effector T cell function and therefore promote the progression of the disease [24]. MDSCs utilize nitric oxide (NO), arginase 1 and methylglyoxal (MGO) with other constituents that cause nitrosylation of T cell receptors, apoptosis of T cells and induction of Tregs [25–27]. The vast detrimental effect of MDSCs is mediated by the strong suppression of Th1 and Th17 immunity along with a decline in the secretion of innate cytokines [28]. Consequently, it becomes crucial to decode the function of unexplored proteins exploited by *Mtb* to support the generation of MDSCs to escape the immune system.

MPT64 is a secretory protein (m.wt. ~ 24 kDa) and is less studied for its immunomodulatory role [29]. It belongs to a new family of beta grasp proteins [30]. The level of MPT64 is high in the serum and sputum of active TB patients [31]. Moreover, MPT64 enhances the secretion of IL-1β, IL-6, TNF-α and IL-10 by the macrophages, and therefore may be responsible for suppressing the immune system [32]. Recently, it has been shown that MPT64 inhibits the apoptosis of macrophages through upregulation of bcl-2 and increases the survival of *Mtb* [33]. Further, the MPT64 mutant strain (Mtb*Δmpt64*) generates less bacterial burden in mice, as compared to wildtype *Mtb* [34].

Keeping in view the aforesaid facts, we have tried to delineate here the immunomodulatory role of MPT64 on the activation and differentiation of DCs. Interestingly, we observed that the early encounter of DCs with MPT64 (DC^{MPT64}) during their differentiation skewed them towards a myeloid suppressor cell phenotype. The DC^{MPT64} showed the accumulation of methylglyoxal, an advanced glycation end product, which along with other soluble mediators is implicated in suppressing the host immune system. DC^{MPT64} preferably generated Tregs and suppressed the activation of Th1 cells and Th17 cells. The DC^{MPT64} demonstrated decreased tendency to phagocytose and kill *Mtb*. Consequently, it may be concluded from the study that *Mtb* utilizes MPT64 to make DC^{MPT64} a safe shelter for its persistence, and this may be one of the mechanisms adopted by the mycobacterium to escape the host immune system.

Materials and methods

Dendritic cell culture

Bone marrow cells (BMCs) were isolated from the femur and tibiae of C57BL/6 mice and were differentiated into DCs, as mentioned elsewhere [35]. Briefly, the BMCs were treated with ACK lysis buffer (0.15 M NH_4Cl, 10 mM $KHCO_3$, and 88 mM Na_2EDTA) to lyse RBCs. BMCs (2×10^6) were cultured in 24-well plates in complete medium [RPMI-1640 + FCS-10% supplemented with penicillin (100 U/ml), L-glutamine (100 mM), streptomycin (100 mg/ml)] and GM-CSF (2 ng/ml) and IL-4 (4 ng/ml). The cultures were kept for 7d in a humidified CO_2 (5%) incubator at 37 °C. The medium was replenished after 3 d. Abbreviations used in this text: DCs: BMCs cultured with GM-CSF + IL-4; DC^{MPT64}, DC^{CFP-10} and DC^{ESAT-6}: BMCs cultured with GM-CSF + IL-4 along with MPT64, CFP-10 and ESAT-6, respectively.

Arginase activity assay

Arginase was estimated through arginase activity assay. DCs and DC^{MPT64} (5×10^5) were cultured in 48-well plates for 6 d in RPMI-1640 + FCS-10%. The cells were isolated on the 7th day and washed with 1X PBS, and water (100 µl) containing Triton X-100 (0.1%) and protease inhibitor was added and incubated at 37 °C for 30 min. Later, Tris–HCL (100 µl, 25 mM), $MnCl_2$ (333 µM) and pH 7.5 were added followed by heating the reaction mixture at 56 °C for 10 min to activate the enzyme. Later, L-arginine (200 µl, 0.5, mol/L, pH 9.7) was added as an arginase substrate and heated the mixture for 30 min at 37 °C. The reaction was stopped with an acid solution (400 µl, H_2SO_4:H_3PO_4:H_2O; 1:3:7). Finally, α-isonitrosopropiophenone (50 µl, 9% ethanol) was added to the reaction mixture for colorimetric detection of urea, followed by heating the mixture for 45 min at 56 °C. Finally, the reaction mixture was kept in dark at RT for 10 min. The urea formed was calorimetrically determined by taking absorbance at 540 nm [36, 37].

Expression of surface markers by flow cytometer

DCs, DC^{MPT64} and DC^{CFP-10} (5×10^5) were cultured in a complete medium for 6 d. Cells were harvested on the 7th day and surface stained with fluorochrome-labelled Abs to CD11c, CD11b, F4/80, Ly6c, Ly6G, CCR7, Fox-P3, CD25, CD4, CD8, TCRβ and TCRγ/δ. Cells were acquired through flow cytometry and expression was monitored through BD DIVA software.

In vivo cell migration assay

DCs, DC^{MPT64} and DC^{CFP-10} (2×10^6) were cultured in 6-well plates complete medium for 6 d. Next, the cells were re-suspended in CFSE (1 ml, 2 µM) and incubated for 8 min at 37 °C. Later, FBS (2 ml) was added and cultures were centrifuged at 2000 rpm at RT for 3 min. The cell pellet was washed 2× with PBS-1X + FBS-20%. The CFSE-labelled

cells were intravenously injected into C57BL/6 mice. After 24 h and 48 h, the animals were sacrificed and splenocytes were monitored for the presence of CFSE-labelled DCs by flow cytometer. Results were analyzed through BD DIVA software and represented in terms of fold-change migration. Later, the expression of CCR7 was monitored on these cells through flow cytometry.

Soluble antigen uptake assay

DCs and DC^{MPT64} (2×10^5) were cultured in 24-well plates for 6 d in complete media at 37 °C/5% CO_2. Later, cells were pulsed with FITC-dextran (100 µg/ml) and monitored for 30 min/37 °C. The cells were washed 4 × with PBS-1X-BSA-1%. Finally, cells were acquired through a flow cytometer and analyzed for dextran-FITC uptake through BD DIVA software.

Mycobacterial uptake and intracellular survival

DCs and DC^{MPT64} (5×10^5) were cultured in 24-well plate for 6 d in complete media. On the 7th day cells were washed with PBS-1X and infected with *Mtb* strains H37Ra (GFP-*Mtb*) or H37Rv for 4 h (3 h for *M. smegmatis*) at MOI of 1:5 in antibiotic-free RPMI-1640 media. Extensive washings with PBS-1X were given to the cells. Later, to kill the extracellular bacilli, amikacin (2 µg/ml) (for H37Rv) and gentamycin (50 µg/ml) (for H37Ra and *M. smegmatis*) were added to antibiotic-free RPMI-1640 media into cell cultures for 1 h at 37 °C. Then, cells were extensively washed with PBS-1X. To monitor the uptake after 4 h of *Mtb* (GFP-H37Ra, H37Rv, *M. smegmatis*) infection, cells were lysed with saponin (0.1%) and lysates (100 µl) were plated on 7H11 plates. Further, to monitor the survival of *Mtb* (H37Rv) within DCs and DC^{MPT64}, infected cells were rested for 72 h at 37 °C in 5% CO_2. The cells were lysed with saponin (0.1%) and lysates (100 µl) were plated in 7H11 plates. Bacterial growth was enumerated after 21 d by colony-forming units (CFUs).

Isolation of CD4 T cells and CD8 T cells

CD4 T cells and CD8 T cells were isolated from mouse spleen and lymph nodes by magnetic-activated cell sorting (MACS) through negative selection, as per the manufacturer's instruction (BD Biosciences, San Diego, CA). Briefly, splenocytes were isolated from C57BL/6 and BALB/c mice and were processed into a single-cell suspension. Next, CD4 T cells and CD8 T cells enrichment cocktail was added to these splenocytes. Generally, a mouse CD4 T cell enrichment cocktail (5 µl/1×10^6 cells) was added and incubated for 15 min on ice. Then, cells were centrifuged at 300 g for 7 min, and to this pellet streptavidin-magnetic beads (5 µl) were added and incubated for 30 min at 6–12 °C. Afterwards, CD4 T cells were isolated using BD IMagnet™. Similarly, CD8 T cells were isolated using CD8 T cells enrichment kit.

Syngeneic T cell proliferation

CD4 T cells and CD8 T cells were purified from the C57BL/6 mice splenocytes by MACS as per the manufacturer's instruction (BD Biosciences, San Diego, CA). CD4 T cells and CD8 T cells were re-suspended in 1 ml PBS (1X) supplemented with CFSE (2 µM) and incubated for 8 min/37 °C. Later, excess of CFSE was quenched using FCS (2 ml) and cells were washed twice with PBS-1X. T cells were co-cultured with DC^{MPT64} (ratio 10:1) in a 96-well flat bottom plate pre-coated with anti-CD3 (1 µg/ml) and anti-CD28 (0.5 µg/ml) Abs for 72 h. T cell proliferation was assessed through CFSE dye dilution assay by flow cytometry. Data were analyzed through BD DIVA software.

Allogeneic T cell proliferation

CD4 T cells and CD8 T cells were purified from the BALB/c mice splenocytes by MACS as per the manufacturer's instruction (BD Biosciences, San Diego, CA). CD4 T cells and CD8 T cells were re-suspended in 1 ml PBS (1X) supplemented with CFSE (2 µM) and incubated for 8 min/37 °C. Later, excess CFSE was quenched using FCS (2 ml) and cells were washed twice with PBS-1X. T cells (BALB/c) were co-cultured with DC^{MPT64} (C57BL/6) (ratio 10:1) (1.1×10^5 cells/well) in a 96-well flat bottom plate pre-coated with anti-CD3 (1 µg/ml) and anti-CD28 (0.5 µg/ml) Abs for 72 h. T cell proliferation was assessed through CFSE dye dilution assay by flow cytometry. Data were analyzed through BD DIVA software.

The expression of TCRβ and TCRγ/δ chains and apoptosis of T cells

Anti-CD3 and anti-CD28 stimulated naïve CD4 T cells and CD8 T cells were co-cultured with DC^{MPT64} and control DCs and DC^{CFP-10} (DC:T cell, 1:10) for 72 h/37 °C/5% CO_2. Later, the cells were stained with fluorochrome-labelled anti-TCRβ chain and TCRγ/δ chain Abs and analyzed through flow cytometry. Further, the apoptosis in T cells upon culturing with DCs, DC^{MPT64} and DC^{CFP-10} was enumerated through staining with FITC-labelled Annexin V (5 µl/tube) for 15 min in dark. After incubation, the binding buffer (400 µl) was added to these cells and analyzed immediately

by flow cytometry. Data were analyzed through BD DIVA software.

DC^{MPT64}-mediated suppression of CD4 T cells and CD8 T cells through NO secretion

The suppressive activity of DC^{MPT64} was measured through trans-well plate experiments. CFSE-labelled naïve CD4 T cells and CD8 T cells were stimulated with anti-CD3 and CD28 Abs and poured into the lower chamber of the trans-well plate. DC^{MPT64} and control DC^{CFP-10} and DCs were added into the upper chamber of the trans-well plate. Further, the same cultures were set in a normal tissue culture plate. The cells were incubated for 72 h at 37 °C/5% CO_2. Furthermore, the role of NO-mediated suppression of CD4 T cells and CD8 T cells by DC^{MPT64} was validated by treating the cultures with iNOS inhibitor (NM: N-monomethyl-L-arginine) (20 µM) for 72 h. The proliferation of T cells was measured by CFSE dye dilution assay through flow cytometry and analyzed by BD DIVA software.

Statistical analysis

Data analysis was done using '*t* test' (one- and two-tailed) and one-way analysis of variance (ANOVA) (Dunnett and Bonferroni tests) using GraphPad Prism 6 software (GraphPad Software, La Jolla, CA). The '*p* value' of less than 0.05 was considered significant.

Results

MPT64 impairs the maturation of DC^{MPT64}

Mtb uses an array of approaches to elude its destruction by modulating the host immune system. DCs are the only APCs that can activate naïve T cells. Interestingly, it has been observed that DCs upon *Mtb* infection lose their function [38]. Hence, it is crucial to comprehend how *Mtb* implicates its components to detriment the function of DCs. Therefore, we thought to decipher the influence of the exposure of MPT64 on the differentiating DCs. BMCs were cultured in the presence of GM-CSF and IL-4 with (DC^{MPT64}) or without (DCs) MPT64. The control cultures were set using CFP-10 (DC^{CFP-10}) and ESAT-6 (DC^{ESAT-6}) proteins of *Mtb*. We noted a decline in the $CD11c^+$ cells, but augmentation in the pool of $F4/80^+$ cells, in a dose-dependent manner (Fig. 1A). However, the greatest expansion of $F4/80^+$ cells and lowest percentage of $CD11c^+$ cells were observed with 12 µg/ml of MPT64. Hence, this concentration was used in all the subsequent experiments.

To validate that the decline in the frequency of $CD11c^+$ cells was not due to overgrowth and death of the cells, we checked their viability. No change in the viability of neither $CD11c^+$ cells nor $F4/80^+$ cells was noted (Supplementary Fig. 3A). We also checked the specificity of MPT64. To prove this, we used CFP-10 and ESAT-6 proteins of *Mtb*. We noticed that the increase of the $F4/80^+$ cells and decline in the $CD11c^+$ cells were solely associated with a function of MPT64 and not CFP-10 and ESAT-6 proteins (Supplementary Fig. 3B). Thus, it establishes the specificity of MPT64 in transforming the BMCs under DCs differentiating conditions (IL-4 + GM-CSF) into MDSCs.

An optimum expression of co-stimulatory and MHC molecules by the APC is decisive for the presentation of antigen and activation of T cells. Decline or absence in the expression of co-stimulatory molecules leads to T cell anergy, a state of unresponsiveness. Hence, we next evaluated the expression of these molecules on DC^{MPT64}. DC^{MPT64} increased CD40, CD80 and CD11b levels but declined MHC II expression (Fig. 1B). Further, it has been reported that DCs not only activate but also suppress the immunity [39]. Therefore, we were curious to monitor the expression of co-inhibitory molecules on DCs. We noticed that DC^{MPT64} displayed higher levels of PD-L1, TIM-3, and Ly6C, as compared to control DCs (Fig. 1C–D). Both PD-L1 and TIM-3 are known for the induction of tolerance, as well as recognized as co-inhibitory markers [40]. The cells with $Ly6C^{hi}$, $F4/80^{hi}$, $CD11b^{hi}$, $CD40^{hi}$, $CD80^{hi}$, $PD\text{-}L1^{hi}$ and $TIM\text{-}3^{hi}$ phenotypes represent monocytic MDSCs (myeloid-derived suppressor cells). It can be inferred from these findings that pre-exposure of early DCs to MPT64 during differentiation converts them to MDSCs. Recently, MDSCs have been reported to be localized within the TB granulomas along with DCs and macrophages. MDSCs are heterogeneous cell populations having different morphology and functionality.

We have used purified and endotoxin-free MPT64, CFP-10 and ESAT-6 in all the experiments (Supplementary Fig. 1A, B). The MPT64 was characterized through MASCOT, it is the same as wild-type MPT64 protein [29] (Supplementary Fig. 2). We also verified the specificity of the experiments using CFP-10 and ESAT-6 proteins of *Mtb* that were produced under the same conditions [36].

MPT64 inhibits the release of pro-inflammatory cytokines by DC^{MPT64}

DC performs a diametric role, it can activate and suppress the immune response. The cytokines secreted by DCs are very critical for *Mtb* survival [42]. Pro-inflammatory cytokines, like IL-6, IL-12, and TNF-α, inhibit the growth of *Mtb*, whereas anti-inflammatory cytokines, such as IL-10

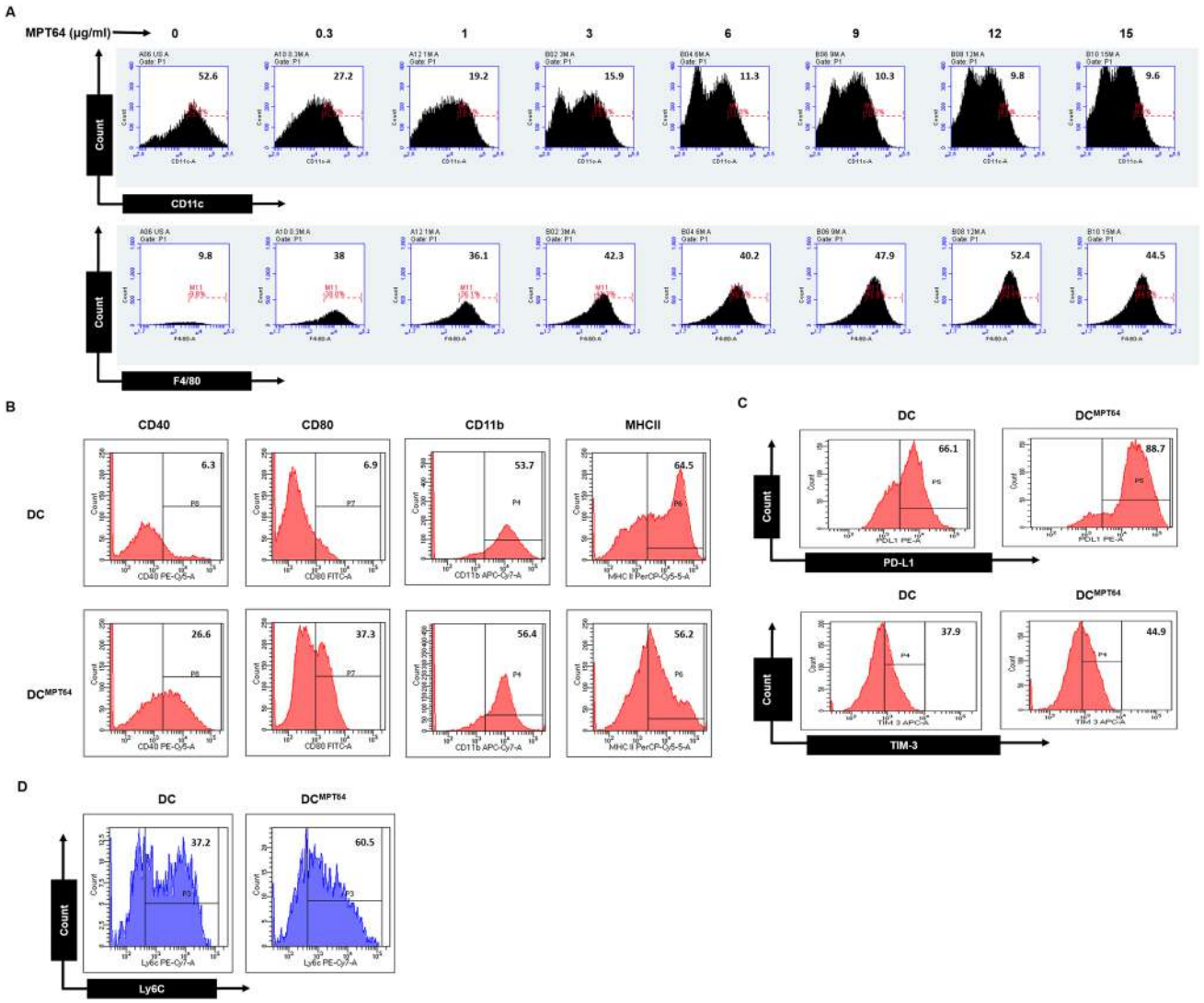

Fig. 1 MPT64 impairs the maturation of DC. Bone marrow cells (BMCs) cultured with GM-CSF + IL-4 (DCs) along with MPT64 (DC^{MPT64}) were monitored for the expression of **A** CD11c and F4/80 through flow cytometry upon exposure to various concentrations of MPT64 (0–15 µg/ml). The insets of the histogram display percentage positive cells. **B** The expression of CD40, CD80, CD11b, MHCII and **C** PD-L1 and TIM-3 was assessed through flow cytometry on DC^{MPT64} and control DCs. The values in the inset of the histogram show percentage of positive cells. **D** The expression of Ly6C on DC^{MPT64} and control DCs was monitored through flow cytometry and shown as histograms. The data are representative of 2–3 independent experiments.*$p < 0.05$, **$p < 0.01$, ***$p < 0.001$, ****$p < 0.0001$

and TGF-β, encourage the persistence of *Mtb* [43, 44]. Moreover, cytokines are the third important signal requisite for the activation of T cells. Therefore, it was imperative to examine the cytokines produced by DC^{MPT64}. DC^{MPT64} showed a significant reduction in the yield of IL-6 ($p < 0.01$), IL-12 ($p < 0.0001$) and TNF-α ($p < 0.0001$), as compared to control DCs and DC^{CFP-10} (Fig. 2A–C). In contrast, a higher level of IL-10 ($p < 0.0001$) was noted in DC^{MPT64} (Fig. 2D). These results illustrate that MPT64 restricts DCs to produce cytokines that impede *Mtb* function but promote cytokines that may help mycobacterium sustenance.

MPT64 induces morphological changes in DC^{MPT64} and obstructs their migratory function

DCs play a decisive role in activating the immune system against *Mtb* infection [45, 46]. DCs have many long arborizing projections on their surface known as dendrites, which help in capturing of antigens and interaction with T cells [47]. Activated DCs appear morphologically vivid with elongated dendrites. They robustly capture antigens for processing and presentation to T cells [48]. Hence, we wanted to monitor the change in the morphology of

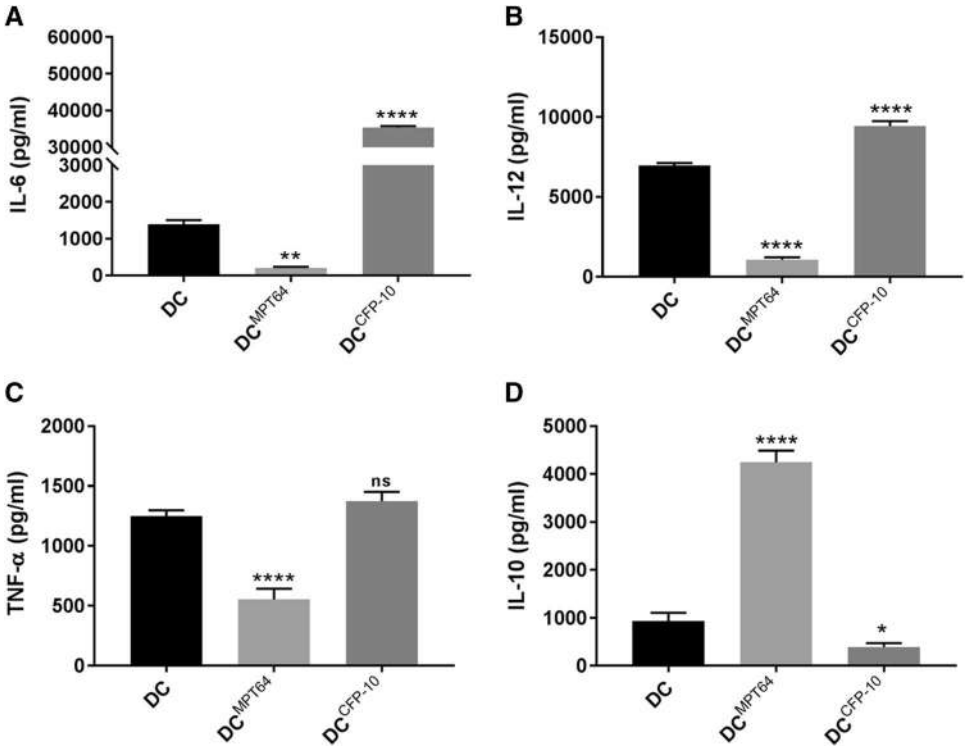

Fig. 2 Exposure of MPT64 to DC^{MPT64} during maturation impedes the secretion of pro-inflammatory cytokines IL-6, IL-12 and TNF-α but augments the release of IL-10. DC^{MPT64} and control DC^{CFP-10} and DCs were cultured for 6 days in complete medium. Later, SNs were collected for the estimation of **A** IL-6, **B** IL-12, **C** TNF-α and **D** IL-10 by ELISA. Data represented as mean ± SD are from triplicate wells ($n=3$) and 2 independent experiments. *$p<0.05$, **$p<0.01$, ***$p<0.001$, ****$p<0.0001$

MPT64-treated DCs. Surprisingly, DC^{MPT64} exhibited an absence of dendrites, as compared to control DCs (Fig. 3A). These changes were further documented by confocal microscopy (Supplementary Fig. 4A). This corroborates with our previous observations that MPT64 prompts the generation of MDSCs, as these cells have diminished morphology with less efficacy of activating adaptive immune response (Fig. 1).

Mtb conventionally infects macrophages and DCs. Lipid depots within the host cells act as an energy reservoir for the survival of *Mtb* [49]. MDSCs have high lipid content and act as a nutrient-rich niche to benefit the *Mtb* survival [50]. Further, the lipid within DCs hampers their functionality [51]. Hence, we planned to check whether lipid accumulation within DC^{MPT64} curbs their functionality. Intriguingly, we observed that DC^{MPT64} showed augmented lipid deposition, as compared to control DCs and DC^{CFP-10} by both flow cytometry and confocal microscopy (Fig. 3B and Supplementary Fig. 4B). It can be inferred from these results that *Mtb* employs its MPT64 protein to promote lipid accumulation in DC^{MPT64}, which might be responsible for their suppressive function.

Migration of antigen-captured APCs to lymphoid organs is crucial for the induction of adaptive immune response. DCs capture antigens from the site of infection and migrate to the secondary lymphoid organs to activate T cells. Such DCs express an optimum level of CCR7, a chemokine that is responsible for their chemotaxis [48]. Migration of DCs to the site of infection or lymphoid organs with captured antigen relies highly on CCR7 expression [52]. Till now, we observed that DC^{MPT64} exhibit high expression of co-inhibitory markers with less expression of MHC II markers and therefore imparts suppressive phenotype. Hence, we were eager to know, whether DC^{MPT64} have retained their migratory potential or not. Surprisingly, DC^{MPT64} exhibited a significant ($p<0.05$) reduction in the expression of CCR7 (Fig. 3C, D and Supplementary Fig. 5A). Further, to confirm this finding in vivo, we adoptively transferred CFSE-labelled DC^{MPT64} into mice. A significant drop was apparent in the migration of DC^{MPT64} but not control DCs to the spleen after 24 h ($p<0.0001$) and 48 h ($p<0.001$) of inoculation (Fig. 3E, F). Such DC^{MPT64} displayed a significantly ($p<0.01$) lower level of CCR7 (Fig. 3G, H). Our results correlate well with the findings that the deposition of high lipid content in the cells hampers their migration and functionality [51].

MPT64 abates the efficacy of DC^{MPT64} to activate and differentiate T cells

For the complete elimination of pathogens, both innate and adaptive immunity play a very important role. APCs upon recognizing pathogens activate the primary immune response through the secretion of antibodies, cytokines and other soluble mediators. Pathogen-captured DCs migrate to secondary lymphoid organs to activate pathogen-reactive T cells [53]. Inhibition of the activation of T cells has been referred to as a 'gold' standard for

considering any cell as MDSCs [54]. Since DC^{MPT64} exhibited an MDSCs-like phenotype, we were next interested to see whether DC^{MPT64} inhibit the proliferation of CD4 T cells and CD8 T cells. We co-cultured DC^{MPT64} with syngeneic CD4 T cells ($p < 0.0001$) and CD8 T cells ($p < 0.001$) and observed a significant decrease in their proliferation (Fig. 4A, B). Likewise, these results were further supported by observing a substantial decline in the proliferation of allogeneic CD4 T cells ($p < 0.05$) and CD8 T cells ($p < 0.001$) (Fig. 4C, D). These findings suggest the suppressive nature of DC^{MPT64}, as has been reported in the case of MDSCs. Therefore, DC^{MPT64} exhibit their tendency to inhibit the induction of T cell response.

The adaptive immune system plays a compelling contribution in controlling the spread of *Mtb*. Lymphocytes have a significant role in the pathogenesis and development of immunity [55]. Activation of T cells by DCs leads to the secretion of array of cytokines, such as IL-17, IFN-γ, TGF-β and IL-10. These cytokines have a robust role in the induction and differentiation of Th1 cells, Th17 cells and Treg cells. Th1 cells and Th17 cells play a central role in protecting against *Mtb* [56]. In contrast, Th2 cells and Tregs support the progression of the disease [57, 58]. We detected a reduction in IFN-γ ($p < 0.0001$) and IL-17 ($p < 0.0001$), but an increase in IL-10 ($p < 0.0001$) and TGF-β ($p < 0.0001$) when syngeneic CD4 T cells were cultured with DC^{MPT64} (Fig. 4E–H). These results were confirmed using allogeneic CD4 T cells. A reduction in IFN-γ ($p < 0.0001$) and IL-17 ($p < 0.0001$), but an increase in the IL-10 ($p < 0.0001$) and TGF-β ($p < 0.0001$), was noticed (Fig. 4I–L). Therefore, these results testify that DC^{MPT64} obstruct the differentiation of Th1 cells and Th17 cells but supports the generation of Tregs.

DC^{MPT64} induce the generation of Tregs

Tolerance of immune response has been identified in the case of diseases, like TB and cancer. Conventionally, immune system of host always maintain a balance between the generation of immune response and tolerance. DCs not only stimulate innate and adaptive immunity but also impart tolerance [39, 59]. Till now, we have noticed that DC^{MPT64} exhibit high expression of PD-L1, TIM-3 and IL-10. Both PD-L1 and TIM-3 are well known for the generation of tolerance in DCs [40, 60]. Moreover, we have shown that DC^{MPT64} have the efficacy to abate the activation and differentiation of CD4 T cells and CD8 T cells. T cells stimulated by DC^{MPT64} produced significantly higher levels of TGF-β and IL-10 (Fig. 4G, H, K, L). Therefore, we examined if DC^{MPT64} can in vivo evoke the generation of $FoxP3^+$ Tregs. Hence, OVA pulsed-DC^{MPT64} were adoptively transferred into mice twice at an interval of 7d (Fig. 5A). A significant augmentation was demonstrated in the percentage of $CD4^+$ and $CD8^+$ Tregs ($p < 0.05$) (Fig. 5B–E and Supplementary Fig. 5B, C). Our data substantiate the previous findings that MDSCs promote Tregs during TB infection [61]. These results also suggest that *Mtb* may be exploiting its MPT64 to elude the immune response by engendering Tregs.

MPT64 impairs the ability of DC^{MPT64} to phagocytose mycobacterium

DCs and macrophages are the most potent immune cells with strong phagocytic activity. DCs upon uptake of pathogen translocate MHC I or II complex on its surface with enhanced expression of co-stimulatory molecules and cytokines [48]. Surprisingly, we observed that MPT64-exposed DC^{MPT64} show less expression of MHC II. Interestingly, it has been well reported that MDSCs have less phagocytosis potential and favor the survival of the pathogen [62]. *Mtb*-infected macrophages and DCs show deterioration in engulfing antigens. To check this, we infected DC^{MPT64} with *Mtb* GFP-H37Ra, *Mtb* H37Rv and *M. smegmatis* and examined their uptake by flow cytometer (GFP-H37Ra) and CFUs (H37Rv and *M. smegmatis*). DC^{MPT64} indicated significant downregulation in phagocytosis of both the virulent (H37Rv) ($p < 0.001$) and avirulent (H37Ra) ($p < 0.001$) mycobacteria (Fig. 6A, B). These results were further confirmed, when we noted a substantial ($p < 0.0001$) decline by DC^{MPT64} to engulf *M. smegmatis*, another strain of mycobacteria by CFUs (Fig. 6C). Further, impairment in phagocytosis of *Mtb* GFP-H37Ra by DC^{MPT64} was validated by confocal imaging (Fig. 6D). Furthermore, DC^{MPT64} also exhibited remarkable inhibition ($p < 0.0001$) in the uptake of dextran-FITC, a soluble form of an antigen (Fig. 6E, F).

Enhancement of the intracellular survival of *Mtb* in the DC^{MPT64}

Like alveolar macrophages, *Mtb* can also persist in MDSCs [26, 63]. We observed that DC^{MPT64} exhibit a suppressive phenotype and augments the generation of Tregs through inhibition of Th1 cells and Th17 cells. MDSCs have a very contentious role in tuberculosis and literature have shown that through modulation of immune response MDSCs promote *Mtb* survival [64]. Next, we thought of checking the intracellular survival of *Mtb* in DC^{MPT64}. *Mtb* showed remarkably ($p < 0.0001$) higher growth in the DC^{MPT64}, as compared to control DCs (Fig. 7). The results indicate that *Mtb* exploits its MPT64 protein to establish its survival in the DCs by skewing its differentiation to MDSCs.

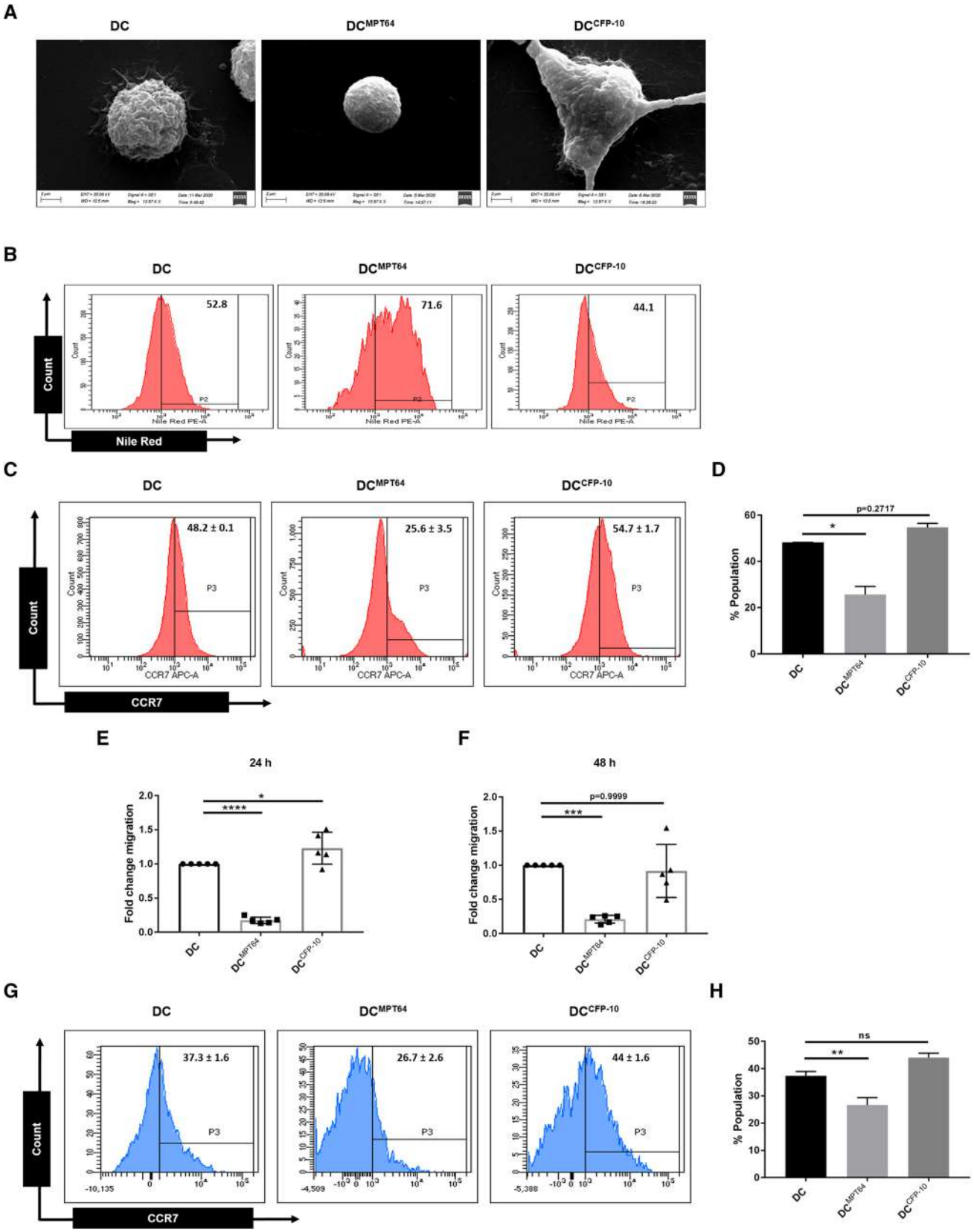
A
DC
DC^MPT64
DC^CFP-10
B
DC
DC^MPT64
DC^CFP-10
52.8
71.6
44.1
Count
Nile Red
Nile Red PE-A
P2
C
DC
DC^MPT64
DC^CFP-10
48.2 ± 0.1
25.6 ± 3.5
54.7 ± 1.7
P3
Count
CCR7
CCR7 APC-A
D
% Population
p=0.2717
*
DC
DC^MPT64
DC^CFP-10
E
24 h
Fold change migration
*
****
F
48 h
p=0.9999
***
G
DC
DC^MPT64
DC^CFP-10
37.3 ± 1.6
26.7 ± 2.6
44 ± 1.6
P3
Count
CCR7
H
% Population
ns
**

◂**Fig. 3** Induction of morphological changes and impairment in the migratory function of DC^{MPT64}. **A** DC^{MPT64} and control DC^{CFP-10} and DCs were cultured on poly-L-Lysine pre-coated glass coverslips in 12-well plates for 6 d. Later, cells were fixed with modified Karnovsky fixative and imaged under scanning electron microscopy (SEM). Pictures were clicked at 13.97 K (scale bar: 2 µm). The data are representative of two independent experiments. **B** DC^{MPT64}, DC^{CFP-10} and DCs were stained with Nile red dye for monitoring the lipid accumulation within cells through flow cytometry. Values in the inset of the histogram depict the percent positive cells ($n=1$). **C–D** DC^{MPT64}, DC^{CFP-10} and DCs were monitored for the surface expression of CCR7 ($n=2$). Data are represented as percentage positive cells (mean ± SEM) through flow cytometer histograms and bar diagrams. **E–F** DC^{MPT64}, DC^{CFP-10} and DCs were CFSE-labelled and injected i.v. in the mice. After 24 and 48 h, the presence of $CFSE^+$ cells was monitored in the spleen. The data are expressed as a fold-change migration of DC^{MPT64} through scatter plots. Each dot denotes an individual animal ($n=5$). **G–H** The surface expression of CCR7 was observed ex vivo on DC^{MPT64} migrated to the spleen ($n=4$). The percentage positive (mean ± SEM) DC^{MPT64} is illustrated through a flow cytometry and bar diagram. Data are representative of 2 independent experiments. $*p<0.05$, $**p<0.01$, $***p<0.001$, $****p<0.0001$, *ns* non-significant

The mechanism involved in suppressing the function of DC^{MPT64} by MPT64 is through the involvement of arginase, STAT-3, NO and IDO

Innate immune cells restrict *Mtb* infection through various mechanisms, such as phagocytosis, opsonization, inflammasome activation and producing various inflammatory mediators [2]. We next elucidated the mechanism involved in imparting suppression by DC^{MPT64}. DC^{MPT64} showed modulation in the expression of $CD11c^{lo}$, $CD11b^{hi}$, $F4/80^{hi}$, $CD40^{hi}$, $CD80^{hi}$, $MHCII^{lo}$, $Ly6C^{hi}$, $Ly6G^{lo}$, $PD\text{-}L1^{hi}$, $TIM\text{-}3^{hi}$, $IL\text{-}10^{hi}$, $TGF\text{-}\beta^{hi}$, $IL\text{-}6^{lo}$, $IL\text{-}12^{lo}$, $TNF\text{-}\alpha^{lo}$ and $CCR7^{lo}$, the molecules that are responsible for immunosuppression (Figs. 1, 2, 3). Based upon the presence of specific set of markers these cells have been characterized as M-MDSC. After extensive analysis, we observed the mechanism involved in suppression was through an elevated level ($p<0.05$) of the arginase in DC^{MPT64}, as tested by biochemical assay and confirmed by Western blotting (Fig. 8A, B). The higher quantity of arginase was well correlated with increased STAT-3 expression (Fig. 8C). STAT-3 controls arginase 1 in MDSCs [65]. MDSCs produce a higher amount of arginase, which contributes to the inhibition of the immunity [66]. We next examined indoleamine 2,3-dioxygenase (IDO) and ROS in DC^{MPT64}. IDO and ROS are important immunosuppressive molecules produced by MDSCs [67–69]. DC^{MPT64} showed augmentation in IDO and a decline in the expression of NF-κB and secretion of ROS (Fig. 8D, F). Similarly, a significant release in the NO ($p<0.0001$) and iNOS was noticed, along with a noticeable upregulation of STAT-1 (Fig. 10I–K). STAT-1 is required for the iNOS activation [70], which establishes the specificity of our results.

During microbial infections, NF-κB contributes to managing the immune response. It enhances the release of pro-inflammatory cytokines and chemokines and fosters the migration of the cells to the site of infection. We observed a remarkable reduction of NF-κB, as compared to control DCs (Fig. 8E). In essence, the results illustrate that *Mtb* skillfully exploits MPT64 to modulate the expression of an array of molecules on DC^{MPT64} to fine-tune the immune system for its survival.

Acquisition of dormant metabolic phenotype by DC^{MPT64}

Various mechanisms have been delineated for the immune surveillance and elicitation of the optimum immune response against infections [55, 71]. MDSCs work as a double edge sword against host in TB infection, as they not only provide a safer resort for *Mtb* survival but also slash the adaptive immune response. *Mtb* utilizes lipids as a potent nutritional source for its survival and progression within host cells [49]. During TB infection, MDSCs shift their glycolysis machinery to the fatty acid oxidation [72]. Therefore, we analyzed the metabolic components of DC^{MPT64}. Initially, we monitored the glucose uptake potential of DC^{MPT64} and noted a significant decline ($p<0.001$) in the glucose (2-NBDG) level, as compared to control DCs (Fig. 9A, B). These results were further confirmed by confocal microscopy; a significant fall in the glucose uptake was seen in DC^{MPT64} (Fig. 9C). Negative control (DC^{neg}) signifies DCs cultured in media supplemented with glucose (Fig. 9A, B).

Glycolysis plays a significant role in the activation of immune cells [73, 74]. Impairment in glycolysis leads to the induction of a steady state in the cells and makes them metabolically inert. We observed that DC^{MPT64} utilize less glucose from surroundings. Further, accumulation of methylglyoxal (MGO) in MDSCs is an indication of their suppressive nature [27]. Hence, we next wanted to monitor the metabolic status of DC^{MPT64}. Likewise, we observed significantly high ($p<0.001$) MGO in DC^{MPT64} by flow cytometry (Fig. 9D, E). These results were further corroborated by confocal imaging (Fig. 9F). DCs stressed with H_2O_2 served as a positive control (DC^{pos}). Furthermore, we observed a significant reduction in Glut1 ($p<0.05$) in DC^{MPT64} (Fig. 9G). Glut1 is the main glucose transport channel in immune and non-immune cells. Additionally,

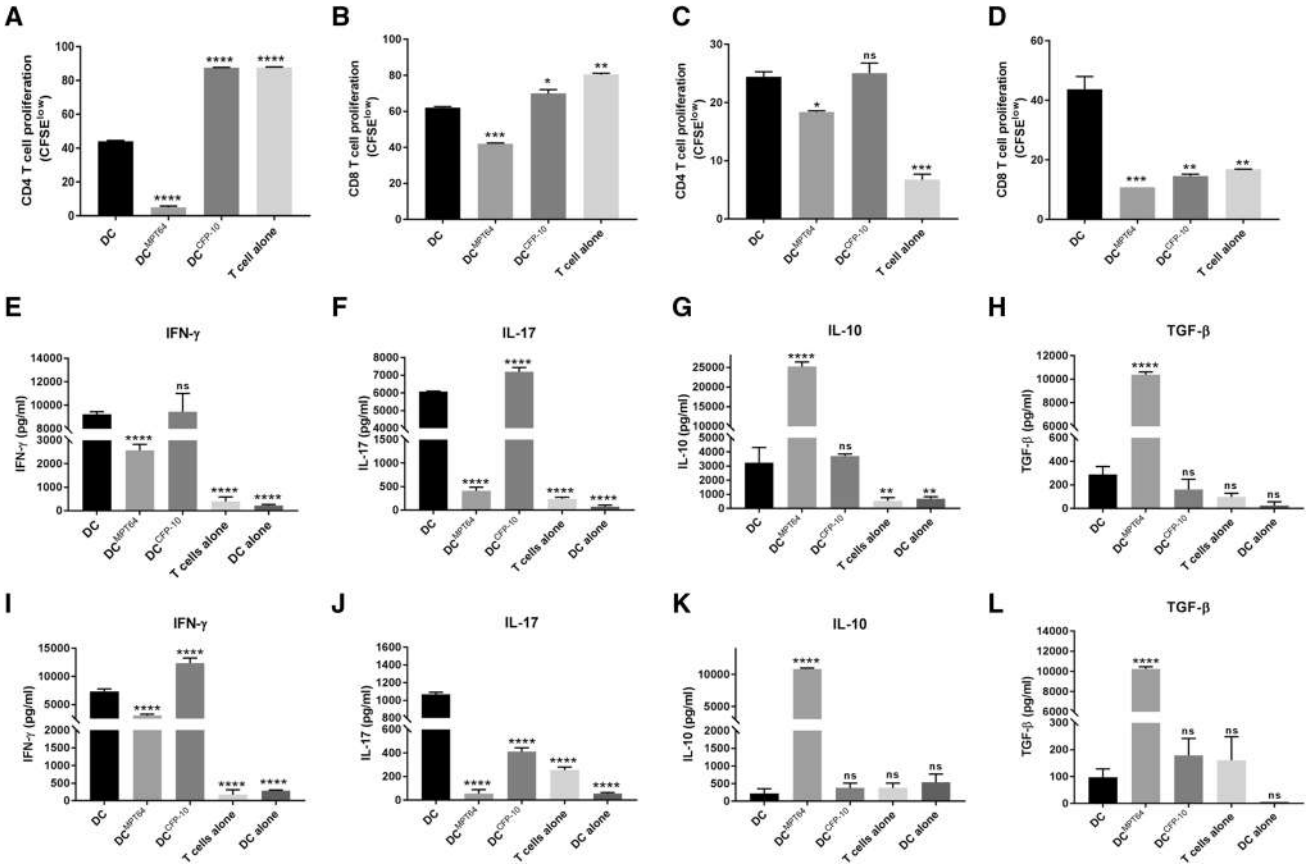

Fig. 4 MPT64 impairs the function of DC^{MPT64} to activate and differentiate CD4 T cells and CD8 T cells. The proliferation of syngeneic CD4 T cells and CD8 T cells by DC^{MPT64}. CFSE-labelled syngeneic naïve **A** CD4 T cells; **B** CD8 T cells were stimulated with plate-bound anti-CD3 and anti-CD28 Abs and co-cultured with syngeneic DC^{MPT64} and control DC^{CFP-10} and DCs (T cell: DCs; 10:1 ratio). The allogeneic proliferation of CD4 T cells and CD8 T cells by DC^{MPT64}. Allogeneic naïve **C** CD4 T cells; **D** CD8 T cells isolated from BALB/c mice were co-cultured with allogeneic (C57BL/6) DCs (T cell: DCs; 10:1 ratio). **A**–**D** After 72 h, T cell proliferation was enumerated by CFSE dye dilution assay. The bar diagram represents the percentage of positive cells (mean ± SEM) ($n = 2$), and data are representative of 2–3 independent experiments. **E**–**L** Estimation of the production of cytokines. After 72 h of culture, the SNs were collected from syngeneic (**E**–**H**) and allogeneic (**I**–**L**) and monitored by ELISA for the production of IFN-γ, IL-17, IL-10 and TGF-β. Data represented as mean ± SD are of triplicate wells and ($n = 3$) from 2 independent experiments.*$p < 0.05$, **$p < 0.01$, ***$p < 0.001$, ****$p < 0.0001$, *ns* non-significant

a striking reduction in the expression of the hexokinase 2 ($p < 0.05$) enzyme was detected in DC^{MPT64} (Fig. 9H). Noteworthy, augmentation in the messenger RNA of semicarbazide-sensitive amine oxidase (SSAO) ($p < 0.01$) was seen in DC^{MPT64} (Fig. 9I). It has been reported that intracellular MGO was regulated by glyoxalase and glutathione [75]. A marked reduction in the expression of glyoxalase 1 ($p < 0.01$) in DC^{MPT64} was noticed (Fig. 9J). This finding depicts that there was dysregulation between generation and neutralization of MGO. MGO generation occurs through the by-products (glyceraldehyde3-phosphate and dihydroxyacetone phosphate) of glycolysis, and acetone and aminoacetone by SSAO [76–78]. Together, these results imply that DCs encountering MPT64 during their differentiation renders them metabolically dormant with suppressive function.

The mechanism of inhibition of the proliferation of T cells is through methylglyoxal

During TB infection, innate immune cells engulf the pathogen and initiate a cascade of events. Due to the non-specificity of the innate immune system, the adaptive immune system operates finally to curtail the infection. T cells play a crucial role in the pathogenesis and protection of TB disease [55]. Till now, the results suggest that DC^{MPT64} secrete soluble mediators, as well as displays certain molecules on its surface that are responsible for their suppressive activity. It has been well evidenced that the expression of co-inhibitory molecules, such as PD-L1 and TIM-3, over the surface of myeloid cells imparts suppressive functionality that leads to the induction of tolerance [40, 60]. Moreover, the presence of methylglyoxal in MDSCs dampens T cell function

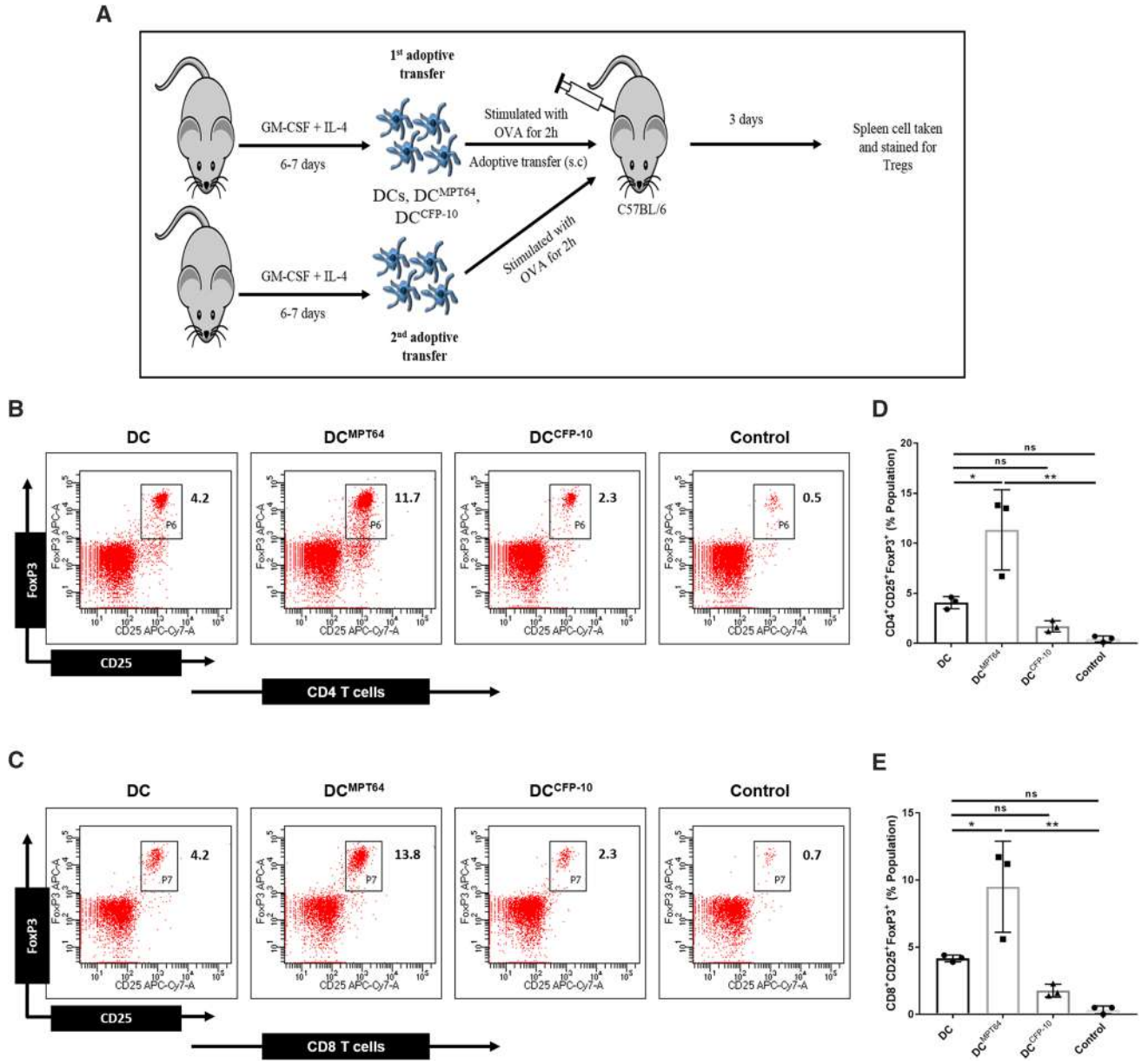

Fig. 5 MPT64-stimulated DC^{MPT64} supports the in vivo generation of Tregs. **A** Diagrammatic representation of the experimental design. Antigen-pulsed DC^{MPT64} and control DC^{CFP-10} and DCs were injected (s.c) twice at an interval of 7 d into the mice. After 3 d, animals were sacrificed and the pool of **B** CD4 T cells; **C** CD8 T cells expressing $CD25^+$ and $FoxP3^+$ were enumerated by flow cytometry and depicted as (**B**, **C**) dot plots; (**D**, **E**) bar diagrams. DCs adoptively transferred without antigen (OVA) were taken as a control. Each dot in the scatter plot signifies data from one mouse ($n=3$). The values (mean ± SEM), in the inset are percentage positive cells and representative of 3 independent experiments. $*p<0.05$, $**p<0.01$, $***p<0.001$, $****p<0.0001$, *ns* non-significant

[27]. Hence, we were curious to know whether inhibition in T cell proliferation by DC^{MPT64} was through secretory molecules or cognate interaction. Consequently, DC^{MPT64} were cultured with CD4 T cells either in a normal tissue culture plate (contact dependent) or in a trans-well culture plate (contact independent). We observed a significant reduction in CD4 T cells ($p<0.001$) proliferation when cultured with DC^{MPT64} either in a contact-dependent or -independent fashion (Fig. 10A, B). These results were further validated with CD8 T cells ($p<0.01$) (Fig. 10C, D). Thus, the DC^{MPT64} inhibit the proliferation of T cells through the secretory, as well as surface molecules.

Nitric oxide is reported to inhibit T cell proliferation [79]. Nitric oxide and iNOS, and their transcription regulator STAT-1 are expressed in higher amounts by DC^{MPT64} (Fig. 10I–K). Consequently, we wanted to examine if NO may be a soluble factor responsible for deterring T cell proliferation. Therefore, the iNOS inhibitor

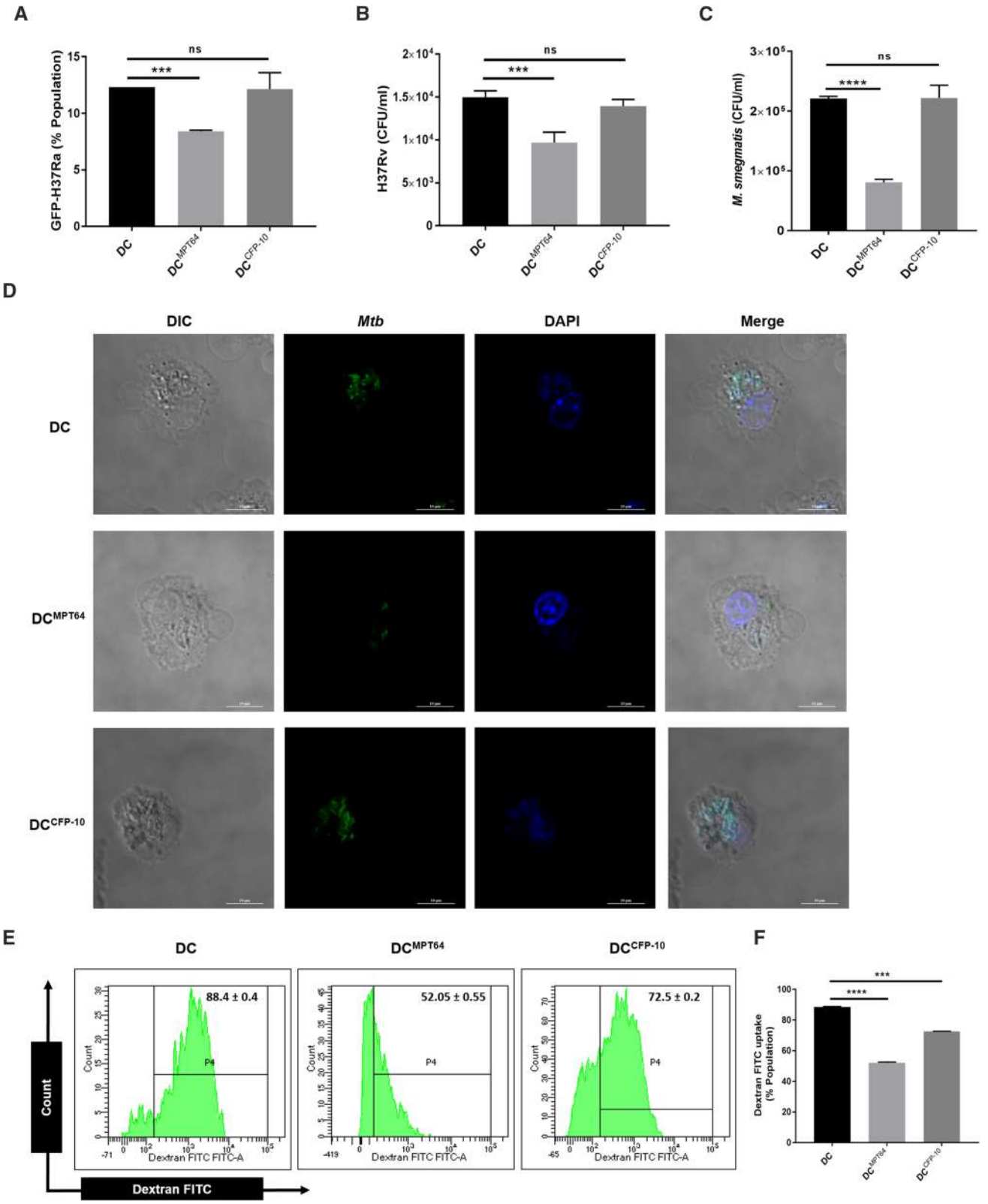

N-monomethyl-L-arginine (NM) was added to the cultures of DC^{MPT64} and CD4 T cells. We observed slight regaining (non-significant) in the proliferation of CD4 T cells (Fig. 10E, F) and CD8 T cells (Fig. 10G, H).

◂**Fig. 6** MPT64 restricted *Mtb* uptake by DC^{MPT64}. The DC^{MPT64} and control DCs were monitored for phagocytosis (3–4 h) (MOI—1:5, DC: bacterium) of **A** GFP-H37Ra; **B** H37Rv; **C** *M. smegmatis*. The extracellular bacilli were killed by incubating cultures with gentamycin/amikacin for 1 h. The engulfment of the bacteria was enumerated by **A** flow cytometer ($n=2$); **B**, **C** CFUs ($n=3$); **D** confocal microscopy (scale bar: 10 µM; magnification: 60×). **E**, **F** DC^{MPT64} were also monitored for antigen (dextran-FITC) uptake by flow cytometry and depicted as **E** histogram and **F** bar diagram ($n=2$). Data are illustrative of 2–3 independent experiments. *$p<0.05$, **$p<0.01$, ***$p<0.001$, ****$p<0.0001$

Myeloid cells depict different metabolic statuses depending upon their state. These metabolic variations can be from a glycolytic metabolism to lipid metabolism, leading to induction or inhibition of various functional and differentiation processes [80]. The adaptive immune system plays a decisive role in controlling TB. Hence, we examined whether DC^{MPT64} induce a metabolically quiescent stage in T cells. A sizeable decline in glucose uptake by CD4 T cells and CD8 T cells was noticed when cultured with DC^{MPT64} (Fig. 11A, B). Further, a remarkable decrease in the MGO level of CD4 T cells was noticed when cultured with DC^{MPT64} but not with control $DC^{CFP\text{-}10}$ and DCs (Fig. 11C). These results were further confirmed with CD8 T cells (Fig. 11D). Thus, it may be concluded that MGO produced by DC^{MPT64} might be restricting the proliferation of T cells. Ultimately, it can be inferred from these results that DC^{MPT64} inhibit the proliferation of T cells through molecules expressed on its surface and soluble mediators.

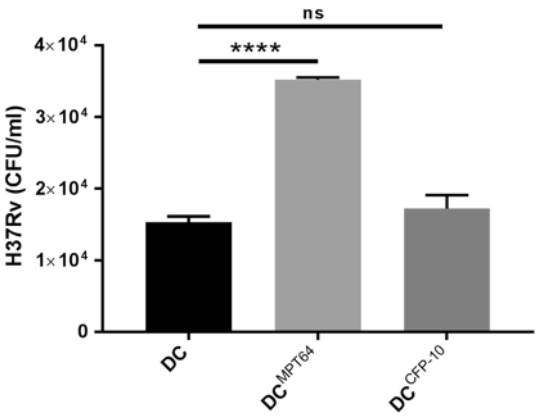

Fig. 7 MPT64 augmens *Mtb* survival in DC^{MPT64}. The DC^{MPT64} were infected with H37Rv (MOI – 1:5) for 4 h. The extracellular bacilli were killed by incubating the cultures with amikacin for 1 h. DC^{MPT64} were further cultured for 72 h. Later, the infected DC^{MPT64} were lysed and the survival of *Mtb* was estimated by CFUs. The data (mean ± SD) shown as bar diagrams are indicative of CFU/ml of *Mtb* and representative of triplicate samples ($n=3$) and two independent experiments. *$p<0.05$, **$p<0.01$, ***$p<0.001$, ****$p<0.0001$

MPT64-stimulated DC^{MPT64} downregulate the expression of T cell receptors and augment T cell apoptosis

T cell recognizes peptide-MHC complex presented on the surface of DCs through its T cell receptor (TCR). The TCR is composed of α and β or γ and δ glycoproteins. The TCRs chains get downregulated in the presence of a high level of NO and ROS [79]. We noticed remarkable downregulation in the expression of the TCRβ chain ($p<0.01$) and TCRγ/δ ($p<0.05$) of CD4 T cells when T cells were cultured with DC^{MPT64} but not control $DC^{CFP\text{-}10}$ and DCs (Fig. 12A–D). These results were further validated with CD8 T cells since a significant decline in the TCRβ chain ($p<0.05$) and TCRγ/δ ($p<0.05$) was noted (Fig. 12E–H).

Literature suggests that myeloid suppressor cell induces apoptosis of T cells. Furthermore, it has been shown that nitrogen and oxygen intermediates impede T cell function through nitration of TCR and apoptosis [81, 82]. We have shown that DC^{MPT64} exhibit high NO secretion along with expression of various other co-inhibitory markers. Therefore, we were interested to examine the effect of DC^{MPT64} in the induction of apoptosis in T cells. Likewise, we noticed considerable apoptosis ($p<0.01$) in CD4 T cells, when co-cultured with DC^{MPT64} but not control DCs or $DC^{CFP\text{-}10}$ (Fig. 12I, J). These results were further authenticated with CD8 T cells ($p<0.001$) (Fig. 12K, L).

Overall the results suggest that MPT64 impairs the function DCs if encountered during their differentiation.

Discussion

Mycobacterium tuberculosis has latently infected nearly 2 billion people globally and therefore is a great threat to society [83]. *Mtb* is a smart pathogen, which has developed various immune evasion strategies against the host [10, 84–86]. *Mtb* secretes an array of molecules, which are involved in subverting the immune response for its persistence. Hence, it is imperative to identify such components. It has been hypothesized that secretory proteins of *Mtb* are the first moieties to encounter the host immune system [87]. Among secretory proteins, Ag85 family, ESAT-6 family, MPT63, MPT64, Acr1 and lipoproteins constitute a major part of the secretome [88]. MPT64 (Rv1980c) is one of the actively secretory proteins of replicating *Mtb* with m.wt. of 24 kDa [29, 89]. It has been observed that the expression level of MPT64 in serum, sputum and granulomas of active TB patients is fairly high [90]. It is recognized by Th1 cells and is a potential diagnostic or vaccine candidate. The modulatory role of MPT64 has been explored to some extent on macrophages, epithelioid cells and multinucleated

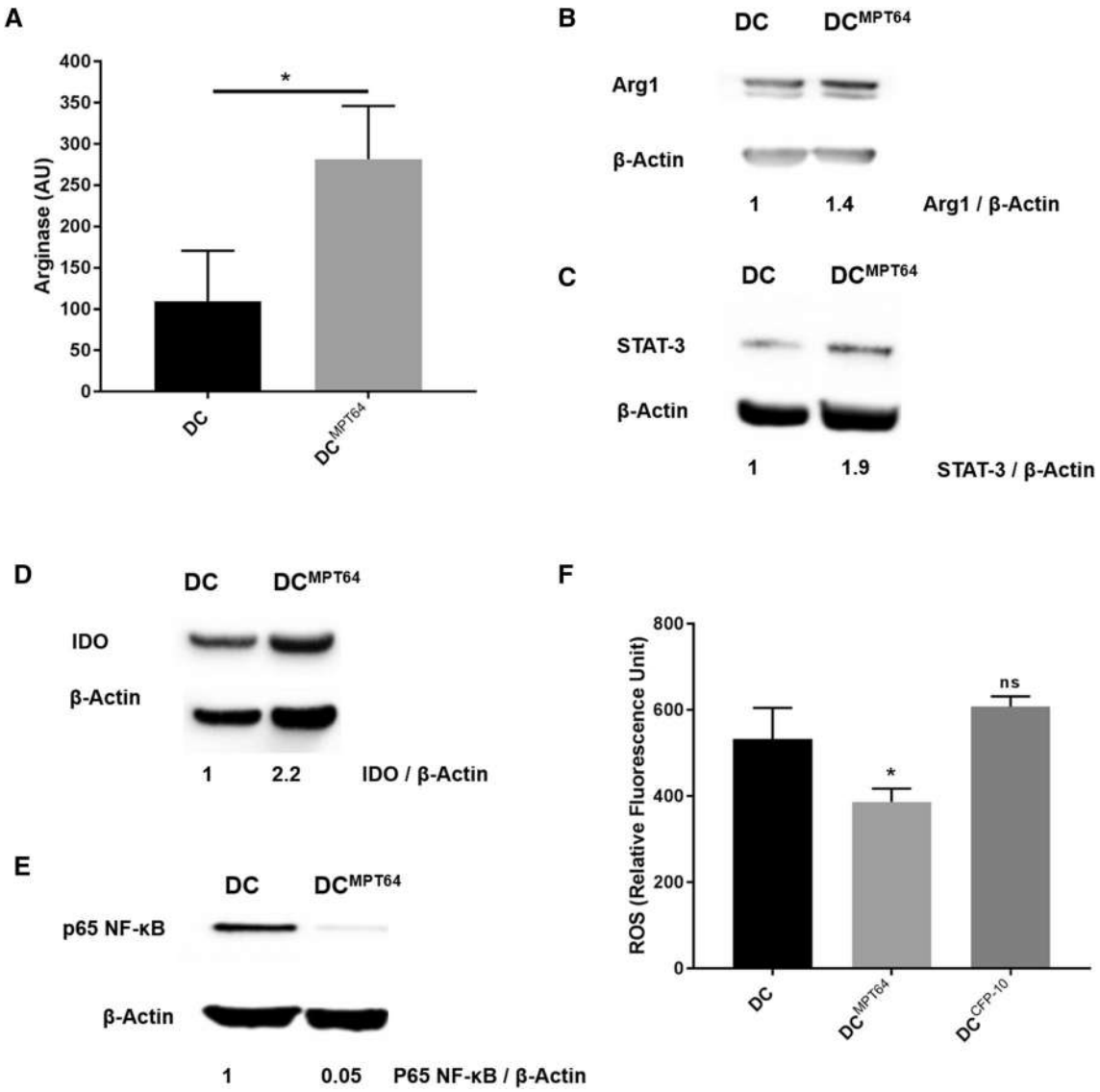

Fig. 8 MPT64 upregulates Arg1 and IDO but inhibits ROS and NF-κB expression in DC^{MPT64}. DC^{MPT64} and control DC^{CFP-10} and DCs were cultured for 6 d in a complete medium. Later, **A** arginase was estimated by arginase activity assay ($n=3$). The cell lysate was used for Western blotting for the expression of **B** arginase 1; **C** STAT-3; **D** IDO; **E** NF-κB p65. **F** ROS were analysed by labelling with oxidation-sensitive dye H2DCFDA ($n=3$). The data are representative of 2–3 independent experiments. *$p<0.05$, **$p<0.01$, ***$p<0.001$, ****$p<0.0001$, *ns* non-significant

giant cells but its influence on differentiating DCs remains elusive [91, 92].

For the first time, we have delineated the role of MPT64 in evading the immune system by impairing the differentiation of the DCs and the following major findings were observed: MPT64 (i) skewed the maturation of BMDCs to MDSCs but not DCs, under DC differentiating milieu (IL-4 + GM-CSF); (ii) suppressed the function of DCs by upregulating the expression of the co-inhibitory molecules PD-L1, TIM-3 and Ly6C; (iii) downregulating the display of MHC II molecules the display of MHC II molecules and inhibiting the secretion of pro-inflammatory cytokines; (iv) impaired the migratory function of DCs by reducing CCR7 expression; (v) promoted the generation of Tregs and restricted the expansion of Th1 cells and Th17 cells; (vi) inhibited the function of DCs to phagocytose *Mtb* but augmented its intracellular survival; and (vii) the mechanism of immunosuppression deciphered was due to the surface exhibition of co-inhibitory molecules and induction of metabolically quiescent morphology.

It was amazing to note that on exposure to MPT64 during their differentiation, DCs failed to activate both CD4 T cells and CD8 T cells and developed a suppressive phenotype like of MDSCs, viz., $CD11c^{lo}$, $MHCII^{lo}$, $Ly6C^{hi}$, $TIM\text{-}3^{hi}$,

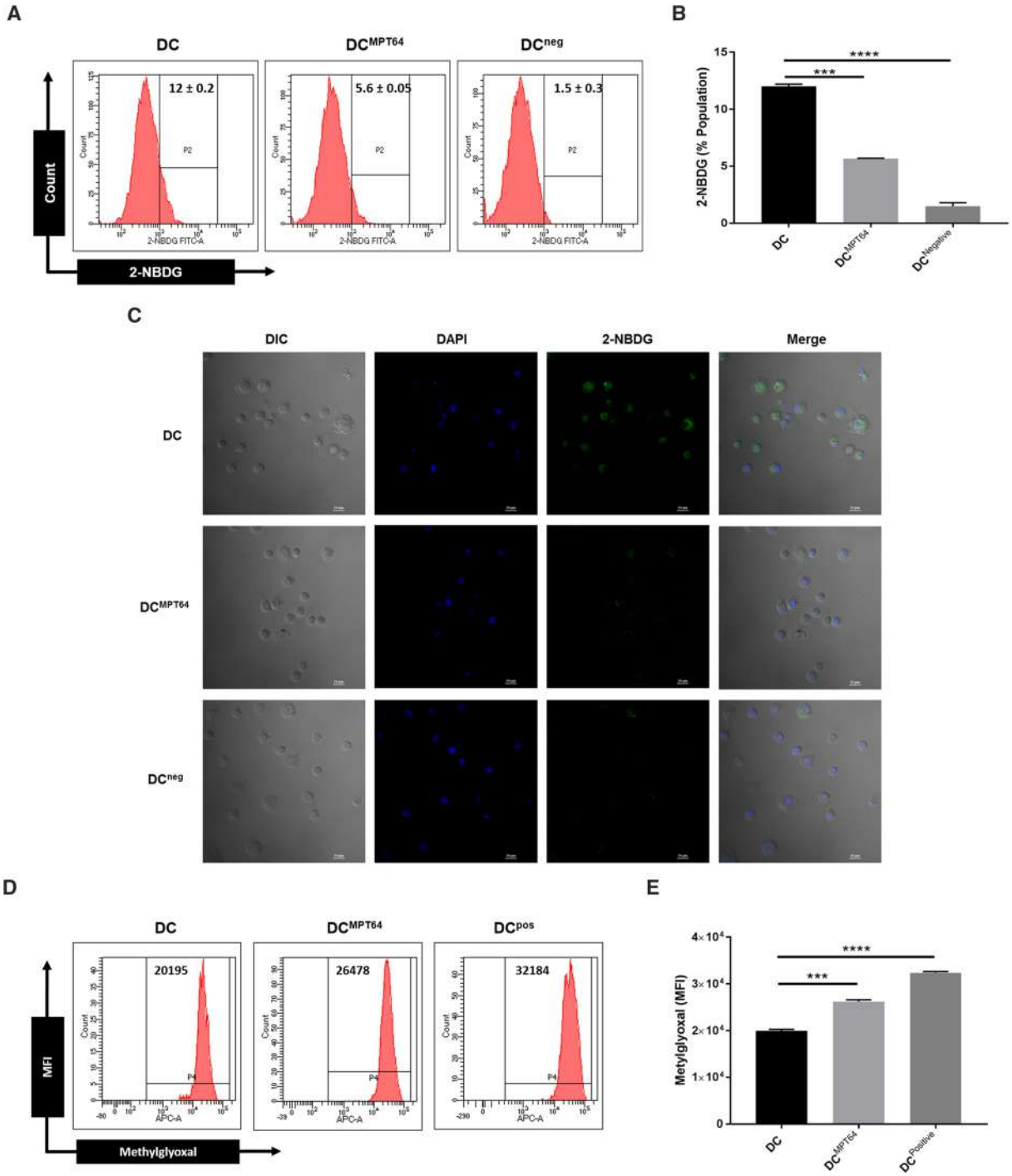

Fig. 9 Acquisition of dormant metabolic phenotype by DC^{MPT64} upon MPT64 exposure. DC^{MPT64} were metabolically characterized and studied for the **A**–**B** impairment of the uptake of glucose analogue 2-NBDG by flow cytometry. The histogram and bar diagrams show the percentage of positive cells (mean ± SEM). DCs cultured with glucose were taken as a negative control (DC^{neg}) ($n = 2$). **C** The decreased level of glucose uptake was monitored by confocal microscopy (scale bar: 10 µM, magnification: 60×). **D** The expression of methylglyoxal was examined by flow cytometry. H_2O_2-treated DCs (DC^{pos}) were taken as a positive control. Data are represented as histograms showing MFI and **E** bar diagrams ($n = 2$). **F** DC^{MPT64} were stained with anti-methylglyoxal Abs (red), along with DAPI (blue) to visualize the nucleus and phalloidin (green) for actin. The images were obtained through a confocal microscope (scale bar: 10 µm, magnification: 60×). The histogram (right side) depicts the intensity of methylglyoxal, actin and DAPI, as indicated by white arrows. **G**–**J** The expression of Glut1, Hk2, SSAO and GLO1 was monitored by RT-qPCR ($n = 3$). The data are representative of 2–3 independent experiments. $^{*}p < 0.05$, $^{**}p < 0.01$, $^{***}p < 0.001$, $^{****}p < 0.0001$

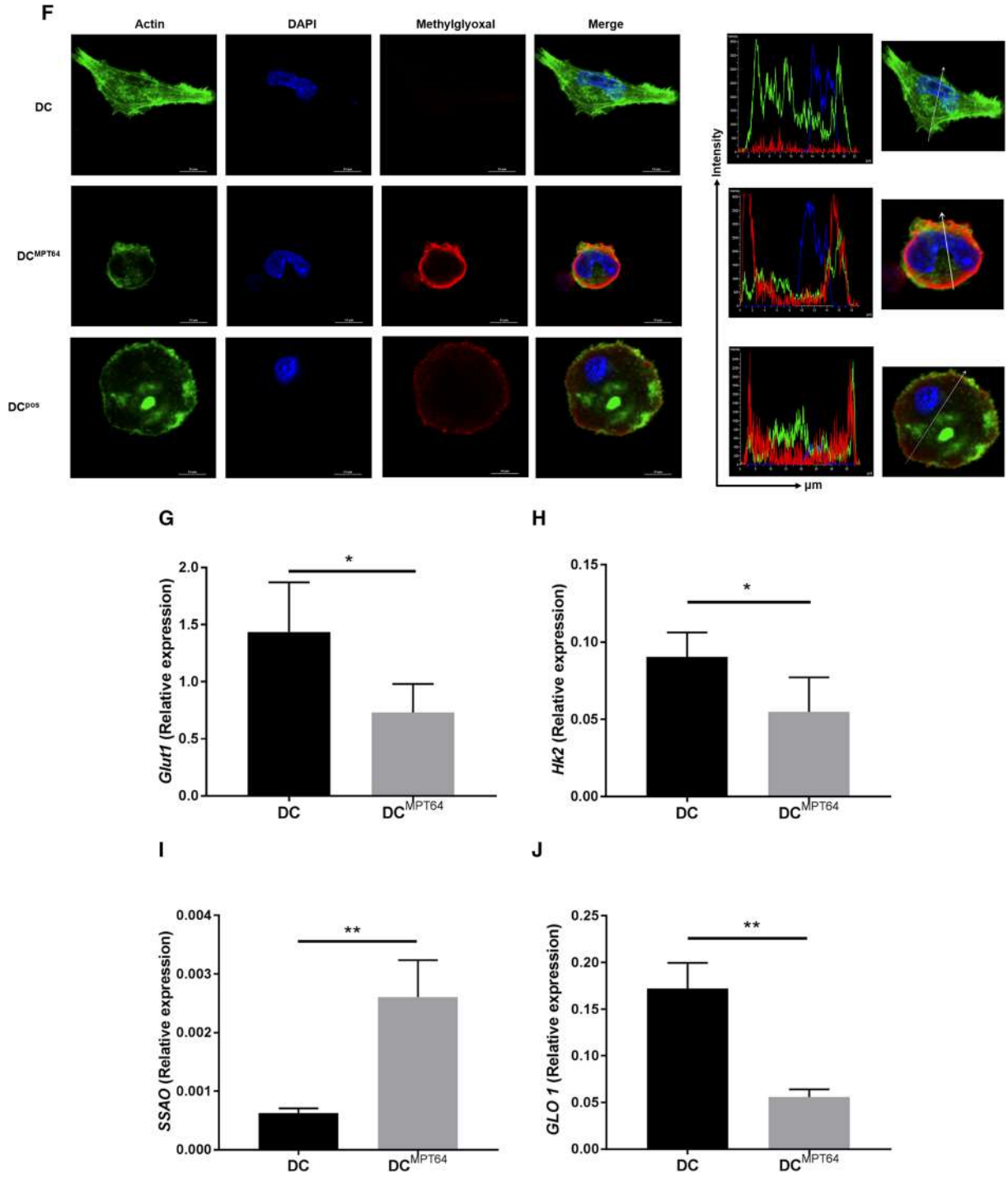

Fig. 9 (continued)

PD-L1^{hi}, CCR7^{lo}, IL-10^{hi}, TGF-β^{hi}, arginase^{hi} and IDO^{hi}. Furthermore, the inhibitory nature of DC^{MPT64} was further validated by the accumulation of lipids and MGO, reduced glucose (2-NBDG) uptake, weakened Glut1 and hexokinase 2 expressions and reduced ability to kill *Mtb*. DC^{MPT64} showed reduced expression of MHCII; hence, their antigen

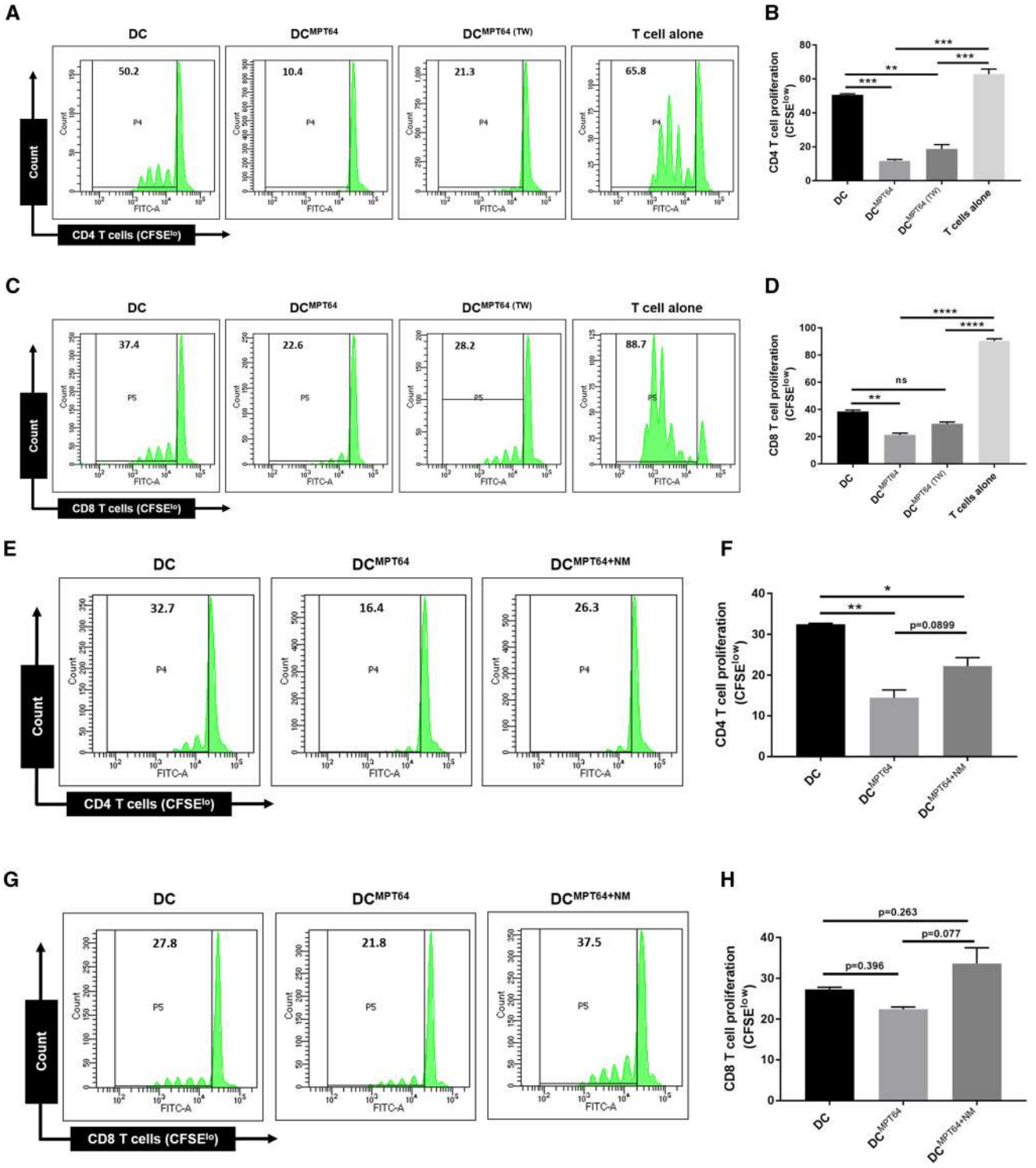

Fig. 10 MPT64-exposed DC^{MPT64} released NO and inhibited the proliferation of CD4 T cells and CD8 T cells. DC^{MPT64} and control DCs were co-cultured in 'regular' and 'trans-well' (TW) plates with CFSE-labelled and anti-CD3 and CD28 Abs stimulated naïve **A**, **B** CD4 T cells; **C**, **D** CD8 T cells. Similarly, DC^{MPT64} and control DCs were co-cultured with CFSE-labelled and anti-CD3 and CD28 Abs stimulated **E**, **F** CD4 T cells; **G**, **H** CD8 T cells in the presence or absence of iNOS inhibitor (NM). The cultures were set for 72 h and proliferation was demonstrated by flow cytometry ($n=2$). **F**, **H** The results (mean ± SEM) are also illustrated as a bar diagram of the percentage of CFSE^{lo} CD4 T cells and CD8 T cells. The SNs of the cultures were used to estimate **I** NO ($n=3$). The lysate of the cells was used to check the expression of **J** iNOS; **K** STAT-1 by Western blotting. The data are representative of 2–3 independent experiments. *$p<0.05$, **$p<0.01$, ***$p<0.001$, ****$p<0.0001$

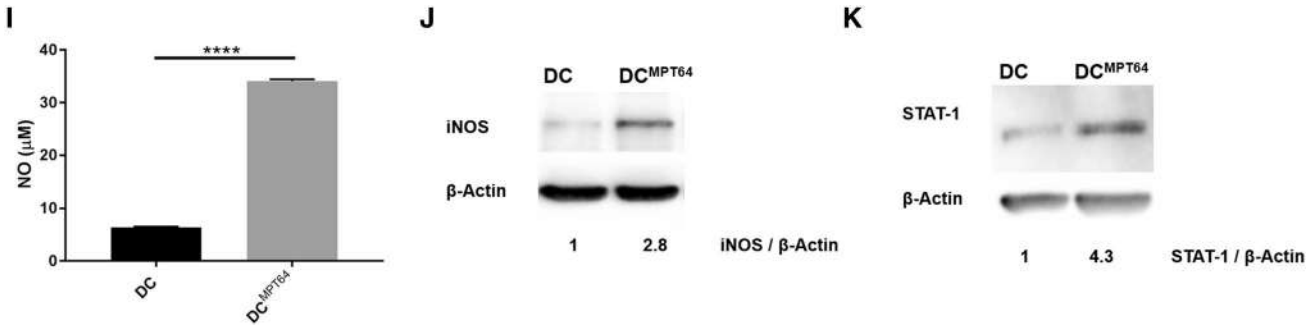

Fig. 10 (continued)

presentation capacity to T cells was compromised. *Mtb* has evolved a mechanism to modulate the MHC expression [55]. Inhibitory markers on DC^{MPT64} point towards their MDSCs-like function. The predominance of MDSCs is noticed in the TB granulomas, which promotes the survival of *Mtb* [93, 94]. Although, MDSCs role is well established in cancer but not yet in TB.

DC^{MPT64} showed upregulation of PD-$L1^{hi}$/TIM-3^{hi} and promoted Tregs development. The interaction of APCs with T cells through PD-L1-PD1 supports Tregs formation [95]. In TB patients, suppression of T cell proliferation is reported due to PD-$L1^{hi}$ on APCs [63]. MDSCs secrete anti-inflammatory cytokines, but pro-inflammatory cytokines to a lesser extent [96]. Likewise, DC^{MPT64} exhibited a high yield of IL-10 and TGF-β. DC^{MPT64} expressed a lower level of CCR7 chemokine that compromised their ability to migrate to lymphoid organs and prime T cells. The migration of DCs to the site of infection to capture antigens or lymph nodes to prime T cells depends on the level of expression of chemokines [97].

Lipids depot in the immune cells impairs their function but serves as an energy reservoir for *Mtb* survival [49]. MDSCs have high lipids content and inhibit the Th1 cell and Th17 cell activation [98]. Similarly, DC^{MPT64} showed high lipid content and inhibited Th1 cell and Th17 cell but stimulated Tregs. MDSCs prefer Tregs induction [99]. Tregs play a cardinal role in suppressing immunity. Further, lipid-rich DC^{MPT64} showed reduced capacity to phagocytose and kill intracellular mycobacteria and served as a protective niche for *Mtb* survival.

It may be important to delineate the metabolic activity of the cells during an infection. *Mtb* utilizes lipids as an energy source from the foamy macrophages [100]. Additionally, on shortage of carbon sources, it initiates glyoxylate shunt for its existence and metabolism of lipids [101]. In the case of MDSCs, the metabolic shift from glycolysis to fatty acid

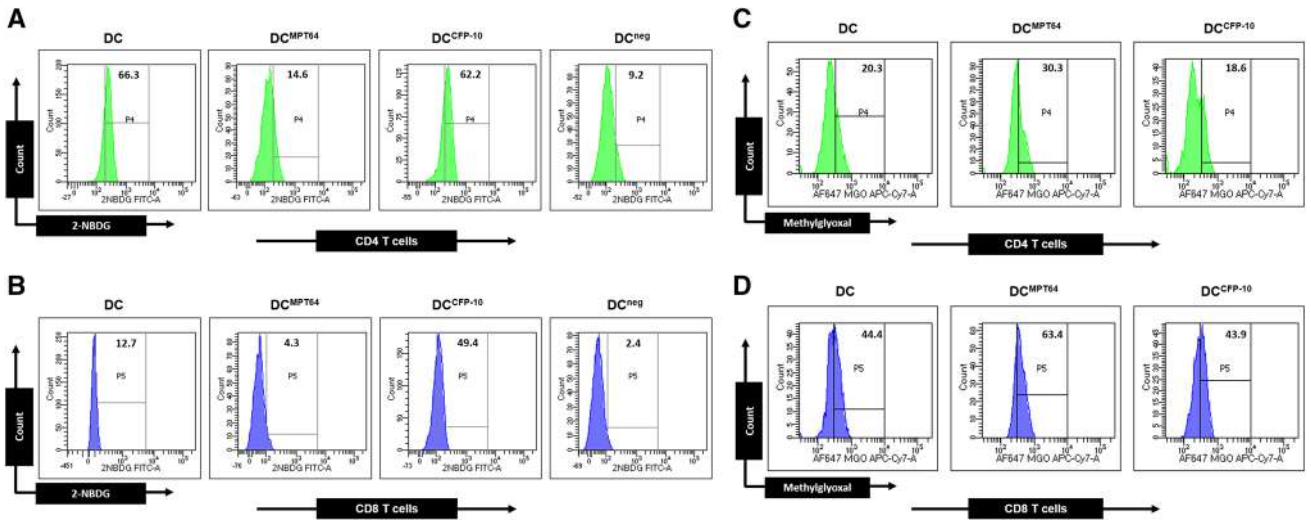

Fig. 11 DC^{MPT64} acquires a metabolically dormant phenotype. DC^{MPT64} and control DCs were co-cultured with the naïve **A**, **C** CD4 T cells; **B**, **D** CD8 T cells and assessed for the uptake of **A**–**B** glucose analogue (2-NBDG); **C**, **D** methylglyoxal through flow cytometry. Values in the inset of histograms refer to the percentage of positive cells for 2-NBDG and methylglyoxal uptake. DCs cultured in glucose conditioned media were used as a negative control (DC^{neg}) for glucose uptake assay. Data are representative of 2–3 independent experiments

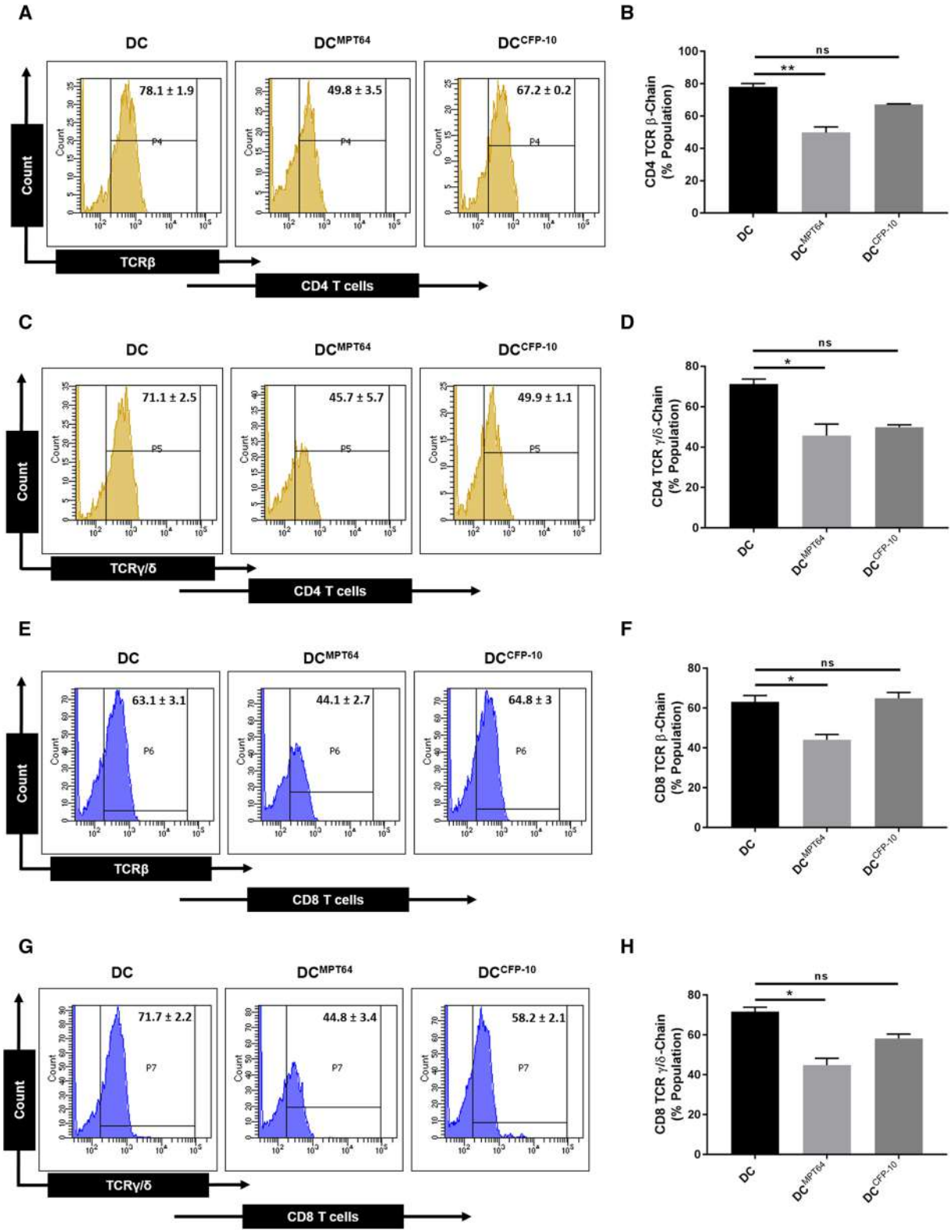

Fig. 12 MPT64-stimulated DC^{MPT64} downregulates the expression of T cells receptor and augments apoptosis of T cells. DC^{MPT64} and control DCs were cultured with the anti-CD3 and CD28 Abs-stimulated naïve **A**–**D** CD4 T cells; **E**–**H** CD8 T cells for 72 h. Later, the cells were analysed for the expression of **A**, **B** TCRβ; **C**, **D** TCRγ/δ chains on CD4 T cells; **E**, **F** TCRβ; **G**, **H** TCRγ/δ chain on CD8 T cells by flow cytometry. The data are expressed as histograms and bar diagrams. Likewise, **I**, **J** CD4 T cells; **K**, **L** CD8 T cells were monitored for apoptosis by staining with Annexin V through flow cytometry. Data (mean ± SEM) ($n = 2$) denoted as histograms and bar diagrams are the percentage of positive cells and representative of 2–3 independent experiments. *$p < 0.05$, **$p < 0.01$, ***$p < 0.001$, ****$p < 0.0001$, *ns* non-significant

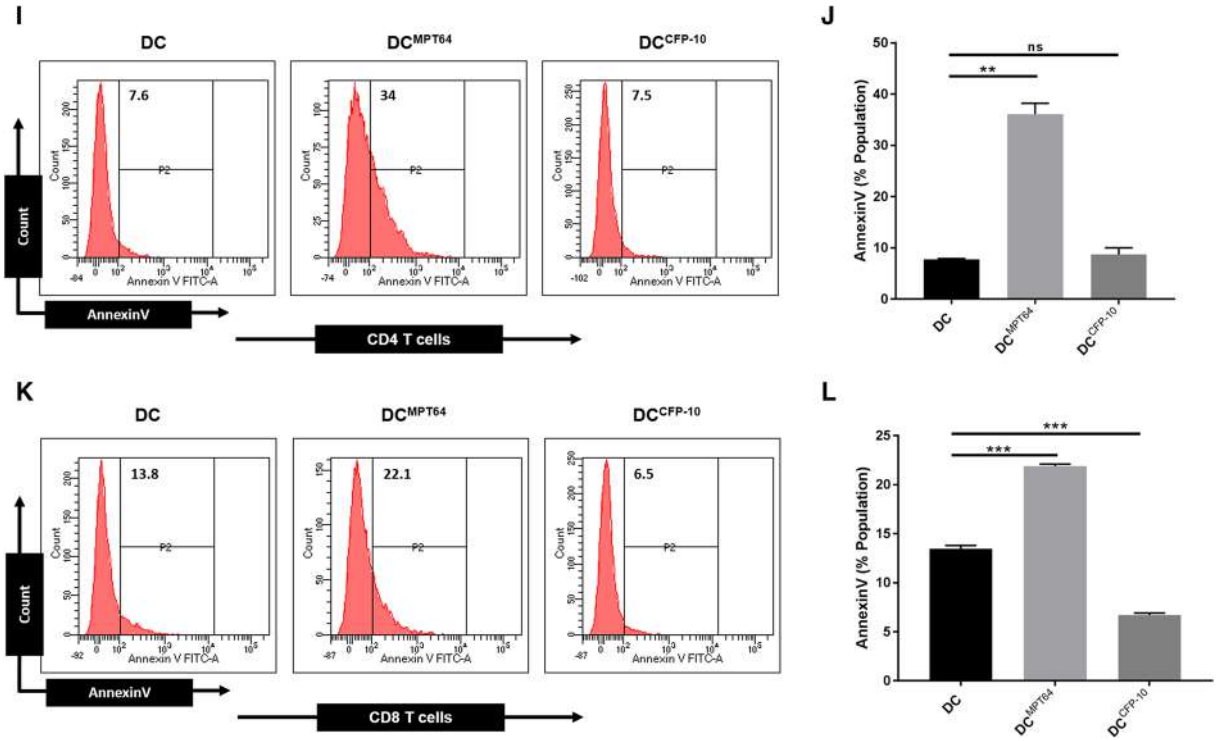

Fig. 12 (continued)

oxidation is known in the case of cancer [72]. Accumulation of methylglyoxal (MGO) imparts suppressive characteristics in MDSCs [27]. Generation of MGO occurs through glyceraldehyde3-phosphate and dihydroxyacetone phosphate during glycolysis and from acetone and aminoacetone by SSAO [76–78]. DC^{MPT64} showed reduced 2-NBDG uptake with impaired Glut1 and hexokinase 2 expression. A deposit of MGO in DC^{MPT64} was noted, which was unutilized due to a decline in glyoxalase 1 level. It showed a decrease in the glycolysis cycle and the generation of advanced glycation end products (MGO), from by-products of glycolysis and aminoacetone. The accumulation of MGO in DC^{MPT64} was further confirmed by flow cytometry and confocal microscopy. It may be inferred that *Mtb* may employ MPT64 to induce MGO for instilling suppressive characteristics in MDSCs.

Finally, we were curious to delineate the mechanism involved by DC^{MPT64} in executing the inhibitory activity. IDO is linked with tolerogenic DCs and Tregs induction by MDSCs [61]. Further, a higher level of NO/iNOS and arginase inhibits the T cell activation [102]. DC^{MPT64} which inhibited T cell proliferation showed augmented expression of NO/iNOS, IDO and arginase 1 and a decline in ROS and NF-κB. Enhanced expression of STAT-1 upregulates iNOS followed by NO secretion, and increased exhibition of STAT-3 stimulates the arginase 1 level, which utilizes L-arginine and generates urea and ornithine, confirming the specificity of our results. Further, induction of iNOS and arginase 1 leads to the generation of ONOO- and RNS that induces malfunctioning of TCR and inhibits T cell proliferation followed by apoptosis. Augmentation of IDO leads to consumption of tryptophan from the cell and surroundings, and therefore deprivation of amino acids in the cell and its microenvironment. Reduction in glucose uptake along with a decline in the expression of Glut1 and Hk2 leads to the formation of MGO, as supported by high levels of SSAO and low expression of GLO1. Augmentation in the secretion of IL-10 and TGF-β leads to Tregs differentiation and inhibition of Th1 cells and Th17 cells. Downregulation in pro-inflammatory response is marked by reduced expression of p65 NF-κB. Higher lipid accumulation works as a source of nutrition for *Mtb* survival in the M-MDSC, as demonstrated by higher the survival rate of *Mtb* [27, 103, 104] (Fig. 13).

DCs have an imperative role in the induction of immune response, but along with that their role in the generation of immune tolerance to self-antigens is also well established. Hence, DCs imparting immune tolerance has been characterized as tolerogenic DCs. Tolerogenic DCs can be well defined on the basis of high expression of co-inhibitory markers, like PD-L1/2, Mer tyrosine kinase, IL-10 and TGF-β [105, 106]. Low expression of co-stimulatory molecules (CD80, CD86, MHC II) and pro-inflammatory

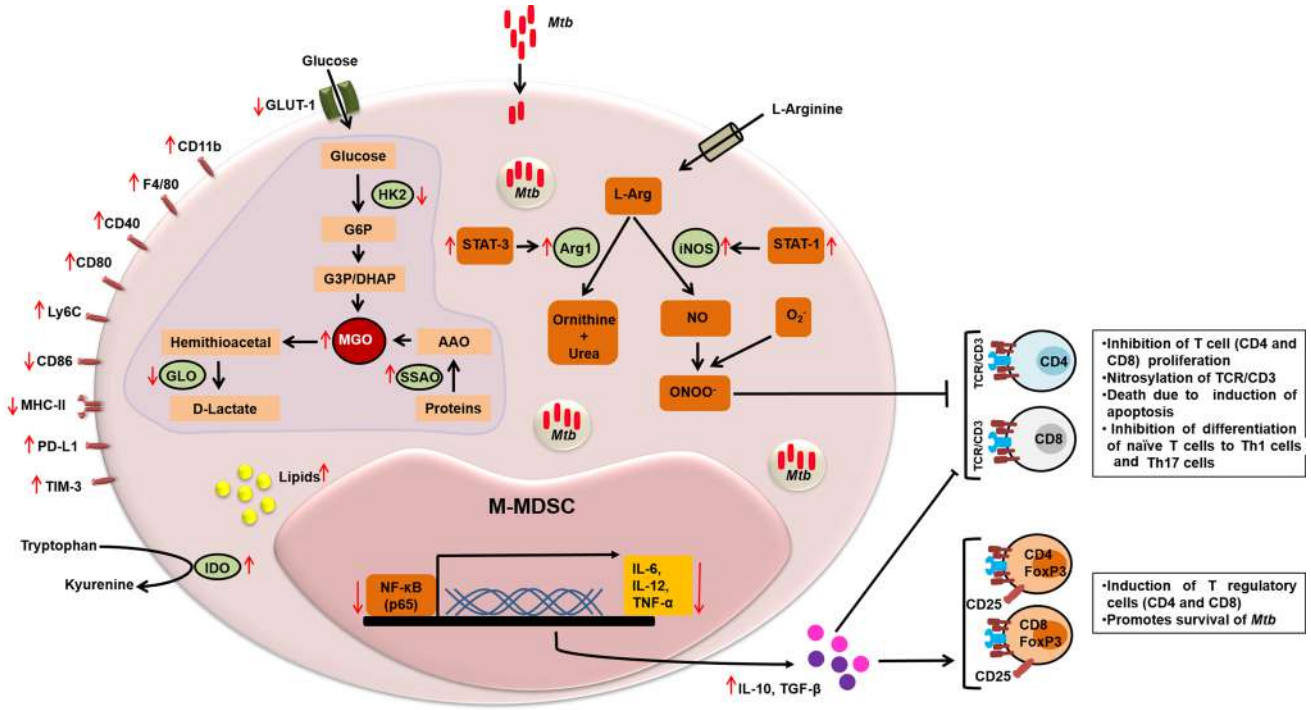

Fig. 13 Proposed mechanism of skewing BMCs towards M-MDSCs by MPT64 protein of *Mtb* under DCs differentiation conditions. Pre-exposure of BMCs to MPT64 under DC differentiating conditions (GM-CSF + IL-4) promotes the generation of M-MDSCs, as evidenced by the enhanced expression of CD11b, Ly6C, F4/80, CD40, CD80, PD-L1, TIM-3 and reduction in the expression of CD86 and MHC II. Enhanced expression of STAT-1 elicits the upregulation of iNOS followed by NO secretion; increased STAT-3 leads to arginase 1 that utilizes L-arginine and generates urea and ornithine. Induction of iNOS and arginase 1 leads to the generation of $ONOO^-$ and RNS that induces malfunctioning of TCR and inhibits T cell proliferation followed by apoptosis. Augmentation of IDO leads to the consumption of tryptophan from the cell and surroundings, and therefore deprivation of amino acids in the cell and its microenvironment. Reduction in glucose uptake along with a decline in the expression of Glut1 and Hk2 leads to the formation of MGO, as supported by high levels of SSAO and low expression of GLO1. Increased secretion of IL-10 and TGF-β leads to Tregs differentiation and inhibition of Th1 cells, Th2 cells and Th17 cells. Downregulation in pro-inflammatory response is marked by reduced expression of p65 NF-κB. Higher lipid accumulation works as a source of nutrition for *Mtb* survival in the M-MDSC, as demonstrated by the higher survival rate of *Mtb*

cytokines (TNF-α, IL-12 and IL-6) are exhibited by these cells [107]. Interestingly, MPT64 stimulation of differentiating DCs leads to the generation of M-MDSCs. These are also well-known immunosuppressive cells resembling tolerogenic DCs in terms of high expression of PD-L1, TIM-3, IL-10 and TGF-β. In contrast to tolerogenic DCs, MDSCs express Ly6C marker along with CD40 and CD80 molecules. These are not exhibited by tolerogenic DCs. Surprisingly, MDSCs do exhibit a high expression of arginase 1 and iNOS, due to which it depletes essential amino acids from the surrounding T cells and limits their proliferation [108, 109]. Hence, contrary to tolerogenic DCs, MDSCs have diverse immune suppressive machinery, which differentiates them from other suppressive immune cells.

In essence, this study for the first time decodes a novel mechanism of immune evasion adopted by *Mtb* through its MPT64 protein. This study suggests that MPT64 may be an excellent drug target to inhibit the persistence of *Mtb* in human cells.

Supplementary Information The online version contains supplementary material available at https://doi.org/10.1007/s00018-022-04596-5.

Acknowledgements SS received a fellowship from the Indian Council of Medical Research (ICMR); MA was the recipient of fellowships from the Department of Science and Technology (DST); SKM and HB were the recipients of fellowships from CSIR.

Author contributions JNA conceptualized the study. JNA, SS and SKM designed the experiments and analyzed data. SS, SKM, MA and HB performed experiments. SS, JNA and VB wrote the manuscript. AA cloned, expressed and purified the proteins. All the authors finally reviewed and approved the submitted manuscript.

Funding The work was supported through funding from the Council of Scientific and Industrial Research (CSIR), India.

Data availability All data generated or analyzed during this study are included in this article and its supplementary information file.

Additionally, data are available from the corresponding author upon reasonable request.

Declarations

Conflict of interest The authors have no relevant financial or non-financial interests to disclose.

Ethical approval The use of *Mtb* for this study was approved by the Biosafety committee of Institute of Microbial Technology (CSIR-IMTECH/IBSC/2018/31). All animal studies were approved by the Institutional Animal Ethics Committee (55/GO/Re/Rc/Bi/Bt/S/99/CPCSEA) and experiments were performed as per the approved protocols and guidelines issued by CPCSEA (Committee for the Purpose of Supervision of Experiments on Animals), Govt. of India.

References

1. Mehra A, Zahra A, Thompson V, Sirisaengtaksin N, Wells A, Porto M et al (2013) Mycobacterium tuberculosis type VII secreted effector EsxH targets host ESCRT to impair trafficking. PLoS Pathog 9(10):e1003734. https://doi.org/10.1371/journal.ppat.1003734
2. Lerner TR, Borel S, Gutierrez MG (2015) The innate immune response in human tuberculosis. Cell Microbiol 17(9):1277–1285. https://doi.org/10.1111/cmi.12480
3. Queval CJ, Brosch R, Simeone R (2017) The macrophage: a disputed fortress in the battle against *Mycobacterium tuberculosis*. Front Microbiol 8:2284. https://doi.org/10.3389/fmicb.2017.02284
4. Wang Z, Jiang H, Chen S, Du F, Wang X (2012) The mitochondrial phosphatase PGAM5 functions at the convergence point of multiple necrotic death pathways. Cell 148(1–2):228–243. https://doi.org/10.1016/j.cell.2011.11.030
5. Cambier CJ, Falkow S, Ramakrishnan L (2014) Host evasion and exploitation schemes of *Mycobacterium tuberculosis*. Cell 159(7):1497–1509. https://doi.org/10.1016/j.cell.2014.11.024
6. Harding CV, Boom WH (2010) Regulation of antigen presentation by *Mycobacterium tuberculosis*: a role for toll-like receptors. Nat Rev Microbiol 8(4):296–307. https://doi.org/10.1038/nrmicro2321
7. Velmurugan K, Chen B, Miller JL, Azogue S, Gurses S, Hsu T et al (2007) Mycobacterium tuberculosis nuoG is a virulence gene that inhibits apoptosis of infected host cells. PLoS Pathog 3(7):e110. https://doi.org/10.1371/journal.ppat.0030110
8. Ouimet M, Koster S, Sakowski E, Ramkhelawon B, van Solingen C, Oldebeken S et al (2016) Mycobacterium tuberculosis induces the miR-33 locus to reprogram autophagy and host lipid metabolism. Nat Immunol 17(6):677–686. https://doi.org/10.1038/ni.3434
9. Mayer-Barber KD, Andrade BB, Barber DL, Hieny S, Feng CG, Caspar P et al (2011) Innate and adaptive interferons suppress IL-1alpha and IL-1beta production by distinct pulmonary myeloid subsets during *Mycobacterium tuberculosis* infection. Immunity 35(6):1023–1034. https://doi.org/10.1016/j.immuni.2011.12.002
10. Zhai W, Wu F, Zhang Y, Fu Y, Liu Z (2019) The immune escape mechanisms of *Mycobacterium tuberculosis*. Int J Mol Sci 20(2):340. https://doi.org/10.3390/ijms20020340
11. Ernst JD (2018) Mechanisms of *M. tuberculosis* immune evasion as challenges to TB vaccine design. Cell Host Microbe 24(1):34–42. https://doi.org/10.1016/j.chom.2018.06.004
12. Siddiqui KF, Amir M, Gurram RK, Khan N, Arora A, Rajagopal K et al (2014) Latency-associated protein Acr1 impairs dendritic cell maturation and functionality: a possible mechanism of immune evasion by *Mycobacterium tuberculosis*. J Infect Dis 209(9):1436–1445. https://doi.org/10.1093/infdis/jit595
13. Amir M, Aqdas M, Nadeem S, Siddiqui KF, Khan N, Sheikh JA et al (2017) Diametric role of the latency-associated protein acr1 of *Mycobacterium tuberculosis* in modulating the functionality of pre- and post-maturational stages of dendritic cells. Front Immunol 8:624. https://doi.org/10.3389/fimmu.2017.00624
14. Dulphy N, Herrmann JL, Nigou J, Rea D, Boissel N, Puzo G et al (2007) Intermediate maturation of *Mycobacterium tuberculosis* LAM-activated human dendritic cells. Cell Microbiol 9(6):1412–1425. https://doi.org/10.1111/j.1462-5822.2006.00881.x
15. Gehring AJ, Dobos KM, Belisle JT, Harding CV, Boom WH (2004) *Mycobacterium tuberculosis* LprG (Rv1411c): a novel TLR-2 ligand that inhibits human macrophage class II MHC antigen processing. J Immunol 173(4):2660–2668. https://doi.org/10.4049/jimmunol.173.4.2660
16. Noss EH, Pai RK, Sellati TJ, Radolf JD, Belisle J, Golenbock DT et al (2001) Toll-like receptor 2-dependent inhibition of macrophage class II MHC expression and antigen processing by 19-kDa lipoprotein of *Mycobacterium tuberculosis*. J Immunol 167(2):910–918. https://doi.org/10.4049/jimmunol.167.2.910
17. Pecora ND, Gehring AJ, Canaday DH, Boom WH, Harding CV (2006) *Mycobacterium tuberculosis* LprA is a lipoprotein agonist of TLR2 that regulates innate immunity and APC function. J Immunol 177(1):422–429. https://doi.org/10.4049/jimmunol.177.1.422
18. Sinha A, Singh A, Satchidanandam V, Natarajan K (2006) Impaired generation of reactive oxygen species during differentiation of dendritic cells (DCs) by *Mycobacterium tuberculosis* secretory antigen (MTSA) and subsequent activation of MTSA-DCs by mycobacteria results in increased intracellular survival. J Immunol 177(1):468–478. https://doi.org/10.4049/jimmunol.177.1.468
19. Simeone R, Bobard A, Lippmann J, Bitter W, Majlessi L, Brosch R et al (2012) Phagosomal rupture by *Mycobacterium tuberculosis* results in toxicity and host cell death. PLoS Pathog 8(2):e1002507. https://doi.org/10.1371/journal.ppat.1002507
20. Wong D, Bach H, Sun J, Hmama Z, Av-Gay Y (2011) *Mycobacterium tuberculosis* protein tyrosine phosphatase (PtpA) excludes host vacuolar-H+-ATPase to inhibit phagosome acidification. Proc Natl Acad Sci USA 108(48):19371–19376. https://doi.org/10.1073/pnas.1109201108
21. Miller JL, Velmurugan K, Cowan MJ, Briken V (2010) The type I NADH dehydrogenase of *Mycobacterium tuberculosis* counters phagosomal NOX2 activity to inhibit TNF-alpha-mediated host cell apoptosis. PLoS Pathog 6(4):e1000864. https://doi.org/10.1371/journal.ppat.1000864
22. Sun J, Singh V, Lau A, Stokes RW, Obregon-Henao A, Orme IM et al (2013) *Mycobacterium tuberculosis* nucleoside diphosphate kinase inactivates small GTPases leading to evasion of innate immunity. PLoS Pathog 9(7):e1003499. https://doi.org/10.1371/journal.ppat.1003499
23. Jayakumar D, Jacobs WR Jr, Narayanan S (2008) Protein kinase E of *Mycobacterium tuberculosis* has a role in the nitric oxide stress response and apoptosis in a human macrophage model of infection. Cell Microbiol 10(2):365–374. https://doi.org/10.1111/j.1462-5822.2007.01049.x
24. Ribechini E, Eckert I, Beilhack A, Du Plessis N, Walzl G, Schleicher U et al (2019) Heat-killed *Mycobacterium tuberculosis* prime-boost vaccination induces myeloid-derived suppressor cells with spleen dendritic cell-killing capability. JCI Insight. https://doi.org/10.1172/jci.insight.128664
25. El Daker S, Sacchi A, Tempestilli M, Carducci C, Goletti D, Vanini V et al (2015) Granulocytic myeloid derived suppressor cells expansion during active pulmonary tuberculosis is

associated with high nitric oxide plasma level. PLoS ONE 10(4):e0123772. https://doi.org/10.1371/journal.pone.0123772
26. Knaul JK, Jorg S, Oberbeck-Mueller D, Heinemann E, Scheuermann L, Brinkmann V et al (2014) Lung-residing myeloid-derived suppressors display dual functionality in murine pulmonary tuberculosis. Am J Respir Crit Care Med 190(9):1053–1066. https://doi.org/10.1164/rccm.201405-0828OC
27. Baumann T, Dunkel A, Schmid C, Schmitt S, Hiltensperger M, Lohr K et al (2020) Regulatory myeloid cells paralyze T cells through cell-cell transfer of the metabolite methylglyoxal. Nat Immunol 21(5):555–566. https://doi.org/10.1038/s41590-020-0666-9
28. Yang B, Wang X, Jiang J, Zhai F, Cheng X (2014) Identification of CD244-expressing myeloid-derived suppressor cells in patients with active tuberculosis. Immunol Lett 158(1–2):66–72. https://doi.org/10.1016/j.imlet.2013.12.003
29. Wang Z, Potter BM, Gray AM, Sacksteder KA, Geisbrecht BV, Laity JH (2007) The solution structure of antigen MPT64 from *Mycobacterium tuberculosis* defines a new family of beta-grasp proteins. J Mol Biol 366(2):375–381. https://doi.org/10.1016/j.jmb.2006.11.039
30. Sehnal D, Bittrich S, Deshpande M, Svobodova R, Berka K, Bazgier V et al (2021) Mol* viewer: modern web app for 3D visualization and analysis of large biomolecular structures. Nucleic Acids Res 49(W1):W431–W437. https://doi.org/10.1093/nar/gkab314
31. Mehaffy C, Dobos KM, Nahid P, Kruh-Garcia NA (2017) Second generation multiple reaction monitoring assays for enhanced detection of ultra-low abundance *Mycobacterium tuberculosis* peptides in human serum. Clin Proteom 14:21. https://doi.org/10.1186/s12014-017-9156-y
32. Fan Q, Lu M, Xia ZY, Bao L (2013) *Mycobacterium tuberculosis* MPT64 stimulates the activation of murine macrophage modulated by IFN-gamma. Eur Rev Med Pharmacol Sci 17(24):3296–3305
33. Wang Q, Liu S, Tang Y, Liu Q, Yao Y (2014) MPT64 protein from *Mycobacterium tuberculosis* inhibits apoptosis of macrophages through NF-kB-miRNA21-Bcl-2 pathway. PLoS ONE 9(7):e100949. https://doi.org/10.1371/journal.pone.0100949
34. Stamm CE, Pasko BL, Chaisavaneeyakorn S, Franco LH, Nair VR, Weigele BA et al (2019) Screening *Mycobacterium tuberculosis* secreted proteins identifies mpt64 as a eukaryotic membrane-binding bacterial effector. mSphere. https://doi.org/10.1128/mSphere.00354-19
35. Lutz MB, Kukutsch N, Ogilvie AL, Rossner S, Koch F, Romani N et al (1999) An advanced culture method for generating large quantities of highly pure dendritic cells from mouse bone marrow. J Immunol Methods 223(1):77–92. https://doi.org/10.1016/s0022-1759(98)00204-x
36. Corraliza IM, Campo ML, Soler G, Modolell M (1994) Determination of arginase activity in macrophages: a micromethod. J Immunol Methods 174(1–2):231–235. https://doi.org/10.1016/0022-1759(94)90027-2
37. Cowburn AS, Crosby A, Macias D, Branco C, Colaco RD, Southwood M et al (2016) HIF2alpha-arginase axis is essential for the development of pulmonary hypertension. Proc Natl Acad Sci USA 113(31):8801–8806. https://doi.org/10.1073/pnas.1602978113
38. Wolf AJ, Linas B, Trevejo-Nunez GJ, Kincaid E, Tamura T, Takatsu K et al (2007) *Mycobacterium tuberculosis* infects dendritic cells with high frequency and impairs their function in vivo. J Immunol 179(4):2509–2519. https://doi.org/10.4049/jimmunol.179.4.2509
39. Popov A, Schultze JL (2008) IDO-expressing regulatory dendritic cells in cancer and chronic infection. J Mol Med (Berl) 86(2):145–160. https://doi.org/10.1007/s00109-007-0262-6
40. Sumpter TL, Thomson AW (2011) The STATus of PD-L1 (B7–H1) on tolerogenic APCs. Eur J Immunol 41(2):286–290. https://doi.org/10.1002/eji.201041353
41. Meher AK, Bal NC, Chary KV, Arora A (2006) *Mycobacterium tuberculosis* H37Rv ESAT-6-CFP-10 complex formation confers thermodynamic and biochemical stability. FEBS J 273(7):1445–1462. https://doi.org/10.1111/j.1742-4658.2006.05166.x
42. Zhu J, Yamane H, Paul WE (2010) Differentiation of effector CD4 T cell populations (*). Annu Rev Immunol 28:445–489. https://doi.org/10.1146/annurev-immunol-030409-101212
43. Redford PS, Murray PJ, O'Garra A (2011) The role of IL-10 in immune regulation during *M. tuberculosis* infection. Mucosal Immunol 4(3):261–270. https://doi.org/10.1038/mi.2011.7
44. Domingo-Gonzalez R, Prince O, Cooper A, Khader SA (2016) Cytokines and Chemokines in *Mycobacterium tuberculosis* Infection. Microbiol Spectr. https://doi.org/10.1128/microbiolspec.TBTB2-0018-2016
45. Prendergast KA, Kirman JR (2013) Dendritic cell subsets in mycobacterial infection: control of bacterial growth and T cell responses. Tuberculosis (Edinb) 93(2):115–122. https://doi.org/10.1016/j.tube.2012.10.008
46. Banchereau J, Steinman RM (1998) Dendritic cells and the control of immunity. Nature 392(6673):245–252. https://doi.org/10.1038/32588
47. Swetman CA, Leverrier Y, Garg R, Gan CH, Ridley AJ, Katz DR et al (2002) Extension, retraction and contraction in the formation of a dendritic cell dendrite: distinct roles for Rho GTPases. Eur J Immunol 32(7):2074–2083. https://doi.org/10.1002/1521-4141(200207)32:7%3c2074::AID-IMMU2074%3e3.0.CO;2-S
48. van Vliet SJ, den Dunnen J, Gringhuis SI, Geijtenbeek TB, van Kooyk Y (2007) Innate signaling and regulation of dendritic cell immunity. Curr Opin Immunol 19(4):435–440. https://doi.org/10.1016/j.coi.2007.05.006
49. Daniel J, Maamar H, Deb C, Sirakova TD, Kolattukudy PE (2011) *Mycobacterium tuberculosis* uses host triacylglycerol to accumulate lipid droplets and acquires a dormancy-like phenotype in lipid-loaded macrophages. PLoS Pathog 7(6):e1002093. https://doi.org/10.1371/journal.ppat.1002093
50. Hossain F, Al-Khami AA, Wyczechowska D, Hernandez C, Zheng L, Reiss K et al (2015) Inhibition of fatty acid oxidation modulates immunosuppressive functions of myeloid-derived suppressor cells and enhances cancer therapies. Cancer Immunol Res 3(11):1236–1247. https://doi.org/10.1158/2326-6066.CIR-15-0036
51. Herber DL, Cao W, Nefedova Y, Novitskiy SV, Nagaraj S, Tyurin VA et al (2010) Lipid accumulation and dendritic cell dysfunction in cancer. Nat Med 16(8):880–886. https://doi.org/10.1038/nm.2172
52. Saban DR (2014) The chemokine receptor CCR7 expressed by dendritic cells: a key player in corneal and ocular surface inflammation. Ocul Surf 12(2):87–99. https://doi.org/10.1016/j.jtos.2013.10.007
53. Lenschow DJ, Walunas TL, Bluestone JA (1996) CD28/B7 system of T cell costimulation. Annu Rev Immunol 14:233–258. https://doi.org/10.1146/annurev.immunol.14.1.233
54. Hongo D, Tang X, Baker J, Engleman EG, Strober S (2014) Requirement for interactions of natural killer T cells and myeloid-derived suppressor cells for transplantation tolerance. Am J Transplant 14(11):2467–2477. https://doi.org/10.1111/ajt.12914
55. Cooper AM (2009) Cell-mediated immune responses in tuberculosis. Annu Rev Immunol 27:393–422. https://doi.org/10.1146/annurev.immunol.021908.132703

56. Lyadova IV, Panteleev AV (2015) Th1 and Th17 cells in tuberculosis: protection, pathology, and biomarkers. Mediat Inflamm 2015:854507. https://doi.org/10.1155/2015/854507
57. Cardona P, Cardona PJ (2019) Regulatory T cells in *Mycobacterium tuberculosis* Infection. Front Immunol 10:2139. https://doi.org/10.3389/fimmu.2019.02139
58. McLaughlin TA, Khayumbi J, Ongalo J, Tonui J, Campbell A, Allana S et al (2020) CD4 T cells in *Mycobacterium tuberculosis* and *Schistosoma mansoni* co-infected individuals maintain functional TH1 responses. Front Immunol 11:127. https://doi.org/10.3389/fimmu.2020.00127
59. Shklovskaya E, de St F, Groth B (2007) Balancing tolerance and immunity: the role of dendritic cell and T cell subsets. Methods Mol Biol 380:25–46. https://doi.org/10.1007/978-1-59745-395-0_2
60. Alderton GK (2012) Tumour immunology: TIM3 suppresses antitumour DCs. Nat Rev Immunol 12(9):620–621. https://doi.org/10.1038/nri3288
61. Zoso A, Mazza EM, Bicciato S, Mandruzzato S, Bronte V, Serafini P et al (2014) Human fibrocytic myeloid-derived suppressor cells express IDO and promote tolerance via Treg-cell expansion. Eur J Immunol 44(11):3307–3319. https://doi.org/10.1002/eji.201444522
62. Ahn D, Penaloza H, Wang Z, Wickersham M, Parker D, Patel P et al (2016) Acquired resistance to innate immune clearance promotes Klebsiella pneumoniae ST258 pulmonary infection. JCI Insight 1(17):e89704. https://doi.org/10.1172/jci.insight.89704
63. Agrawal N, Streata I, Pei G, Weiner J, Kotze L, Bandermann S et al (2018) Human monocytic suppressive cells promote replication of *Mycobacterium tuberculosis* and alter stability of in vitro generated granulomas. Front Immunol 9:2417. https://doi.org/10.3389/fimmu.2018.02417
64. Davids M, Pooran A, Smith L, Tomasicchio M, Dheda K (2021) The Frequency and effect of granulocytic myeloid-derived suppressor cells on mycobacterial survival in patients with tuberculosis: a preliminary report. Front Immunol 12:676679. https://doi.org/10.3389/fimmu.2021.676679
65. Vasquez-Dunddel D, Pan F, Zeng Q, Gorbounov M, Albesiano E, Fu J et al (2013) STAT3 regulates arginase-I in myeloid-derived suppressor cells from cancer patients. J Clin Invest 123(4):1580–1589. https://doi.org/10.1172/JCI60083
66. Grzywa TM, Sosnowska A, Matryba P, Rydzynska Z, Jasinski M, Nowis D et al (2020) Myeloid cell-derived arginase in cancer immune response. Front Immunol 11:938. https://doi.org/10.3389/fimmu.2020.00938
67. Kumar V, Patel S, Tcyganov E, Gabrilovich DI (2016) The nature of myeloid-derived suppressor cells in the tumor microenvironment. Trends Immunol 37(3):208–220. https://doi.org/10.1016/j.it.2016.01.004
68. Platten M, Wick W, Van den Eynde BJ (2012) Tryptophan catabolism in cancer: beyond IDO and tryptophan depletion. Cancer Res 72(21):5435–5440. https://doi.org/10.1158/0008-5472.CAN-12-0569
69. Fleming V, Hu X, Weber R, Nagibin V, Groth C, Altevogt P et al (2018) Targeting myeloid-derived suppressor cells to bypass tumor-induced immunosuppression. Front Immunol 9:398. https://doi.org/10.3389/fimmu.2018.00398
70. Montorsi W, Annoni F, Doldi SB, Germiniani R, Longoni F (1975) Letter: plasma concentration of zinc and copper after intestinal shunt. Nouv Presse Med 23:1734
71. Spitzer MH, Carmi Y, Reticker-Flynn NE, Kwek SS, Madhireddy D, Martins MM et al (2017) Systemic immunity is required for effective cancer immunotherapy. Cell 168(3):487–502.e415. https://doi.org/10.1016/j.cell.2016.12.022
72. Al-Khami AA, Rodriguez PC, Ochoa AC (2016) Metabolic reprogramming of myeloid-derived suppressor cells (MDSC) in cancer. Oncoimmunology 5(8):e1200771. https://doi.org/10.1080/2162402X.2016.1200771
73. O'Neill LA, Pearce EJ (2016) Immunometabolism governs dendritic cell and macrophage function. J Exp Med 213(1):15–23. https://doi.org/10.1084/jem.20151570
74. Ganeshan K, Chawla A (2014) Metabolic regulation of immune responses. Annu Rev Immunol 32:609–634. https://doi.org/10.1146/annurev-immunol-032713-120236
75. Rabbani N, Thornalley PJ (2008) The dicarbonyl proteome: proteins susceptible to dicarbonyl glycation at functional sites in health, aging, and disease. Ann NY Acad Sci 1126:124–127. https://doi.org/10.1196/annals.1433.043
76. Phillips SA, Thornalley PJ (1993) The formation of methylglyoxal from triose phosphates. Investigation using a specific assay for methylglyoxal. Eur J Biochem 212(1):101–105. https://doi.org/10.1111/j.1432-1033.1993.tb17638.x
77. Ray S, Ray M (1983) Formation of methylglyoxal from aminoacetone by amine oxidase from goat plasma. J Biol Chem 258(6):3461–3462
78. Lyles GA, Chalmers J (1992) The metabolism of aminoacetone to methylglyoxal by semicarbazide-sensitive amine oxidase in human umbilical artery. Biochem Pharmacol 43(7):1409–1414. https://doi.org/10.1016/0006-2952(92)90196-p
79. Hardy LL, Wick DA, Webb JR (2008) Conversion of tyrosine to the inflammation-associated analog 3'-nitrotyrosine at either TCR- or MHC-contact positions can profoundly affect recognition of the MHC class I-restricted epitope of lymphocytic choriomeningitis virus glycoprotein 33 by CD8 T cells. J Immunol 180(9):5956–5962. https://doi.org/10.4049/jimmunol.180.9.5956
80. Pearce EL, Pearce EJ (2013) Metabolic pathways in immune cell activation and quiescence. Immunity 38(4):633–643. https://doi.org/10.1016/j.immuni.2013.04.005
81. Nagaraj S, Gupta K, Pisarev V, Kinarsky L, Sherman S, Kang L et al (2007) Altered recognition of antigen is a mechanism of CD8+ T cell tolerance in cancer. Nat Med 13(7):828–835. https://doi.org/10.1038/nm1609
82. Mannick JB, Hausladen A, Liu L, Hess DT, Zeng M, Miao QX et al (1999) Fas-induced caspase denitrosylation. Science 284(5414):651–654. https://doi.org/10.1126/science.284.5414.651
83. Zaman K (2010) Tuberculosis: a global health problem. J Health Popul Nutr 28(2):111–113. https://doi.org/10.3329/jhpn.v28i2.4879
84. Collins FM (1997) Tuberculosis research in a cold climate. Tuber Lung Dis 78(2):99–107. https://doi.org/10.1016/s0962-8479(98)80002-6
85. Cohen SB, Gern BH, Delahaye JL, Adams KN, Plumlee CR, Winkler JK et al (2018) Alveolar macrophages provide an early *Mycobacterium tuberculosis* niche and initiate dissemination. Cell Host Microbe 24(3):439–446.e434. https://doi.org/10.1016/j.chom.2018.08.001
86. Aqdas M, Singh S, Amir M, Maurya SK, Pahari S, Agrewala JN (2021) Cumulative signaling through NOD-2 and TLR-4 eliminates the *Mycobacterium tuberculosis* concealed inside the mesenchymal stem cells. Front Cell Infect Microbiol 11:669168. https://doi.org/10.3389/fcimb.2021.669168
87. Jiang Y, Liu H, Wang H, Dou X, Zhao X, Bai Y et al (2013) Polymorphism of antigen MPT64 in *Mycobacterium tuberculosis* strains. J Clin Microbiol 51(5):1558–1562. https://doi.org/10.1128/JCM.02955-12
88. Malen H, Berven FS, Fladmark KE, Wiker HG (2007) Comprehensive analysis of exported proteins from *Mycobacterium*

tuberculosis H37Rv. Proteomics 7(10):1702–1718. https://doi.org/10.1002/pmic.200600853
89. Gaillard T, Fabre M, Martinaud C, Vong R, Brisou P, Soler C (2011) Assessment of the SD Bioline Ag MPT64 Rapid and the MGIT TBc identification tests for the diagnosis of tuberculosis. Diagn Microbiol Infect Dis 70(1):154–156. https://doi.org/10.1016/j.diagmicrobio.2010.12.011
90. Baba K, Dyrhol-Riise AM, Sviland L, Langeland N, Hoosen AA, Wiker HG et al (2008) Rapid and specific diagnosis of tuberculous pleuritis with immunohistochemistry by detecting *Mycobacterium tuberculosis* complex specific antigen MPT64 in patients from a HIV endemic area. Appl Immunohistochem Mol Morphol 16(6):554–561. https://doi.org/10.1097/PAI.0b013e31816c3f79
91. Latchumanan VK, Singh B, Sharma P, Natarajan K (2002) Mycobacterium tuberculosis antigens induce the differentiation of dendritic cells from bone marrow. J Immunol 169(12):6856–6864. https://doi.org/10.4049/jimmunol.169.12.6856
92. Mustafa T, Wiker HG, Morkve O, Sviland L (2008) Differential expression of mycobacterial antigen MPT64, apoptosis and inflammatory markers in multinucleated giant cells and epithelioid cells in granulomas caused by *Mycobacterium tuberculosis*. Virchows Arch 452(4):449–456. https://doi.org/10.1007/s00428-008-0575-z
93. Kato K, Yamamoto K (1982) Suppression of BCG cell wall-induced delayed-type hypersensitivity by BCG pre-treatment. II. Induction of suppressor T cells by heat-killed BCG injection. Immunology 45(4):655–661
94. Bennett JA, Rao VS, Mitchell MS (1978) Systemic bacillus Calmette-Guerin (BCG) activates natural suppressor cells. Proc Natl Acad Sci USA 75(10):5142–5144. https://doi.org/10.1073/pnas.75.10.5142
95. Hassan SS, Akram M, King EC, Dockrell HM, Cliff JM (2015) PD-1, PD-L1 and PD-L2 gene expression on T-cells and natural killer cells declines in conjunction with a reduction in PD-1 protein during the intensive phase of tuberculosis treatment. PLoS ONE 10(9):e0137646. https://doi.org/10.1371/journal.pone.0137646
96. Haist M, Stege H, Grabbe S, Bros M (2021) The functional crosstalk between myeloid-derived suppressor cells and regulatory T cells within the immunosuppressive tumor microenvironment. Cancers (Basel) 13(2):210. https://doi.org/10.3390/cancers13020210
97. Liu J, Zhang X, Cheng Y, Cao X (2021) Dendritic cell migration in inflammation and immunity. Cell Mol Immunol 18(11):2461–2471. https://doi.org/10.1038/s41423-021-00726-4
98. Knight M, Braverman J, Asfaha K, Gronert K, Stanley S (2018) Lipid droplet formation in *Mycobacterium tuberculosis* infected macrophages requires IFN-gamma/HIF-1alpha signaling and supports host defense. PLoS Pathog 14(1):e1006874. https://doi.org/10.1371/journal.ppat.1006874
99. Lei GS, Zhang C, Lee CH (2015) Myeloid-derived suppressor cells impair alveolar macrophages through PD-1 receptor ligation during pneumocystis pneumonia. Infect Immun 83(2):572–582. https://doi.org/10.1128/IAI.02686-14
100. Peyron P, Vaubourgeix J, Poquet Y, Levillain F, Botanch C, Bardou F et al (2008) Foamy macrophages from tuberculous patients' granulomas constitute a nutrient-rich reservoir for *M. tuberculosis* persistence. PLoS Pathog 4(11):e1000204. https://doi.org/10.1371/journal.ppat.1000204
101. Russell DG, Cardona PJ, Kim MJ, Allain S, Altare F (2009) Foamy macrophages and the progression of the human tuberculosis granuloma. Nat Immunol 10(9):943–948. https://doi.org/10.1038/ni.1781
102. Dilek N, Vuillefroy de Silly R, Blancho G, Vanhove B (2012) Myeloid-derived suppressor cells: mechanisms of action and recent advances in their role in transplant tolerance. Front Immunol 3:208. https://doi.org/10.3389/fimmu.2012.00208
103. Huang B, Pan PY, Li Q, Sato AI, Levy DE, Bromberg J et al (2006) Gr-1+CD115+ immature myeloid suppressor cells mediate the development of tumor-induced T regulatory cells and T-cell anergy in tumor-bearing host. Cancer Res 66(2):1123–1131. https://doi.org/10.1158/0008-5472.CAN-05-1299
104. Bronte V, Serafini P, Mazzoni A, Segal DM, Zanovello P (2003) L-arginine metabolism in myeloid cells controls T-lymphocyte functions. Trends Immunol 24(6):302–306. https://doi.org/10.1016/s1471-4906(03)00132-7
105. Comi M, Amodio G, Gregori S (2018) Interleukin-10-producing DC-10 is a unique tool to promote tolerance via antigen-specific t regulatory type 1 cells. Front Immunol 9:682. https://doi.org/10.3389/fimmu.2018.00682
106. Cabezon R, Carrera-Silva EA, Florez-Grau G, Errasti AE, Calderon-Gomez E, Lozano JJ et al (2015) MERTK as negative regulator of human T cell activation. J Leukoc Biol 97(4):751–760. https://doi.org/10.1189/jlb.3A0714-334R
107. Naranjo-Gomez M, Raich-Regue D, Onate C, Grau-Lopez L, Ramo-Tello C, Pujol-Borrell R et al (2011) Comparative study of clinical grade human tolerogenic dendritic cells. J Transl Med 9:89. https://doi.org/10.1186/1479-5876-9-89
108. Rodriguez PC, Ochoa AC (2008) Arginine regulation by myeloid derived suppressor cells and tolerance in cancer: mechanisms and therapeutic perspectives. Immunol Rev 222:180–191. https://doi.org/10.1111/j.1600-065X.2008.00608.x
109. Srivastava MK, Sinha P, Clements VK, Rodriguez P, Ostrand-Rosenberg S (2010) Myeloid-derived suppressor cells inhibit T-cell activation by depleting cystine and cysteine. Cancer Res 70(1):68–77. https://doi.org/10.1158/0008-5472.CAN-09-2587

International Journal of Biological Macromolecules 274 (2024) 133188

Contents lists available at ScienceDirect

International Journal of Biological Macromolecules

journal homepage: www.elsevier.com/locate/ijbiomac

A novel strategy to elicit enduring anti-morphine immunity and relief from addiction by targeting Acr1 protein nano vaccine through TLR-2 to dendritic cells

Sidhanta Nanda [a], Mohammad Adeel Zafar [a], Taruna Lamba [a], Jonaid Ahmad Malik [a], Mohammad Affan Khan [a], Priya Bhardwaj [c], Bhawana Bisht [c], Rohan Ghadi [b], Gurpreet Kaur [e], Vijayender Bhalla [c], Mohammad Owais [d], Sanyog Jain [b], Sharvan Sehrawat [f], Javed N. Agrewala [a,*]

[a] Immunology Laboratory, Department of Biomedical Engineering, Indian Institute of Technology Ropar, Rupnagar, India
[b] Centre for Pharmaceutical Nanotechnology, Department of Pharmaceutics, National Institute of Pharmaceutical Education and Research, Mohali, India
[c] CSIR-Institute of Microbial Technology, Chandigarh, India
[d] Department of Interdisciplinary Biotechnology Unit, Aligarh Muslim University, Aligarh, India
[e] Department of Biotechnology, Chandigarh Group of Colleges, Mohali, India
[f] Department of Biological Sciences, Indian Institute of Science Education and Research, Mohali, India

ARTICLE INFO

Keywords:
Morphine
Vaccines
Opioid substitution therapy
Drug addiction
Nanotechnology
Adjuvant

ABSTRACT

Morphine addiction poses a significant challenge to global healthcare. Current opioid substitution therapies, such as buprenorphine, naloxone and methadone are effective but often lead to dependence. Thus, exploring alternative treatments for opioid addiction is crucial. We have developed a novel vaccine that presents morphine and Pam3Cys (a TLR-2 agonist) on the surface of Acr1 nanoparticles. This vaccine has self-adjuvant properties and targets TLR-2 receptors on antigen-presenting cells, particularly dendritic cells. Our vaccination strategy promotes the proliferation and differentiation of morphine-specific B-cells and Acr1-reactive CD4 T-cells. Additionally, the vaccine elicited the production of high-affinity anti-morphine antibodies, effectively eliminating morphine from the bloodstream and brain in mice. It also reduced the expression of addiction-associated μ-opioid receptor and dopamine genes. The significant increase in memory CD4 T-cells and B-cells indicates the vaccine's ability to induce long-lasting immunity against morphine. This vaccine holds promise as a prophylactic measure against morphine addiction.

1. Introduction

Opioid Use Disorder (OUD) is a pervasive substance abuse condition characterized by persistent, compulsive opioid consumption despite adverse consequences [1]. An estimated 35 million people are affected by substance use disorders (SUD) globally [2]. Additionally, since the onset of COVID-19, there has been a 23 % increase in alcohol abuse and a 16 % increase in drug abuse compared to pre-pandemic levels [3]. Morphine is a potent opioid analgesic commonly used to manage moderate to severe pain [2,4].

Nevertheless, prolonged morphine use can lead to addiction and profoundly impact the immune system, heightening susceptibility to infections [1]. Research has revealed that morphine, besides its addictive potential, hinders vaccine response. It impeded T-cell activation and antibody (Ab) production [1,5–9]. Additionally, it compromises the function of macrophages, reducing the production of vital pro-inflammatory cytokines and diminishing the expression of toll-like receptors (TLRs) and other crucial cell-surface molecules required for macrophage activation [10–13].

Vaccines have been instrumental in eradicating diseases such as smallpox, polio, measles, mumps, and rubella [14]. Numerous research groups worldwide are diligently working on developing vaccines against drug abuse. Recently, a study demonstrated that an anti-heroin vaccine countered the effects of heroin in non-human primates, resulting in the absence of withdrawal symptoms [6,15]. A recent study investigated a vaccine candidate utilizing a small fragment of heroin as the antigen,

* Corresponding author.
E-mail addresses: jagrewala@gmail.com, Jagrewala@iitrpr.ac.in (J.N. Agrewala).

https://doi.org/10.1016/j.ijbiomac.2024.133188
Received 22 May 2024; Received in revised form 11 June 2024; Accepted 13 June 2024
Available online 14 June 2024

coupled with an adjuvant of aluminum hydroxide and polyoxyethylene sorbitan monolaurate. While this vaccine candidate did not reach the desired level of effectiveness, it signifies progress in the development of a clinically viable heroin vaccine [6,8]. However, these vaccines are limited in their ability to neutralize opioids in the bloodstream, provide insufficient immunity against opioids, and fail to counter opioid-induced immunosuppression [16–21]. Moreover, these vaccines rely on external adjuvants, which can affect the binding of receptors with antigens and diminish Ab affinity. Studies suggest that conjugate-based vaccines generate Abs with a limited active duration and may require multiple booster shots [6,22].

Nanoparticle-based vaccines hold tremendous promise in enhancing immunological interventions in the anti-opioid vaccine developments [23]. Nanoparticles offer several advantages over conventional vaccine delivery methods, including heightened antigen specificity, protection against antigen degradation, targeted delivery to specific cells, and sustained antigen release [24–28]. Moreover, nanoparticles can augment immunogenicity due to their size and eliminate the need for additional adjuvants [29,30]. Antigens on nanoparticle surfaces render nanoparticle vaccines highly efficient, as antigens become readily accessible to antigen-presenting cells (APCs) [31,32].

Vaccine effectiveness hinges on generating high-affinity antibodies. Toll-like receptor 2 (TLR-2) plays a pivotal role in modulating the immune system by targeting APCs, activating both adaptive and innate immunity [33–37]. TLR ligands can reduce the required antigen dosage for vaccine effectiveness, alleviating traditional vaccines' economic burdens and adverse effects. TLR-2 is abundantly expressed on the surface of dendritic cells (DCs), making them ideal targets for vaccine delivery. DCs are the sole APCs capable of activating naïve T-cells and play a pivotal role in orchestrating robust immune responses [38].

We have pioneered a novel vaccination strategy against morphine, surpassing previous limitations. Our vaccine displays Pam3Cys and morphine on Acr1 nanoparticles. Acr1 is derived from *Mycobacterium tuberculosis* that activates T-cells and binds to TLR-2, providing both potent adjuvant properties and robust activation of T cells. This stimulates B-cells to produce high-affinity anti-morphine Abs. Additionally, Pam3cys targets dendritic cells via the TLR2 receptor, activating T-cells. Our engineered nanoparticle vaccine effectively neutralizes morphine's effects in experimental animal models, offering a promising solution to combat morphine addiction.

2. Results

2.1. Synthesis and characterization of morphine-Acr1-Pam3Cys nanoparticle vaccine (MAPNV)

The Acr1 nanoparticles were surface conjugated with morphine and TLR-2 agonist Pam3Cys (Fig. 1A). The particle size distribution analysis of the Acr1 nanoparticles (AN) revealed a mean size of 86 ± 19.2 nm, with a concentration of 8.4×10^9 particles/ml, low polydispersity index 0.2 and positive zeta potential charge of 42.4 v (Fig. 1B–D). The Nano-Tracking Analysis (NTA) of the Morphine-Acr1-Pam3Cys Nanoparticles Vaccine (MAPNV) showed a mean particle diameter of 106.1 ± 23.9 nm, polydispersity index (PI) of 0.22, a concentration of 2.0×10^4 particles/ml and the charge 37.3 mV (Fig. 1E–G). The results of the SEM image analysis showed that the nanoparticles had a spherical shape with a smooth surface texture, were highly distinguished, and were not aggregated. The particles displayed a high degree of crystallinity. The analysis revealed that the AN had a slight degree of aggregation (Supplementary Fig. 1A). In contrast, the Morphine Acr1 Nanoparticles (MAN) and MAPNV particles were more distinctively segregated (Fig. 1H, Supplementary Fig. 1B). The FTIR spectra of AN showed a broad peak at 1650 cm^{-1}, indicating the presence of an amide group. The transmittance of MAPNV revealed two distinct peaks at 1664 cm^{-1} and 1620 cm^{-1}, denoting the presence of an amide group and a peptide bond, respectively. Additionally, an absorbance peak at 1415 cm^{-1} was observed, signifying the presence of a hydroxyl group in MAPNV (Fig. 1I). Further, results from surface spectral scans exhibited a shift from 320 to 350 nm and 450–550 nm, illustrating the successful conjugation of morphine and Pam3Cys to the MAPNV surface (Supplementary Fig. 2). Morphine is a hydrophobic molecule, and conjugating it to the MAPNV's surface resulted in a change in the surface tension and a shift in the peak of the surface scan at 320–350 nm. The presence of the Pam3Cys molecule on the MAPNV surface increases the negative charge on the nanoparticle surface, resulting in a further surface scan peak shift at 450–550 nm (Supplementary Fig. 2). These results suggested that the surface tension of the nanoparticle had changed, confirming the successful surface coating of morphine and Pam3Cys on the MAPNV.

Biotinylated Pam3Cys was used to further validate the presence of Pam3Cys on the surface of MAPNV. A significantly ($p < 0.0001$) higher absorbance (1.946 ± 0.16 nm) of MAPNV, as compared to the controls Acr1 nanoparticles displaying Pam3Cys on the surface (ANP) (2.7 ± 0.23 nm), AN (0.04 ± 0.01 nm) and MAN (0.06 ± 0.02 nm), was noted (Fig. 1J). These results confirmed the presence of Pam3Cys on the surface of MAPNV. Similarly, the presence of morphine (2.014 ± 0.97 nm) on the MAPNV surface was substantially ($p < 0.0001$) detected by anti-morphine Abs on MAPNV, but not the controls AN (OD: 0.0614 ± 0.01 nm) and ANP (OD: 0.0668 ± 0.08 nm), which were without morphine (Fig. 1K). These results confirmed the effective conjugation of morphine on the surface of MAPNV.

The stability of MAPNV remained consistent for up to 180 days, as indicated by the surface spectrum analysis, demonstrating no observable changes over time (Supplementary Fig. 3). Furthermore, the UV–visible spectrophotometer analysis confirmed that the surface cross-linking of the MAPNV was more stable at pH 7 than pH 4 or pH 9 (Supplementary Fig. 4), indicating the stability of MAPNV at physiological pH 7. We detected negligible cytotoxicity of MAPNV on L929 cells at a physiological dose of up to 20 μg/ml for 24 h and 48 h. However, significant cytotoxicity was noticed at a 50 μg/ml dose (Supplementary Fig. 5). Consequently, 20 μg/ml of MAPNV was used for all the subsequent experiments.

2.2. MAPNV has self-adjuvant properties and activates B-cells and T cells to clear morphine from the brain and blood through anti-morphine Abs

The animals were vaccinated, as mentioned (Fig. 2A). Mice vaccinated with MAPNV showed an increase in the pool of morphine-specific B-cells ($p < 0.0001$) and production of anti-morphine Abs ($p < 0.0001$) in a dose-dependent manner, as compared to the unvaccinated control group. The subtype of anti-morphine Abs was chiefly IgG ($p<0001$) (Fig. 2B–E, Supplementary Fig. 6). A substantial decline in the level of unbound morphine in the serum ($p < 0.0001$) and brain ($p < 0.0001$) was noticed (Fig. 2F–G). It may be deduced from these results that MAPNV stimulated the secretion of anti-morphine Abs that successfully removed the morphine from the brain and blood. Hence, we were curious to examine the affinity of the anti-morphine Abs. We observed that the Kd values of anti-morphine Abs in a group of 5 mice immunized with MAPNV were 5.42 nM, 4.91 nM, 7.10 nM, 5.07 nM, and 4.84 nM (mean Kd: 5.468 nM). No anti-morphine Abs were detected in the placebo group (Fig. 2H). The MAPNV samples with high Kd values indicate the presence of high-affinity Abs that bind antigens more tightly for a longer duration. We were inquisitive about whether anti-morphine Abs-cleared morphine or MAPNV-vaccinated animals showed down-regulated expression of morphine addiction-associated receptors, like μ-opioid and dopamine D1 receptors [39,40]. These findings reveal that free morphine is not be available to bind its receptors. MAPNV-vaccinated animals showed optimum levels of μ-opioid receptors. Therefore, this proves that high-affinity anti-morphine Abs neutralizes the function of morphine by not allowing it to bind to the μ-opioid receptor (Fig. 2I). MAPNV-vaccinated animals showed an active state of movements ($p < 0.0001$), sensitivity to heat ($p < 0.0001$), and no dark-seeking nature ($p < 0.0001$) compared to the unvaccinated-control

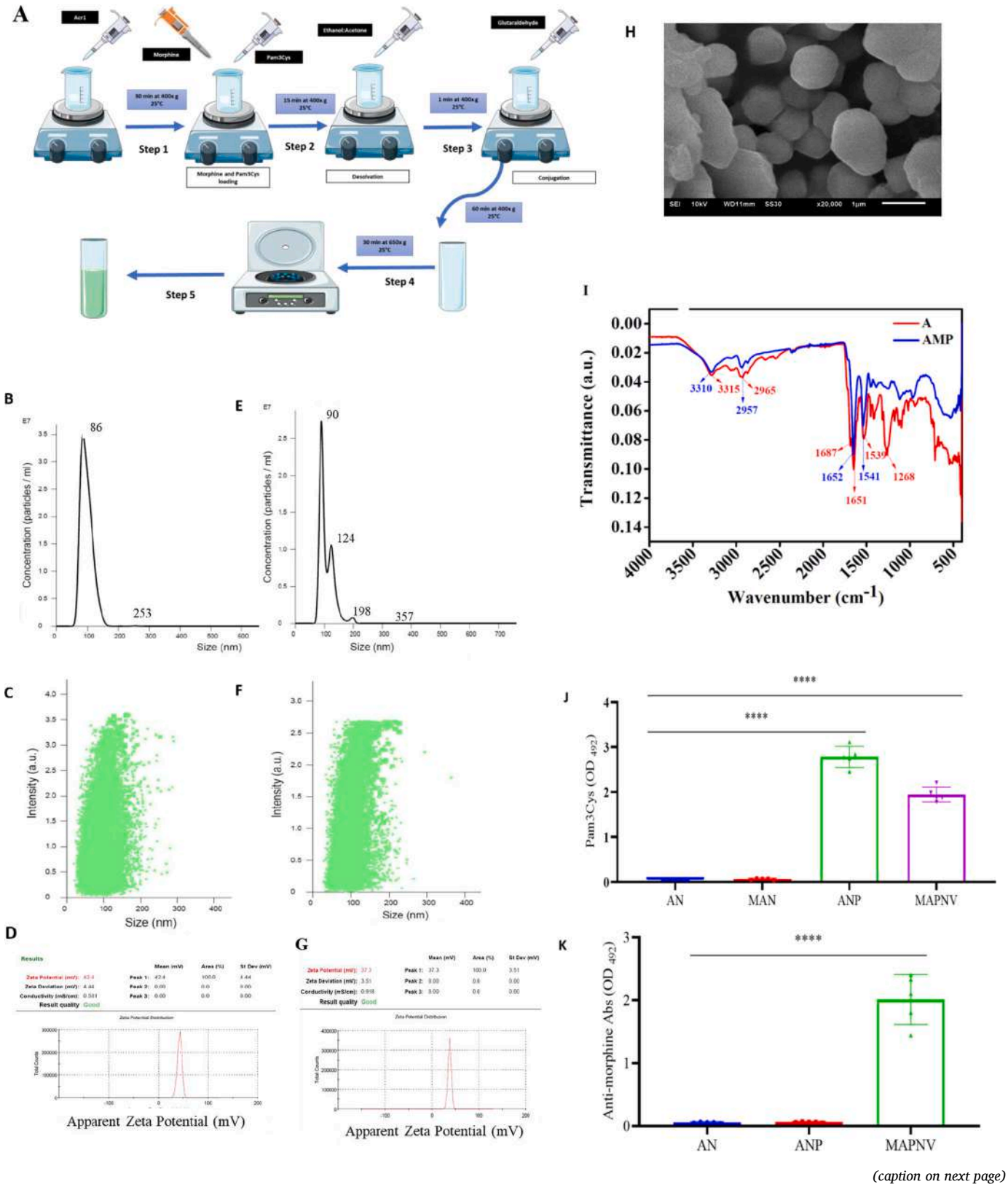

(caption on next page)

Fig. 1. The morphine-Acr1-Pam3Cys nanoparticle vaccine (MAPNV) was engineered using the Acr1 protein of *Mycobacterium tuberculosis (Mtb)* with morphine and Pam3Cys coated on the surface. (A) The process for creating and purifying Acr1 nanoparticles. In step 1, Acr1 (0.1 mg) was dissolved in deionized water (10 ml). In step 2, morphine (1 mg) and Pam3Cys (1 mg) were dissolved in ethanol, added to the Acr1 solution, and mixed for 15 min. In step 3, a desolating solution consisting of acetone (1 ml) and ethanol (1 ml) was added to the Acr1 solution at a 1 ml/min rate, and glutaraldehyde solution (25 %, 0.2 ml) was added. Step 4: stirred the mixture at 400 xg at 25 ± 2 °C for 1 h. In step 5, the solution was centrifuged at 650 ×*g* for 30 min at 4 °C, the supernatent (SN) was collected, and the pellet was dissolved in MES buffer (1:1000 dilution). (B–E) The AN (1 mg/ml) was synthesized and analyzed using Nano Sight NS300 (Malvern Analytica Ltd, Malvern, UK) for size, concentration, intensity, and charge. (E–G) The MAPNV (1 mg/ml) was analyzed for size and concentration, size and intensity, and charge. (H) The SEM images of MAPNV depict the particles of adequate sizes and shapes with a smooth surface texture. The pictures were taken at 20000–23000 X magnification (scale: 1 μm). (I) FTIR characterized the surface of the MAPNV. The orange line depicts the surface interferogram of the MAPNV. The AN was taken as a control depicted in the blue line. (J) The coating of Pam3Cys on the surface of the MAPNV was evaluated by biotin-Pam3Cys conjugated on the surface of the MAPNV. The bar graph denotes the optical density $(OD)_{492}$ values of the spectrophotometer after binding biotin-Pam3Cys with avidin-HRP, and the reaction was developed using the substrate. The Acr1 nanoparticles without Pam3Cys (AN), Morphine-Acr1 nanoparticles without Pam3Cys (MAN), and Acr1-Pam3Cys nanoparticles (APN) were used as controls. (K) The presence of morphine on the surface of the MAPNV was estimated using mouse anti-morphine Abs and secondary anti-mouse-HRP Abs through ELISA. The Acr1 nanoparticles without morphine (AN) and Acr1-Pam3Cys nanoparticles without morphine (APN) were negative controls. The ordinary one-way ANOVA was used to perform the statistical analysis. The data are expressed as mean ± SD. *$p < 0.1$; **$p < 0.01$; ***$p < 0.001$; ****$p < 0.0001$; ns = non-significant. (For interpretation of the references to color in this figure legend, the reader is referred to the web version of this article.)

animals (Supplementary Fig. 7A–C). The behavior of the vaccinated animals was not significantly changed with exposure to morphine. This suggests that MAPNV neutralizes the influence of morphine on the behavior of the animals.

2.3. MAPNV displays Pam3Cys, a TLR-2 ligand, on its surface

Pam3Cys is known to possess adjuvant properties. Consequently, we immunized mice with MAPNV supplemented with adjuvant alum to prove MAPNV's self-adjuvant properties. The gating strategies of B-cells depicted in Fig. 2B, J, and L are illustrated in Supplementary Fig. 8A–C. Interestingly, no change was observed in the production of anti-morphine Abs or proliferation of $CD19^+$ B-cells or morphine-reactive B-cells in the animals either inoculated with MAPNV or MAPNV+alum (Fig. 2D–M). Thus, this suggests that MAPNV has self-adjuvant properties and that no exogenous adjuvant is required.

2.4. Immunization with MAPNV induces optimum proliferation, differentiation, and generation of memory CD4 T-cells

The animals were administered MAPNV, as mentioned in Fig. 3A. We observed the proliferation ($p < 0.0001$) of the Acr1-specific $CD4^+$ T cell in a dose-dependent fashion (Fig. 3B–C), as compared to the PBS (placebo) control group by flowcytometry. Further, a substantially higher yield of TNF-α ($p < 0.01$), IL-4 ($p < 0.001$), IL-6 ($p < 0.0001$), and IFN-γ ($p < 0.01$) was noticed by ELISA, suggesting the presence of both Th1 cells and Th2 cells (Fig. 3D). These results were validated by RT-qPCR (Fig. 3E). Furthermore, MAPNV induced a significantly higher ($p < 0.0001$) generation of $CD44^{hi}CD62^{hi}$ memory CD4 T-cells (Fig. 3F–G). No change in the activity of CD4 T-cell was observed in the group administered with MAPNV versus MAPNV+alum (Fig. 3H–I). Thus, CD4 T cell results validated the B cell data of self-adjuvant properties of MAPNV. The gating strategies of T-cells depicted in Fig. 3B, F, and H are illustrated in Supplementary Fig. 8D–F. Further, memory phenotype and cytokines secretion by CD4 T-cells suggest their ability to help B-cells produce high-affinity Abs [33].

2.5. Prior exposure of morphine to animals does not affect the efficacy of MAPNV

Drug addicts are constantly exposed to SOA, which suppresses their immunity [2,41]. Therefore, we wanted to examine the efficacy of MAPNV if the animals were previously exposed to morphine. The mice were inoculated with morphine (10 mg/kg bwt) for 7 days. Later, animals were injected with MAPNV and sacrificed on 12 d after vaccination (Fig. 4A). We could not notice any difference in the proliferation of Acr1-specific CD4 T-cells or morphine-reactive B-cells in the animals exposed to morphine on vaccination with MAPNV (Fig. 4B–E).

Further, we noticed that the DCs derived from the BMCs of the animals exposed to morphine showed uptake of MAPNV-FITC in a dose-dependent fashion (Fig. 4F–G). The gating strategies for B-cells (Fig. 4B), CD4 T-cells (Fig. 4D), and DCs (Fig. 4F) are also shown in Supplementary Fig. 8G–I. It may be concluded from these results that prior exposure of animals to morphine does not interfere with the performance of the MAPNV in activating CD4 T-cells, B-cells, and DCs.

2.6. MAPNV induces therapeutic protections in immunized animals

Finally, to assess the therapeutic efficacy of MAPNV, we conducted a study wherein mice were initially exposed to morphine (10 mg/kg bwt) and subsequently vaccinated with MAPNV (20 mg/kg bwt) (Fig. 5A). The results were striking, revealing a substantial increase in B cell proliferation ($p < 0.0001$) and a remarkable production of IgG anti-morphine Abs ($p < 0.0001$) compared to the control group, which included animals vaccinated with APN, morphine, or PBS (Fig. 5B–D). Furthermore, the anti-morphine Abs efficiently cleared morphine from both the serum and the brain (Fig. 5E–F). These vaccinated animals exhibited non-significant changes in μ-opioid receptor and dopamine D1 receptors, compared to a placebo group, signifying a notable reduction in the expression of addiction-associated genes (Fig. 5G–H). Additionally, there was a prominent expansion of Acr1-specific CD4 T-cells ($p < 0.0001$), accompanied by an increased expression of cytokines, including TNF-α ($p < 0.0001$), IL-6 ($p < 0.0001$), IFN-γ ($p < 0.001$) and IL-4 ($p < 0.001$) (Fig. 5I–K), indicating the presence of both Th1 cells and Th2 cells. Moreover, a substantial increase in the population of memory CD4 T-cells was observed, as evidenced by a significant ($p < 0.0001$) upregulation of the $CD44^{hi}/CD62L^{hi}$ memory CD4 T-cells markers (Fig. 5L–M). The gating strategies were illustrated in the Supplementary Fig. 8J–L. Much like its prophylactic potential, MAPNV also holds considerable promise as a therapeutic vaccine for mitigating the influence of morphine.

2.7. MAPNV triggers dendritic cell (DC) activation via the Toll-like receptor 2 (TLR-2) signaling pathway

Given that MAPNV presents the Toll-like receptor 2 (TLR-2) ligand Pam3Cys on its surface, our interest was piqued regarding its potential interaction with TLR-2 and subsequent endocytosis via the TLR-2-dependent pathway. Dendritic cells (DCs) derived from $TLR\text{-}2^{-/-}$ and wild-type mice were exposed to FITC-labeled MAPNV (Fig. 6A). A significantly enhanced uptake of MAPNV-FITC was observed in DCs of WT ($p < 0.0001$) compared to DCs of $TLR\text{-}2^{-/-}$ (Fig. 6B). DCs of WT demonstrated notably higher expression levels of CD40 compared to DCs of $TLR\text{-}2^{-/-}$ (Fig. 6C–D). The gating strategies were illustrated in the Supplementary Fig. 8M-O. These findings suggest that MAPNV is primarily endocytosed through the TLR-2-dependent pathway, which can enhance antigen uptake, promote optimal antigen presentation, and induce robust germinal center reactions, developing durable memory B

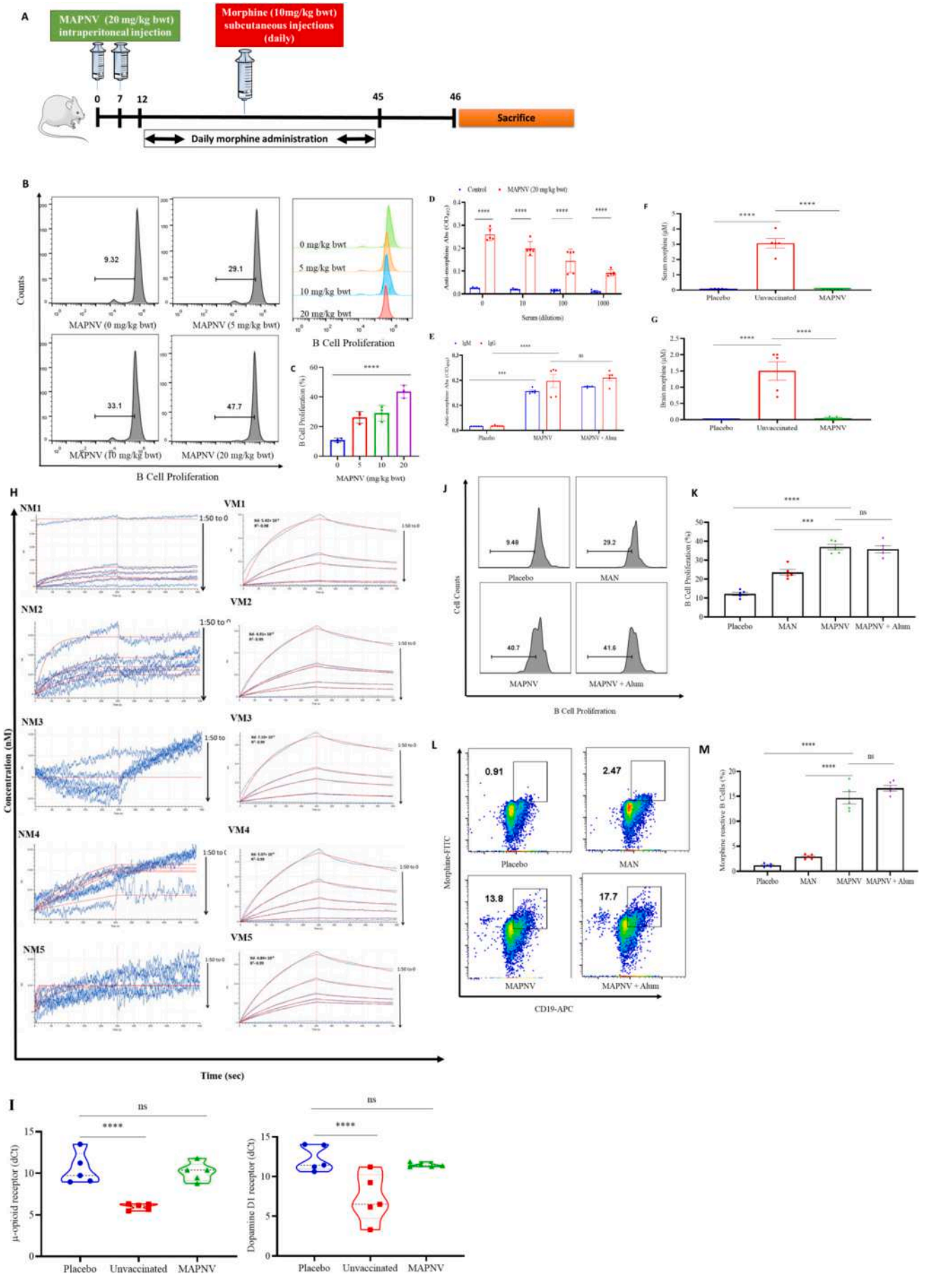

(caption on next page)

Fig. 2. MAPNV vaccination activates B cells to secrete high-affinity anti-morphine Abs and clears morphine from the brain and blood. (A) The mice were immunized with the MAPNV (20 mg/kg bwt) and the control group with PBS (placebo) on days 0 and 7. Later, they were continuously administered morphine (10 mg/kg bwt) from days 12 to 45. On day 46, the mice were bled, and serum anti morphine antibodies were estimated via ELISA. Later, the animals were sacrificed, splenocytes were isolated, labeled with CFSE, and *in vitro* challenged with MAPNV (0–20 μg/ml) for 72 h for monitoring. (B–C) proliferation of $CD19^+$ B cells by CFSE dye-dilution assay by flowcytometry; (D–E) IgM/IgG anti-morphine Abs by ELISA; (F-G) estimation of morphine in the serum and brain by UV–visible spectrophotometer. (H) The Bio-Layer Interferometry study to evaluate the affinity of the anti-morphine Abs generated in the vaccinated animals. The His-tagged morphine-conjugate (2 μg/ml) was immobilized on Ni-NTA sensors for 300 s (200 μL prepared in 1 × PBS). After adjusting the baseline in the working buffer, the immobilized morphine-conjugate was allowed to associate with 200 μL of serum sample (1:1000 in 1× PBS), followed by the dissociation in the working buffer for 250 s each. The binding kinetics was performed with different serum dilutions (1:500, 1:200, 1:100, 1:50) after regeneration and activation of the sensor to immobilize again with morphine-conjugate. The graphs show the binding kinetics of serum samples with the morphine-conjugates globally fit using a 1:1 binding mode. Graphs VM (1–5) show the association-dissociation graphs of vaccinated mice. Graphs NM (1–5) denote the affinity of anti-morphine Abs in the serum of normal mice. (I) The expression of μ-opioid and dopamine D1 receptors in the brains by RT-qPCR. (J–K) The flow cytometry histograms and their descriptive bar diagrams signify the proliferation of $CD19^+$ B cells of the groups vaccinated with MAPNV in the presence/absence of alum. (L–M) The contour plots and their bar diagram depict the percentage of $CD19^+$ morphine-reactive B cells identified using morphine-FITC by the flowcytometry. Each dot represents one mouse. One-way ANOVA and *t*-test for the statistical analysis were used to analyze the data (mean ± SD). $*p < 0.1$; $**p < 0.01$; $***p < 0.001$; $****p < 0.0001$; ns = non-significant.

cell responses and improving MAPNV vaccine efficacy.

3. Discussion

Nanoparticle-based vaccines provide a non-invasive delivery method through inhalation or oral administration, eliminating the need for injections. This characteristic significantly enhances vaccine accessibility, especially in resource-limited settings, and improves patient acceptance [42–50]. Furthermore, nanoparticles can be customized to target specific cells, such as DCs, B-cells, or tissues, enhancing the immune response and overall vaccine effectiveness.

We engineered the vaccine MAPNV, which consists of Acr1 nanoparticles expressing morphine and Pam3Cys on its surface. The experiments involving animals vaccinated with MAPNV yielded the following major findings: 1] proliferation and differentiation of morphine-specific B-cells; 2] induction of high levels of anti-morphine antibodies, effectively clearing morphine from the blood and brain of the animals; 3] proliferation and differentiation of Acr1-reactive CD4 T-cells; 4] expansion of both Th1 and Th2 cells; 5] generation and persistence of memory CD4 T-cells and memory B-cells; 6] self-adjuvant properties of MAPNV, with the addition of an exogenous adjuvant not improving its ability to activate B-cells and CD4 T-cells further; 7] no interference in the efficacy of MAPNV due to prior exposure of mice to morphine; 8] downregulation in the expression of the addiction-associated μ-opioid receptor gene.

The nanoparticles utilized in MAPNV were synthesized using the Acr1 protein of *Mycobacterium tuberculosis (Mtb)*, which binds to TLR-2 and induces potent immunomodulatory activity [51]. Additionally, MAPNV displays morphine and Pam3Cys on its surface, ensuring the binding of morphine to morphine-reactive B cell receptors. Pam3Cys acts as an adjuvant and a targeted delivery via TLR-2 to B-cells and DCs [52–55]. Both of which extensively express TLR-2. As a result, MAPNV activates B cells, bolstering the immune response to produce high-affinity anti-morphine antibodies. TLR-2 is known to increase antibody affinity. Furthermore, we observed that DCs actively uptake MAPNV and present it to CD4 T cells, leading to the proliferation and generation of memory and effector CD4 T cells. TLR-2 pathway is reported to generate and sustain memory T cells [33,35,56–59].

Existing vaccines targeting Substances of Abuse (SoAs) have not achieved optimal or long-lasting immunity, leading to ineffectiveness in combating opioid-induced addiction and immunosuppression [16,60]. Moreover, these vaccines necessitate the incorporation of exogenous adjuvants, significantly diminishing the probability of concurrent engagement of the vaccine and adjuvant with identical B cells, thereby affecting receptor binding to antigens and diminishing antibody affinity. Research indicates that conjugate-based vaccines produce antibodies with a short active duration and may necessitate multiple boosters [6]. In contrast, we chemically conjugated the antigen and adjuvant in the same vaccine, MAPNV, providing ample opportunity for morphine-specific B cells to receive both antigenic and adjuvant signals through MAPNV for their optimum activation, proliferation and secretion of high-affinity anti-morphine antibodies (Supp Fig. 9A). We observed high-affinity IgG anti-morphine antibodies persisting for up to 45 days, demonstrating the presence of bonafide B memory cells capable of producing high-affinity antibodies. Furthermore, nanoparticles function as an adjuvant and can be used for targeted vaccine delivery in substantially low amounts, augmenting antigen specificity, ensuring sustained antigen release, and protecting it from deterioration [26,29,60]. Additionally, the delivery of antigens through nanoparticles enhances the production of high-affinity antibodies [29,61,62].

MAPNV effectively reversed morphine-induced immunosuppression, promoted phagocytosis by DCs, and activated CD4 T and B cells. Furthermore, MAPNV prevented morphine-mediated inhibition in the expression of TNF-α, IL-6, IFN-γ, and IL-4. Additionally, morphine inhibit the expression of TLRs, which are crucial for APC activation. We observed efficient phagocytosis of MAPNV by DCs through TLR-2 signaling pathways. DCs transport antigens from various body sites to secondary lymphoid organs to prime naive T-cells [63,64]. This finding aligns with previous studies suggesting that TLR-2 is a crucial receptor for recognizing and internalizing specific antigens [35,50]. Moreover, the TLR-2 pathway generates long-lasting immunity [35].

The study suggests a MAPNV vaccine engineered with Acr1 nanoparticles coated with morphine and Pam3Cys is targeted through B-cell receptor (BCR) and TLR-2 to morphine-reactive B cells and DCs. Both the APCs will present the Acr1 to CD4 T cells. The effector CD4 T cells will activate and differentiate morphine-specific-B cells to secrete anti-morphine Abs and will finally differentiate into memory CD4-T cells and memory B-cells. The anti-morphine Abs will bind morphine, eliminate it from blood, and prevent it from reaching the brain (Suppl Fig. 9B).

The development of vaccines for SoA treatment began four decades ago, with several candidates entering clinical trials. However, none are approved for clinical use. Further, introducing new molecules like methadone and naltrexone reduced vaccine demand. However, the global pandemic has again significantly increased the need for vaccines. While vaccines for cocaine and nicotine have shown promise in clinical trials, challenges persist, particularly in generating long-lasting and high-affinity neutralizing Abs against SoA [21].

Our vaccine demonstrates an enduring high-affinity Ab response against morphine, necessitating exploration of its efficacy in diverse populations. Before advancing to clinical trials, rigorous testing in various animal models, including macaques, is imperative to validate the vaccine's neutralizing potential and toxicity levels. Furthermore, our vaccine targets multiple antigens, including *Mtb* and morphine, offering a dual solution for treating tuberculosis and morphine addiction. Although protection studies against *Mtb* in animal models are pending. However, previous studies from our group on vaccines using Acr1 and its immunodominant epitopes have shown promising results [50,65–67].

In conclusion, our study suggests that the anti-morphine Abs produced by MAPNV vaccination effectively binds circulating morphine

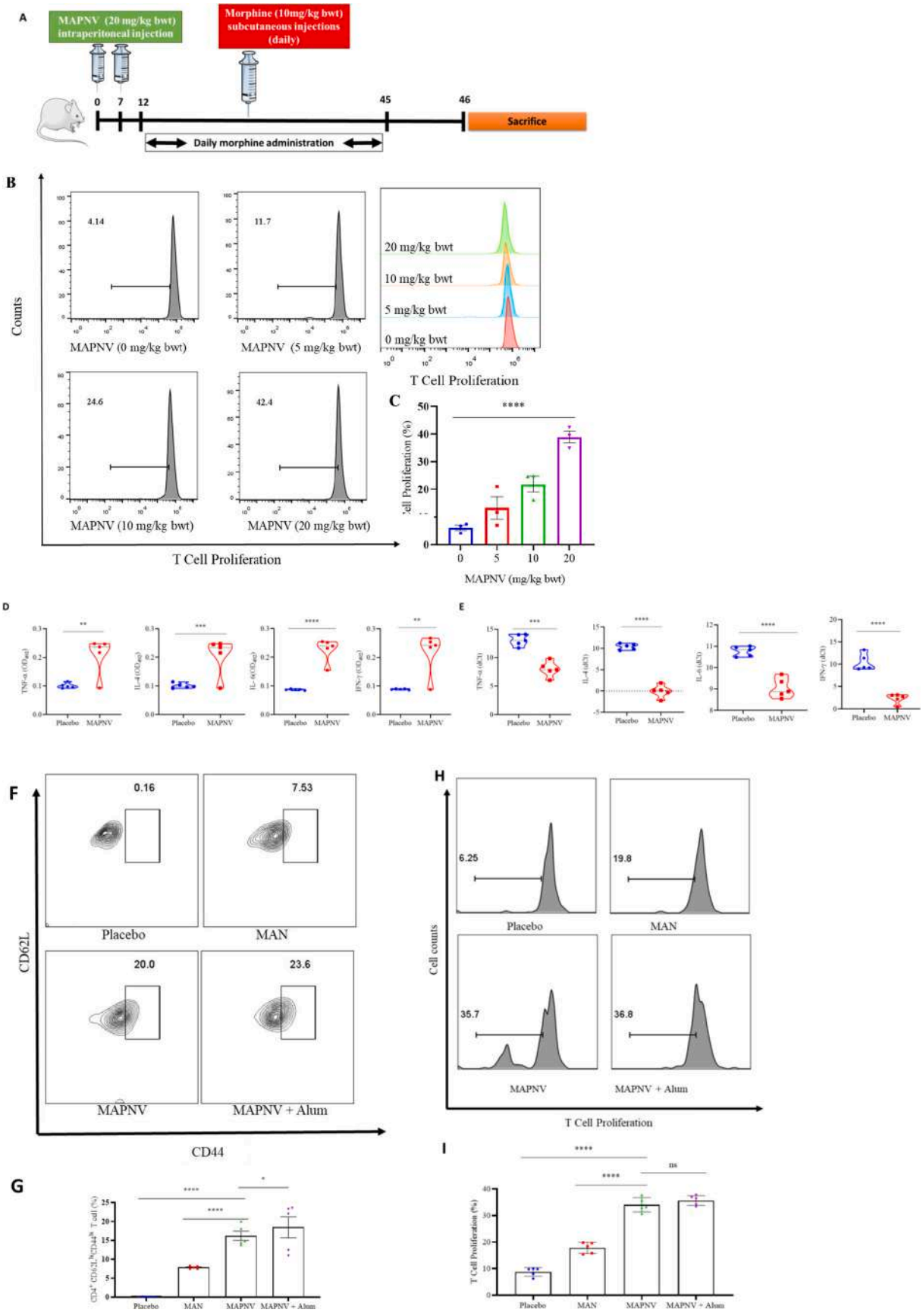

(caption on next page)

Fig. 3. MAPNV immunization induces the proliferation and generation of memory CD4 T cells. (A) The mice were immunized with the MAPNV (0–20 mg/kg bwt) and controlled with PBS (placebo) on 0 d and 7 d. Later, they were daily administered morphine (10 mg/kg bwt) from 12 d to 45 d. On 46 d, the animals were sacrificed, splenocytes were isolated, labeled with CFSE, and *in vitro* challenged with MAPNV for 72 h and examined for the (B–C) proliferation of CD4 T cells by CFSE dye-dilution assay through flowcytometry. Expression of TNF-α, IL-4, IL-6, and IFN-γ cytokines by (D) ELISA and (E) RT-qPCR. (F–G) The flow cytometry histograms and their respective bar diagrams depict the expression of central memory $CD4^+$ T cell markers $CD44^{hi}CD62L^{hi}$. (H–I) The flow cytometry histograms and their descriptive bar diagrams signify the proliferation of CD4 T cells of the groups vaccinated with MAPNV in the presence/absence of alum. Each dot represents one mouse. The data (mean ± SD) were analyzed by One-way ANOVA and *t*-test for the statistical analysis. $^*p < 0.1$; $^{**}p < 0.01$; $^{***}p < 0.001$; $^{****}p < 0.0001$; ns = non-significant.

molecules, thereby efficiently sequestering them from the bloodstream and obstructing their entry into the brain. This mechanistic strategy presents a promising avenue for alleviating the repercussions of opioid dependence and merits continued investigation in clinical contexts.

4. Materials and methods

4.1. Animals

Female BALB/c, C57BL/6 wild type, and TLR-2 knockout mice of C57BL/6 background (aged 6–8 weeks, 22 ± 2 g) were procured from the Animal House Facilities of the National Institute of Pharmaceutical Education and Research (NIPER), Mohali, India, Hylasco Biotechnology Pvt. Ltd. Hyderabad, India and Indian Institutes of Science Education and Research (IISER), Mohali, India. The experiments were approved by the Institutional Animal Ethics Committees (IAEC) of the NIPER (IAEC/19/05), Aligarh Muslim University (AMU), Aligarh (1979/GO/Re/S/17/CPCSEA) and IISER (176/20.03.2019). The animals were kept at the Animal House facility of NIPER, AMU, and IISER with a 12 h day/night cycle, temperature of 22 ± 2 °C, and relative humidity of 45–60 %. The experiments were performed according to the Committee for Control and Supervision of Experiments on Animals (CCSEA) guidelines.

4.2. Chemicals and reagents

Morphine was purchased from the Opium and Alkaloid Factories (Government of India), New Delhi, India (F.No.9/IMP/Sales/1/2019 - Part-IV/2358) with due clearance and approval from the Central Bureau of Narcotics, Gwalior, India (0003023), and Food and Drug Administration, Government of Punjab, Kharar, India. 2019/328). All the reagents and solvents were purchased from Sigma-Aldrich (St. Louis, MO) or otherwise mentioned. Pam3CSK (tlrl-pms) was purchased from InvivoGen (Paris, France).

4.3. Purification of Acr1 protein

The recombinant Acr1 protein was purified as per the protocol mentioned elsewhere [70]. Briefly, The Acr1-expressing recombinant BL21 cells were grown overnight in LB broth (20 ml) supplemented with ampicillin (100 μg/ml). Later, fresh LB broth (99 ml) was added to the culture (1 ml) and incubated until the optical density (OD) reached 0.4–0.6. Later, IPTG (1 mM, 100 μl) was added into the cultures and incubated at 37 °C/4 h. The culture was centrifuged, the pellet was collected and washed with equilibration buffer (50 mM Tris, 250 mM NaCl, 20 mM imidazole), and resuspended in equilibration buffer (25 ml). It was then sonicated in ice for 15 min with a pulse interval of 10 s. Ni-NTA beads were packed in a non-absorbent column and washed 10 times the bed volume with deionized water. The beads were equilibrated with an equilibration buffer 10 to 20 times the bed volume. The lysate SN was applied to the column with a minimal flow rate. The column was washed thoroughly with wash buffer (50 mM tris, 250 mM NaCl, 50 mM imidazole) with a minimum flow rate. The protein was eluted in elution buffer (50 mM Tris, 250 mM NaCl, 20 mM imidazole). Dialysis was done overnight against PBS (1 mM, pH 7.4) to remove excess salt and imidazole.

4.4. Synthesis of Acr1 nanoparticles (AN)

Acr1 (0.1 mg) was mixed with deionized water (10 ml) (Milli-Q type I, Merckmillipore, Burlington, MA) and stirred for 30 min at 400 xg at 25 ± 2 °C. A desolvating solution was prepared by mixing acetone (1 ml) with ethanol (1 ml). After 30 min, the desolvating solution was added to the Acr1 solution at a 1 ml/min rate. Immediately, glutaraldehyde solution (25 %, 0.2 ml) was added. The solution was stirred at 400 xg at 25 ± 2 °C for 1 h, transferred into a 15 ml tube, and centrifuged at 650 xg for 30 min at 4 °C. The SN was collected and stored at 4 °C, while the pellet was dissolved in MES buffer (1:1000 dilution) (0.5 M, pH 7.0) and stored at 4 °C.

4.5. Synthesis of morphine-Acr1-Pam3Cys nanoparticles vaccine (MAPNV)

Acr1 (0.1 g) was dissolved in deionized water (10 ml). The protein solution was stirred for 30 min at 400 xg at 25 ± 2 °C. The 6-succinyl morphine was prepared as mentioned by Akbarzadeh et al. [71]. Concisely, morphine-free base (10 mg) and succinic anhydride (10 mg) in benzene (200 ml) underwent reflux at 2 h, followed by the addition of additional succinic anhydride (10 mg) and continued reflux for 1 h. The reaction mixture was cooled, benzene removed under nitrogen, and the residue dissolved in 100 ml water adjusted to pH 2 with 2 M HCl. After filtration, pH was raised to 8.5 with 2.5 M NaOH, and the solution was filtered to remove unchanged morphine. Crystallization of M-6-S occurred upon overnight refrigeration following adjustment to pH 5.6-succinyl morphine (1 mg) and Pam3Cys (1 mg) were dissolved in ethanol (1 ml), added to the Acr1 solution, and mixed for 15 min. Simultaneously, acetone (1 ml) was mixed with ethanol (1 ml) to create a 1:1 desolating solution. After 30 min, the desolating solution was added to the Acr1 solution at a 1 ml/min rate. Immediately, glutaraldehyde solution (25 %, 0.2 ml) was added for stable coating via the formation of the imino bond. The mixture was stirred at 400 g at 25 ± 2 °C for 1 h. The solution was transferred to a 15 ml tube and centrifuged at 650 *g* for 30 min at 4 °C. The SN was collected and stored at 4 °C. The pellet was dissolved in MES buffer (1:1000 dilution) and stored at 4 °C.

4.6. Particle size distribution and zeta potential measurement

The size and charge of the synthesized Acr1 nanoparticles (AN) and morphine-Acr1-Pam3Cys nanoparticles (MAPNV) were analyzed by Nano Sight NS300 (Malvern Analytica Ltd., Malvern, UK) per the standard protocol. In short, the nanoparticle pellets were suspended in DW (1 ml) and vortexed for 1 min for homogenous distribution. The Nano sight NS300 was set up and calibrated according to the manufacturer's instructions. The sample (10 μl) was loaded onto the flow cell. The flow cell was aligned with the laser beam, and the sample was visualized on the computer screen.

Further, the samples were diluted in deionized water (1 ml) and homogenized for 30 min. The samples were transferred into the cuvettes, and the charge on the particles was measured using the Malvern Zetasizer Nano ZS. A blank sample of deionized water was used as a control. The particles' size distribution and zeta potential were measured by the analysis software Nano Sight Tracker (Malvern Analytica, Malvern, UK).

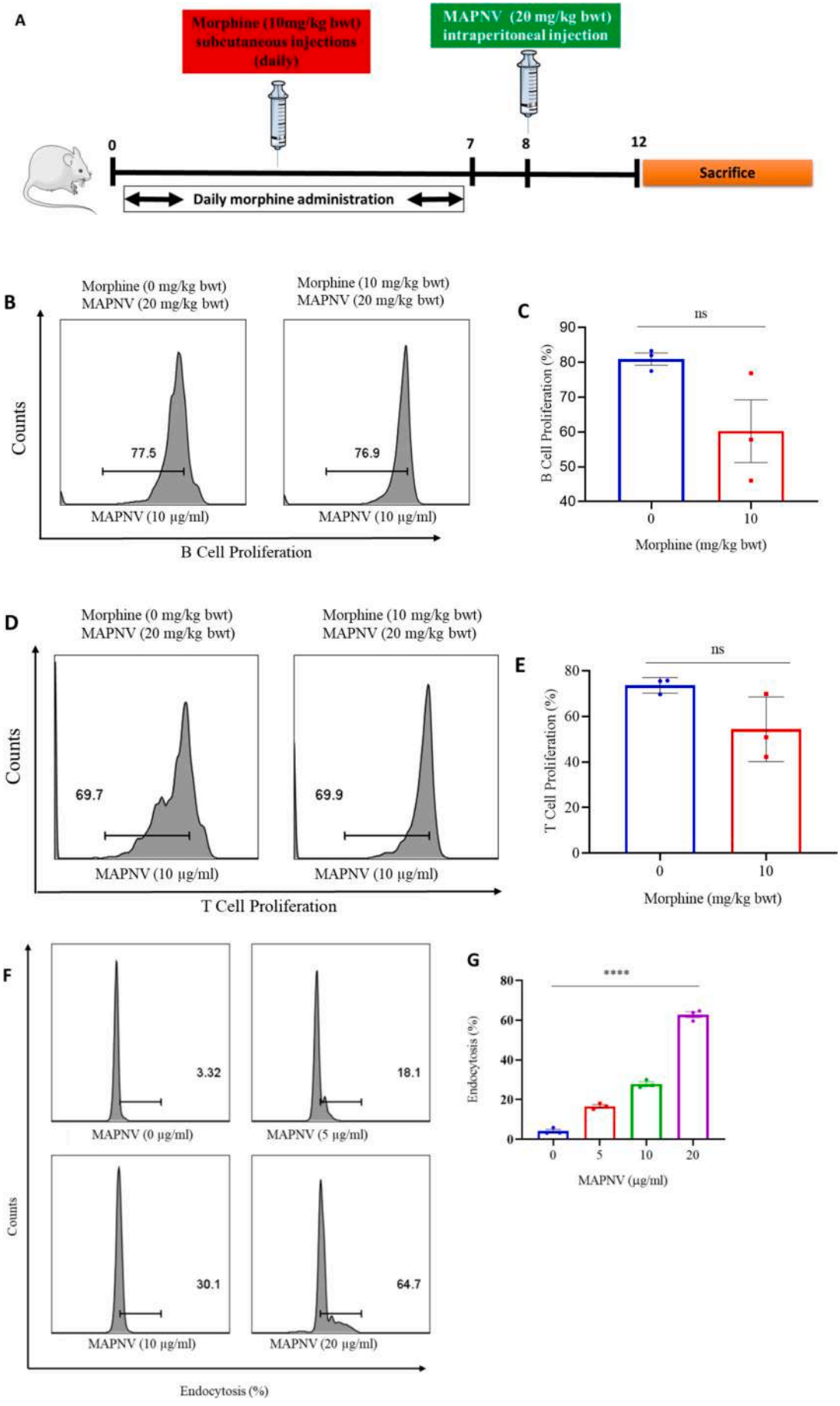

(caption on next page)

Fig. 4. Prior exposure of mice to morphine does not influence the efficacy of MAPNV to activate B cells and T cells. (A) The mice were exposed to morphine (10 mg/kg bwt) for 7 d. Later, they were vaccinated with MAPNV (20 mg/kg bwt). The histograms and their respective bar diagrams denote the proliferation of (B–C) $CD19^+$ B cells; (D-E) $CD4^+$ T cells by CFSE-dye dilution assay by flowcytometry. (F–G) The DCs show endocytosis of MAPNV-FITC in a dose-dependent fashion by flow-cytometry. The data (mean ± SD) was analyzed by *t*-tests. Each dot represents one mouse. *p < 0.1; **p < 0.01; ***p < 0.001; ****p < 0.0001; ns = non-significant.

4.7. Particle morphology demonstrated by scanning electron microscopy (SEM)

The Acr1 nanoparticles (AN), morphine-Acr1 nanoparticles (MAN), and morphine-Acr1-Pam3Cys nanoparticles (MAPNV) were prepared, and the pellets were collected. The pellets were freeze-dried overnight at −80 °C. The samples were loaded onto copper grids and placed on the electron microscope stage. The microscope was adjusted to a magnification (20000−23,000). A series of images were taken of the samples at various magnifications and orientations and recorded digitally as per the Jeol standard operating procedures. The images were analyzed using the Jeol Image software (Jeol, Tokyo, Japan) to measure particle size, shape, and surface texture. The AN and MAN were taken as controls.

4.8. Analysis of MAPNV using Fourier Transform Infrared (FTIR) spectroscopy

The surface of the synthesized nanoparticles was analyzed by the Fourier Transform Infrared spectroscopy (Bruker-TENSOR 2, Billerica, MA), as per the protocol illustrated elsewhere [68]. Freeze-dried AN and MAPNV were prepared and placed on a sample holder. The FTIR spectrometer was set to the appropriate parameters for the analysis. The sample was scanned from spectrum 4000 cm-1 to 600 cm^{-1}. The absorbance of MAPNV was recorded and compared with AN. The spectra were analyzed for differences in the positions of the peaks and intensity between the two samples by Image J software (University of Wisconsin, Madison, WI).

4.9. Surface scanning analysis of MAPNV

The surface of the AN and MAPNV was examined by a Clariostar microplate reader (BMG Labtek, Ortenberg, Germany). In short, the nanoparticles were suspended in deionized water (1 ml) and were pipetted into the triplicate wells (100 μl/wells) of a 96-well plate. Then, the UV–visible spectrophotometer was set for the number of wavelength scan points 278, excitation wavelength 321.0–598.0 nm, step width 1.0, and excitation bandwidth 1.0. The plate was placed in the sample holder, and the surface scan was performed at 200–550 nm wavelengths. The data was analyzed using the Labtek data analyzer software (BMG Labtek, Ortenberg, Germany).

4.10. Conjugation of Pam3Cys on the surface of MAPNV

The coating of Pam3Cys was evaluated, as mentioned elsewhere [50]. In brief, the 96-well plate was coated with cellulose nitrate (1 μg/ml) at 37 °C/1 h. The plate's negatively charged cellulose nitrate surface was incubated with $\log_2$ dilutions of positively charged Acr1-morphine/biotin-P3C at 4 °C/ON. Avidin-HRP was added and incubated at 37 °C/1 h. After each incubation, the wells were washed 3× with phosphate buffer (0.1 M, pH 8). The color was developed using OPD for 20 min, and the reaction was stopped with 7 % H_2SO_4. The absorbance was measured at OD_{492} nm by the Clariostar microplate reader.

4.11. Detection of morphine in the MAPNV

Standard ELISA assay was used to confirm the coating of morphine on the surface of MAPNV. The 96-well ELISA plate was briefly treated with cellulose nitrate (0.1 μg/100 μl) at 37 °C for 2 h. The MAPNV solution (1 μg/ml) was prepared in deionized water (DW) (1 ml). MAPNV solution (100 μl) was added to each well and incubated at 37 °C/2 h. The plate was washed, and 100 μl of the anti-morphine antibodies (1 μg/ml) was added. The plate was incubated at 37 °C for 1h. The wells were washed three times with PBST (PBS 1 M, pH 7.0, + Tween-20 (0.25 %). The HRP-conjugated secondary anti-mouse Abs (1 μg/ml, 100 μl) was added to the wells. The plate was incubated at 37 °C for 1h. The wells were washed 3× with PBST. The substrate buffer was prepared with 5 mg of OPD in 9 ml H_2O and 1 ml H_2O_2. The substrate solution (100 μl) was added to the wells and incubated at 37 °C/10 min. The reaction was stopped by adding 7 % H_2SO_4 (50 μl) to the wells. The absorbance of the solution in the wells was measured at OD_{492} nm using the Clariostar microplate reader.

4.12. UV–visible spectroscopy study revealed the stability of MAPNV

A UV–Vis spectroscopy study was conducted to assess the stability of nanoparticles. MAPNV (1 mg/ml) was prepared in PBS (1 M, pH 7.4, 1 ml). The samples were transferred into a 96-well plate. The absorbance of the samples was measured at 0 h by a UV–visible spectrophotometer. The samples were kept undisturbed at 4 °C for 180 days. Later, the samples were reanalyzed using the microplate reader. The absorbance spectra of the samples were measured. The percentage of particles that remained stable over time was determined.

4.13. Determination of pH-dependent stability of the MAPNV

MAPNV (1 mg/ml) was prepared freshly and dissolved in deionized water. The sample was transferred into a cuvette. The microplate reader was used with a spectrum scan (wavelength 320–540 nm) to detect the surface cross-linking status and examine the stability across the different pHs.

4.14. Demonstration of the cytotoxicity of MAPNV

The toxicity of the MAPNV on the L929 cells was examined by Alamar blue kit (Thermo-Fisher Scientific, Waltham, MA). The assay was performed in 96-well plate using L929 cells (1×10^6 cells/well) in complete RPMI-1640 medium (RPMI-1640 + FBS-10 % + Penicillin-Streptomycin (1 unit)) and different concentrations of MAPNV (0–50 μg/ml). After 24, 48, and 72 h of incubation, Alamar blue reagent (10 μl/well) was added to each well. The plates were incubated at 37 °C/4 h. Later, a microplate reader read the absorbance at 570 and 600 nm.

4.15. The detection of morphine-reactive B-cells in the animals immunized with MAPNV

The mice were immunized with the MAPNV (20 mg/kg bwt) and controlled with PBS on days 0 and 7. Later, morphine (10 mg/kg bwt) was administered from days 12 to 45. On day 46, the animals were sacrificed, and their spleens were collected. Splenocytes were challenged *in vitro* with MAPNV (20 μg/ml) for 72 h. Later, the cells (1×10^5) were stained with morphine-FITC conjugate (1 μg/ml) and anti-mouse CD19-PE Abs (1 μg/ml) and analyzed to detect morphine-reactive B-cells. The cells were acquired using BD Accuri, and analysis was performed using FlowJo software.

4.16. Demonstration of MAPNV-FITC endocytosis in DCs

The mice were injected with morphine (10 mg/kg bwt) for 7 days. On day 8, the mice were sacrificed, and bone marrow cells (BMCs) were collected. The mononuclear cells were then incubated at 400 xg for 10

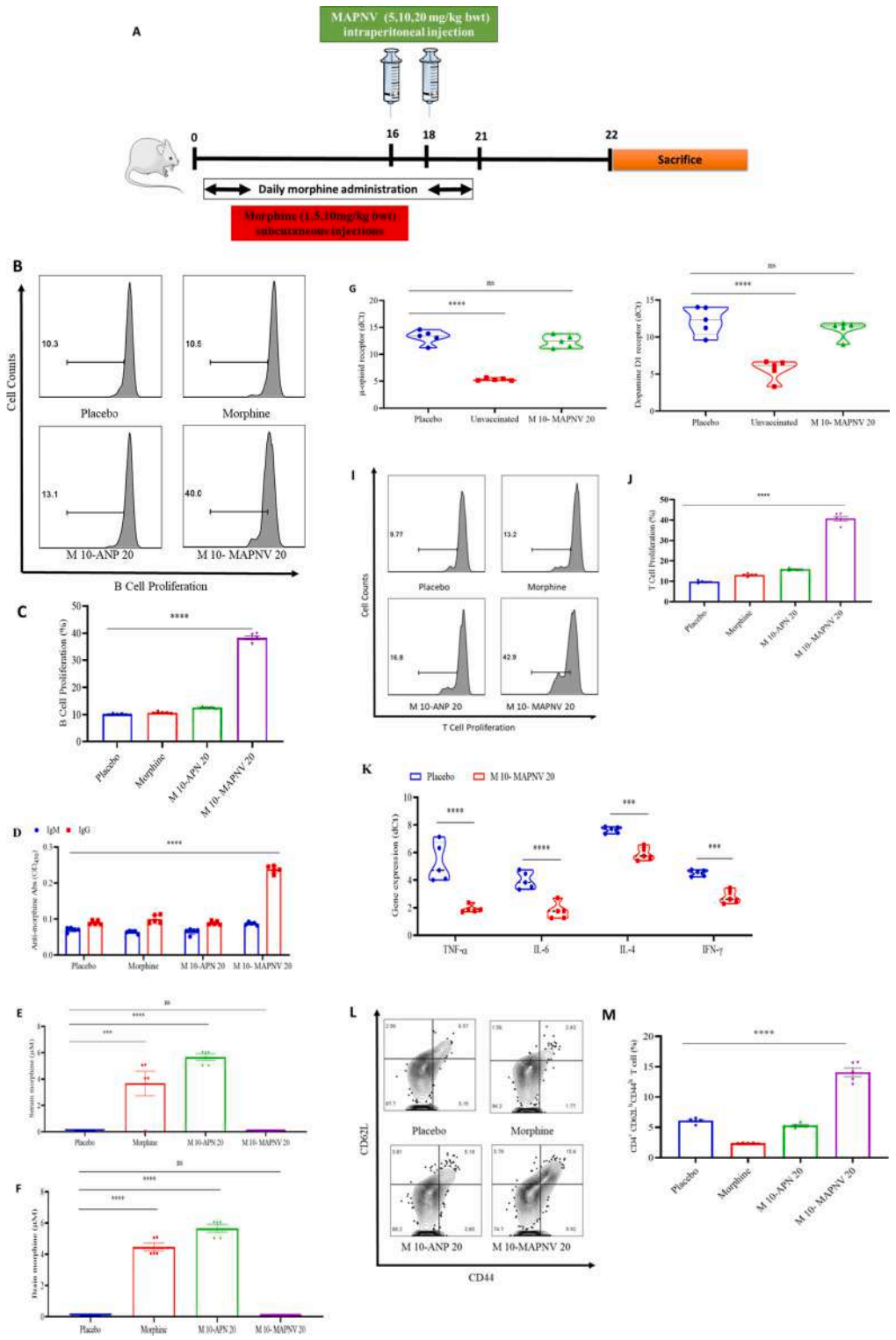

Fig. 5. Vaccination of mice before exposure to morphine demonstrates the therapeutic efficacy of MAPNV. (A) The animals were injected with morphine (10 mg/kg bwt) from 0d to 21d. Later, animals were vaccinated with MAPNV (20 mg/kg bwt) on days 16 and 18. On 22d, the mice were sacrificed, and splenocytes were labeled with CFSE and cultured *in vitro* with MAPNV (10 μg/ml) for 72 h. (B–C) The proliferation of $CD19^{+}$ B cells was enumerated by CFSE-dye-dilution assay through flow cytometry. (D) Levels of IgM/IgG anti-morphine Abs were estimated in the serum by ELISA. (E–F) Estimation of morphine in the blood and brain by UV–visible spectrophotometer. (G–H) The expression of μ-opioid receptor and dopamine D1 receptors were evaluated in the brain by RT-qPCR. (I–J) The CD4 T cells were examined for the (H, I) proliferation by CFSE dye-dilution assay through flow cytometry; (K) expression of TNF-, IL-6, IL-4 and IFN- by RT-PCR; (L-M) expression of CD44/CD62L on CD4 T cells by flowcytometry. Each dot represents one animal. The data (mean ± SD) were analyzed by One-way ANOVA and *t*-test for the statistical analysis. $^{*}p < 0.1$; $^{**}p < 0.01$; $^{***}p < 0.001$; $^{****}p < 0.0001$; ns = non-significant.

min and seeded in a 6-well plate (1×10^6 cells/well) in RPMI-1640-FCS-10 %. The cells were stimulated with IL-4 (20 ng/ml) and GM-CSF (20 ng/ml) and incubated for 6 days. The DCs were harvested using trypsin-EDTA (200 μl) and seeded in a 6-well plate (5×10^4 cells/well). Subsequently, MAPNV-FITC (0–20 μg/ml) was added into the wells and incubated at 37 °C/4 h. The cells were acquired using BD Accuri, and analysis was performed using FlowJo software.

4.17. Examining prophylactic efficacy of MAPNV vaccine

The mice were vaccinated with MAPNV (20 mg/kg bwt) on days 0 and 7. The control groups were injected with placebo (PBS), morphine (10 mg/kg bwt), MAN (20 mg/kg bwt), and MANPV (20 mg/kg bwt) + alum (0.5 mg/kg bwt). Consequently, the mice were injected with morphine (10 mg/kg bwt) from day 12 to 45. On day 46, the animals were sacrificed. The generation of anti-morphine Abs, the proliferation of CD4 T-cells and CD19 B-cells, morphine neutralization ability by vaccine, and opioid receptor expression were monitored.

4.18. Testing of the therapeutic efficiency of MAPNV vaccine

Mice were divided into four groups, with 5 mice/group. The mice were exposed to morphine (10 mg/kg bwt) for 21 days. In between, on 14d and 20d, mice were administered MAPNV (20 mg/kg bwt). The placebo (PBS), morphine (10 mg/kg bwt), and APN (20 mg/kg bwt) groups were taken as control. Later, the mice were sacrificed, and serum, brain, and spleens were collected and analyzed for B cell and T cell proliferation, memory T cell generation, and opioid receptor expression.

4.19. Proliferation of CD4 T and CD19 B-cells obtained from the vaccinated animals

A single-cell suspension of splenocytes isolated from the vaccinated and control groups was prepared. The CFSE-labeled cells were cultured with MAPNV (20 μg/ml) at 37 °C/48 h in a humidified 5 % CO_2 incubator. Later, the cells were washed 3× with PBS-FCS-1 % (PBS (1 mM, pH 7.4) + FCS (1 %)) and fluorochrome-labeled anti-CD19 Abs (1 μg/ml) and anti-CD4 Abs (1 μg/ml) and acquired on BD Accuri and analyzed by FlowJo software.

4.20. Examining the presence of memory, CD4 T-cells on the MAPNV vaccination

The cells were cultured as mentioned above for the CD4 T and B cell proliferation. After 48 h, the cultures were harvested and stained with fluorochrome-labeled anti-mouse CD4, CD44, and CD62L Abs. The cells were acquired through BD Accuri and analyzed by FlowJo software for the expression of the CD44 and CD62L on CD4-gated cells.

4.21. Measuring anti-morphine Abs in the MAPNV vaccinated animals

The 96-well plates were coated with morphine-KLH conjugates (0.001–1 μM, 100 μl/well) ON at 4 °C. Later, the plates were washed 3× with PBS-T20 (Tween 20: 0.025 %) and blocked with skimmed milk (5 %, 150 μl) for 1 h at 4 °C. After the blocking, the plates were washed 3× with PBS-T20. Serum samples (1:10) from vaccinated animals and controls were added to the wells. The plates were incubated at 4 °C for 2 h. Later, the secondary anti-mouse IgG + M + A-HRP Abs (0.1 μg/ml, 100 μl) were added, and the plates were incubated for 1 h at 4 °C. Further, the IgG and IgM subtypes were detected by adding anti-mIgG-HRP Abs or anti-mIgM-HRP Abs in separate wells. The plates were washed 5× with PBST. The color was developed using a tetramethylbenzidine (TMB) substrate (100 μl), and the absorbance was measured at OD_{450} nm wavelength using a microplate reader (BMG Labtek, Ortenberg, Germany).

4.22. Estimation of morphine in the brain and serum on immunization with MAPNV

The brains of MAPNV-vaccinated animals were homogenized with PBS (10 mM, pH 7.4) (10 ml) for 10 s and centrifuged at 1000 x*g* for 10 min at 4 °C. The SN was transferred into a fresh tube and centrifuged at 10000 x*g* for 1 h at 4 °C. The SN was discarded, and the pellet was resuspended in PBS (10 ml). This process was repeated two times. Later, NaCl (2 M, 1 ml) was added and thoroughly mixed with the pellet. The tube was centrifuged at 10000 x*g* for 1 h at 4 °C. The pellet was resuspended in PBS (10 ml), and urea (4 M, 10 ml) was added and mixed with the sample. The sample was centrifuged at 10000 x*g* for 1 h at 4 °C. SDS (10 %) (1 ml) was added to the samples and mixed. The sample was centrifuged at 10000 x*g* for 1 h at 4 °C. The pellet was resuspended in PBS (10 ml). The solution was dialysed against PBS (1 mM, pH 7.4, 50 ml) for 4 h. The sample was centrifuged at 10000 x*g* for 1 h at 4 °C. The pellet was resuspended in PBS (10 ml) and stored at −20 °C. A standard curve was plotted with different doses of morphine (0.01–1 μM). The estimation of the morphine in the serum and the brain was done as per the protocol mentioned [69]. Initially, a standard curve was prepared using various concentrations of solubilized morphine (1–10 μg/ml) in phosphate-buffered saline (PBS, 1 M, pH 7.4). The optical density (OD) was measured at a wavelength of OD_{300} nm using a UV–vis spectrophotometer (BMG Labtek, Ortenberg, Germany). The absorbance values of the blank solution (PBS, 1 M, pH 7.4) and different concentrations of morphine (ranging from 1 to 10 μg/ml) were recorded and plotted to create the standard curve. Serum samples and brain samples (0.1 ml) of immunized animals were extracted first using chloroform and methanol (1:1). In the extraction process, sonication was used for 42 KHz. Then, the solution was allowed to evaporate and mixed with methanol (0.1 ml). Then, NaOH made the pH of the solution. The solutions were pipetted into separate sets of three wells in a 96-well plate. The absorbance of each sample was measured at OD_{300}. Finally, the concentration of morphine in each sample was calculated using the Beer-Lambert law with the aid of the standard morphine curve. Serum and brain samples collected from the unimmunized group were taken as the control.

4.23. Isolation of RNA from the brain and splenocytes of the vaccinated mice

RNA was isolated from the brain and splenocytes of the animals, as per the manufacturer's standard operating protocol (Thermo-Fisher Scientific, Waltham, MA). Briefly, the brain was homogenized using a glass homogenizer in ice in TRIzol reagent (1 ml) (Thermo-Fisher Scientific, Waltham, MA). The homogenate was incubated for 10 min at 22 ± 2 °C. Chloroform (200 μl) was added to the homogenate, vortexed for 30 s, incubated for 10 min at 22 ± 2 °C and centrifuged at 12000 x*g* for 15 min at 4 °C. The SN was transferred into a new tube, and isopropanol (500 μl) was gently mixed. The sample was incubated for 15 min at 22 ± 2 °C, and the mixture was centrifuged at 12000 x*g* for 10 min at 4 °C. The SN was discarded, and the pellet was washed with ethanol (75 %, 200 μl) and centrifuged at 12000 x*g* for 10 min at 4 °C. The pellet was air-dried and dissolved in DEPC-treated water (20 μl), and RNA was quantified using Nano-Drop (Thermo-Fisher Scientific, Waltham, MA).

4.24. Synthesis of cDNA from the RNA

The cDNA was prepared per the manufacturer's protocol using the reverse transcription kit (Thermo-Fisher Scientific. Waltham, MA). The reverse transcription buffer (2.5 μl), dNTP mix (2.5 μl), random primers (2.5 μl), and reverse transcriptase (RT) enzyme (1.0 μl) were added to the RNA (1.0 μl) isolated from splenocytes and brain, separately. The samples were thoroughly mixed with the reaction mixture, briefly spun, and incubated at 25 ± 2 °C for 10 min. Subsequently, RT enzyme (1.0 μl) was added to the tube and gently mixed. The mixture was incubated at 42 °C for 60 min. Finally, the RT enzyme was inactivated by heating at

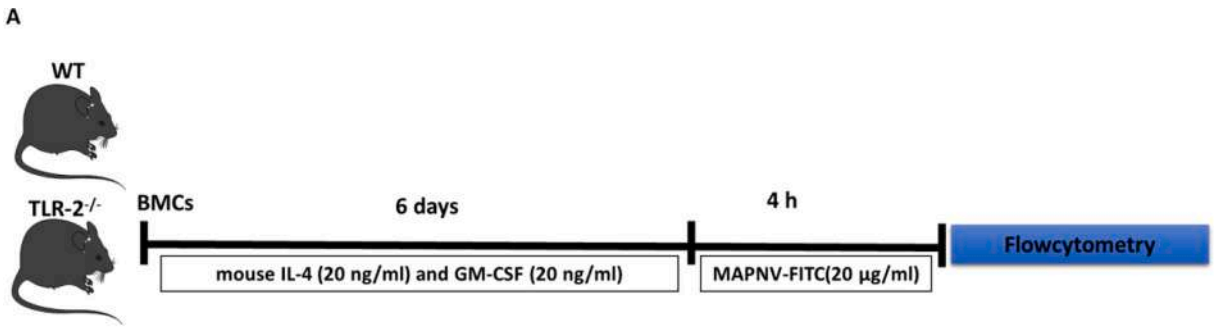

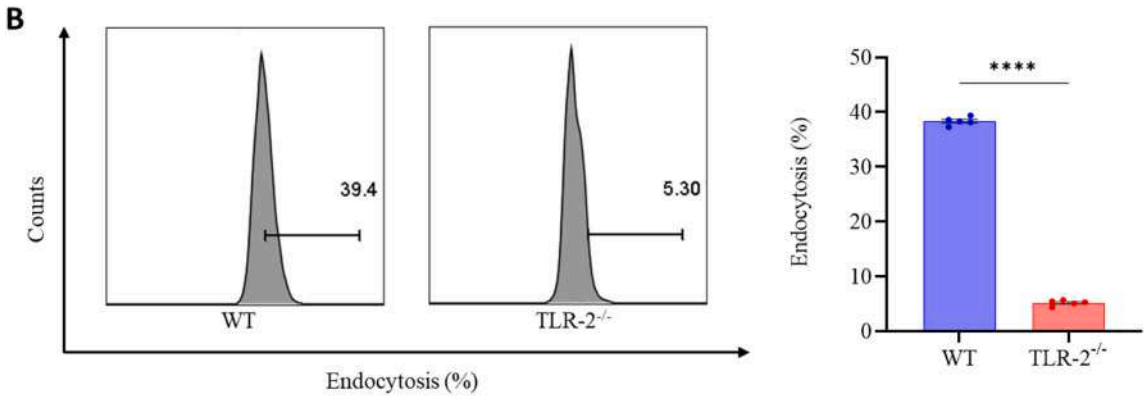

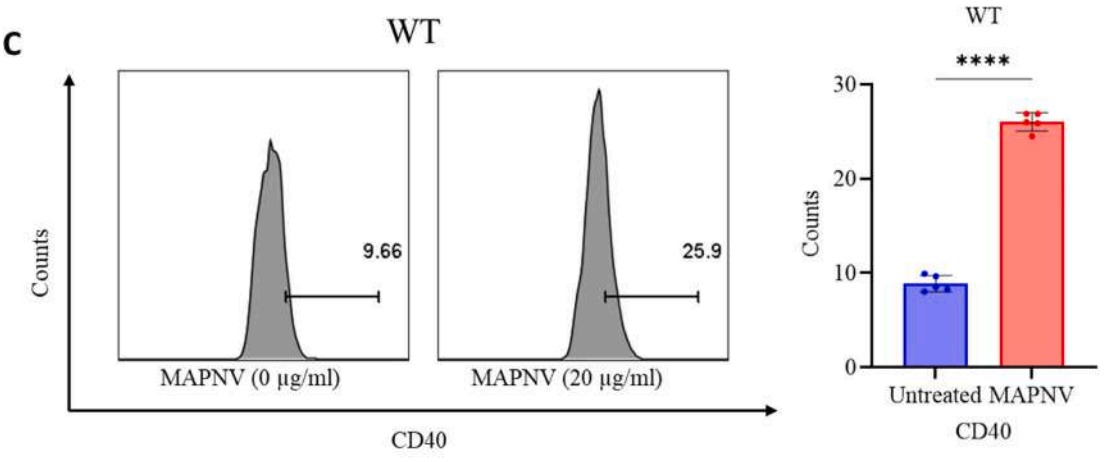

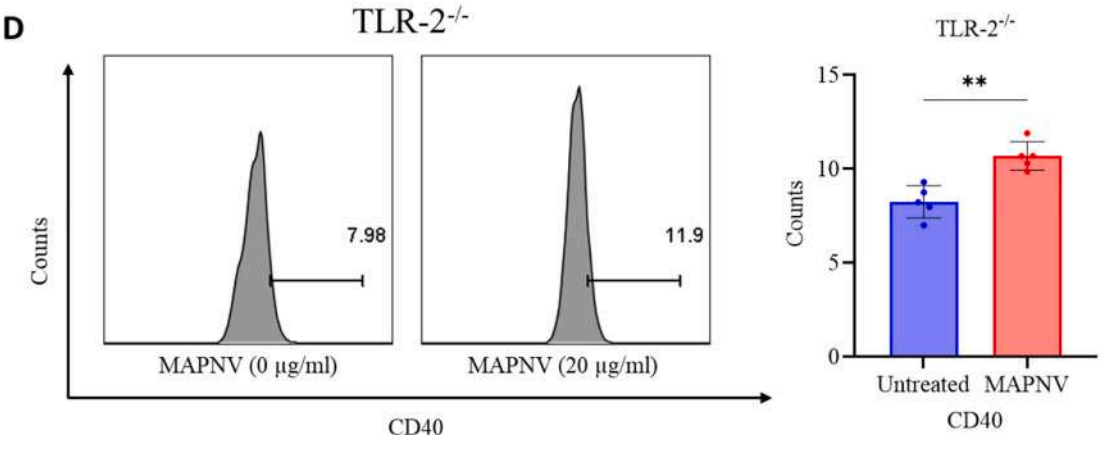

(caption on next page)

Fig. 6. MAPNV activates dendritic cells (DCs) through the Toll-like receptor 2 (TLR-2) pathway. (A) BMCs obtained from C57BL/6J wildtype and TLR-2 knockout mice, stimulated with recombinant mouse IL-4 and GM-CSF for 6-d. (B) DCs derived from both wildtype (DCWT) and TLR-2-deficient (DCTLR-$2^{-/-}$) C57BL/6 mice were cultured with FITC-labeled-MAPNV for 4 h. Subsequent analysis involved (B) assessing the uptake of FITC-labeled-MAPNV-FITC by DCWT and DCTLR-$2^{-/-}$, and (C–D) evaluating the expression of CD40 via flow cytometry. Each dot represents one animal. The data (mean ± SD) were analyzed by t-test for the statistical analysis. *p < 0.1; **p < 0.01; ***p < 0.001; ****p < 0.0001; ns = non-significant.

85 °C for 5 min, and the cDNA sample was stored at −20 °C until use.

4.25. The cytokine gene expression by RT-qPCR in the lymphocytes of vaccinated animals

Forward primer (1 μl) and reverse primer (1 μl) specific for tnf-*α,* il-*6,* il-*4*, and ifn-*γ* were added to a clean, nuclease-free DEPC-treated separate tube. Then, nuclease-free DEPC-treated water (4 μl) was added. Later, Sybr green (3 μl) (Biorad, Sacramento, CA) was added to the tube, and the solution was gently mixed by pipetting. The cDNA (1 μl) was added to the respective tubes and briefly spun to settle down. Finally, the RT-qPCR was performed according to the program specified, step 0: 50 °C for 25 s, step 1: 95 °C for 30 s, step 2: 95 °C for 5 s, step 3: 60 °C for 30 s, step 4: 72 °C for 30 s. Similarly, the RT-qPCR was performed to evaluate the μ-opioid receptor gene in the brain.

4.26. Examining the effects of vaccination on the behavior of animals

The mice were immunized with the MAPNV (20 mg/kg bwt) and controlled with PBS (placebo) on days 0 and 7. Later, they were continuously administered morphine (10 mg/kg bwt) from days 12 to 45. Animal movements, heat sensitivity, and dark-seeking behavior were recorded every alternative day. The behavior was then compared before and after opioid exposure.

4.27. Measurement of the affinity of anti-morphine Abs generated by MAPNV vaccinated mice

The binding of morphine-conjugate with anti-morphine Abs in serum samples was estimated as an equilibrium dissociation constant (Kd) using Bio-Layer Interferometric (BLI) analysis (Octet k2® BLI system, Fortebio – Sartorius, Göttingen, Germany). The data was analyzed using ForteBio data analysis software 9.0. The NTA sensors (Sartorius Part No. 18–5101 [tray]) immobilized His tag containing morphine-conjugate. The experiment was performed in a 96-well, black, flat-bottom polypropylene microplate (Greiner Bio-One Part No. 655209). The entire experiment was performed at 30 °C. Before the experiment, the sensors were allowed to hydrate for 10 min in a working buffer (1× PBS, pH 7.4). The His-tagged morphine-conjugate (2 μg/ml) was immobilized on Ni-NTA sensors for 300 s (200 μl prepared in 1× PBS). After adjusting the baseline in the working buffer, the immobilized morphine-conjugate was allowed to associate with 200 μl of serum sample (1:1000 in 1× PBS), followed by the dissociation in the working buffer for 250 s each. The binding kinetics was performed with different sera dilutions (1:500, 1:200, 1:100, 1:50) after regeneration and activation of the sensor to immobilize again with morphine-conjugate. The regeneration was done for 5 s in 200 μl of regeneration buffer (10 mM glycine pH 1.7), followed by activation of the sensors for 60 s in 200 μl activation buffer (10 mM $NiCl_2$ in H_2O). The control experiment without immobilization was run in parallel. Similarly, the experiment was performed with all the positive and control serum samples.

4.28. E91NP3 activates DCs through the TLR-2 pathway

The bone marrow cells (BMCs) were collected from C57BL/6 wildtype and TLR-$2^{-/-}$ mice. The mononuclear cells were incubated at 400 xg for 10 min and seeded in a 6-well plate (1×10^6 cells/well) in RPMI-1640 + FCS (10 %). The cells were stimulated with recombinant mouse IL-4 (20 ng/ml) and GM-CSF (20 ng/ml) and incubated for 6 days. The dendritic cells (DCs) were harvested using trypsin-EDTA (200 μl) and seeded in a 6-well plate (50×10^4 cells/well). Subsequently, MAPNV-FITC (20 μg/ml) was added into the wells and incubated for 4 h at 37 °C. The cells were acquired using BD Accuri. Furthermore, in another subset, the harvested DCs were incubated for 4 h at 37 °C with MAPNV (20 μg/ml). Later, cells were harvested and stained for CD40 expression using fluorochrome-tagged respective Abs. The cells were acquired using BD Accuri, and analysis was performed using Flowjo software (Franklin Lakes, NJ).

4.29. Statistical analysis

The statistical analysis was performed using the two-tailed student *t*-test and one-way ANOVA multiple comparison tests. All the graphs were analyzed using Graph Pad Prism 8 software (GraphPad Software, Inc., San Diego, CA). The data are represented as mean ± SD unless and otherwise mentioned. *$p < 0.1$, **$p < 0.01$, ***$p < 0.001$, ****$p < 0.0001$, ns = non-significant.

Funding sources

Indian Institute of Technology Ropar-provided ISRD grant, Department of Science and Technology (DST)-Science Education and Research Board (SERB) provided JC Bose Fellowship for this work.

CRediT authorship contribution statement

Sidhanta Nanda: Writing – review & editing, Writing – original draft, Software, Methodology, Formal analysis, Data curation. **Mohammad Adeel Zafar:** Methodology, Investigation, Data curation. **Taruna Lamba:** Methodology, Investigation, Data curation. **Jonaid Ahmad Malik:** Writing – review & editing, Visualization, Methodology, Formal analysis, Data curation. **Mohammad Affan Khan:** Writing – review & editing, Investigation, Data curation. **Priya Bhardwaj:** Data curation. **Bhawana Bisht:** Data curation. **Rohan Ghadi:** Data curation. **Gurpreet Kaur:** Writing – review & editing, Data curation. **Vijayender Bhalla:** Resources, Data curation. **Mohammad Owais:** Supervision, Resources, Data curation. **Sanyog Jain:** Resources, Data curation. **Sharvan Sehrawat:** Resources, Data curation. **Javed N. Agrewala:** Writing – review & editing, Visualization, Validation, Supervision, Software, Resources, Project administration, Methodology, Investigation, Funding acquisition, Conceptualization.

Declaration of competing interest

The authors declare no conflict of interest.

Data availability

Data will be made available on request.

Acknowledgments

SN is the recipient of the fellowship from DST-INSPIRE, MAZ, JAM from MHRD, TL, MAK, RG, and PB from CSIR-UGC funding agencies. Authors are grateful to IIT-Ropar, NIPER-Mohali, IISER-Mohali,CSIR-IMTECH Chandigarh, and AMU-Aligarh for extending their resources for conducting experiments and Grammarly for correcting English grammar.

Appendix A. Supplementary data

Supplementary data to this article can be found online at https://doi.org/10.1016/j.ijbiomac.2024.133188.

References

[1] J.A. Malik, M. Affan Khan, T. Lamba, M. Adeel Zafar, S. Nanda, M. Owais, J. N. Agrewala, Immunosuppressive effects of morphine on macrophage polarization and function, Eur. J. Pharmacol. 975 (2024) 176637, https://doi.org/10.1016/J.EJPHAR.2024.176637.

[2] J.A. Malik, J.N. Agrewala, Morphine acts via TLR4 resulting in neuroinflammation and immunosuppression, Med. Hypotheses 186 (2024) 111335, https://doi.org/10.1016/J.MEHY.2024.111335.

[3] S. Taylor, M.M. Paluszek, G.S. Rachor, D. McKay, G.J.G. Asmundson, Substance use and abuse, COVID-19-related distress, and disregard for social distancing: a network analysis, Addict. Behav. 114 (2021), https://doi.org/10.1016/J.ADDBEH.2020.106754.

[4] J.A. Malik, S. Nanda, M.A. Zafar, S. Sehrawat, J.N. Agrewala, Influence of chronic administration of morphine and its withdrawal on the behaviour of zebrafish, J. Biosci. 2023 483 48 (2023) 1–18. doi:https://doi.org/10.1007/S12038-023-00358-Y.

[5] C. Abdel Shaheed, J. Beardsley, R.O. Day, A.J. McLachlan, Immunomodulatory effects of pharmaceutical opioids and antipyretic analgesics: mechanisms and relevance to infection, Br. J. Clin. Pharmacol. 88 (2022) 3114–3131, https://doi.org/10.1111/BCP.15281.

[6] P.T. Bremer, K.D. Janda, Conjugate vaccine immunotherapy for substance use disorder, Pharmacol. Rev. 69 (2017) 298–315, https://doi.org/10.1124/PR.117.013904.

[7] X. Liang, R. Liu, C. Chen, F. Ji, T.L.-T. perioperative and, undefined 2016, Opioid system modulates the immune function: a review, Ncbi.Nlm.Nih.GovX Liang, R Liu, C Chen, F Ji, T LiTranslational Perioper. Pain Med. 2016•ncbi.Nlm.Nih.Gov (n.d.). https://www.ncbi.nlm.nih.gov/pmc/articles/PMC4790459/ (accessed October 23, 2023).

[8] A. Sulima, R. Jalah, J.F.G. Antoline, O.B. Torres, G.H. Imler, J.R. Deschamps, Z. Beck, C.R. Alving, A.E. Jacobson, K.C. Rice, G.R. Matyas, A stable heroin analogue that can serve as a vaccine hapten to induce antibodies that block the effects of heroin and its metabolites in rodents and that cross-react immunologically with related drugs of abuse, J. Med. Chem. 61 (2018) 329–343, https://doi.org/10.1021/ACS.JMEDCHEM.7B01427.

[9] H. Friedman, S. Pross, T.W. Klein, Addictive drugs and their relationship with infectious diseases, FEMS Immunol. Med. Microbiol. 47 (2006) 330–342, https://doi.org/10.1111/J.1574-695X.2006.00097.X.

[10] C. Gallego, D. Golenbock, M.A. Gomez, N.G. Saravia, Toll-like receptors participate in macrophage activation and intracellular control of Leishmania (Viannia) panamensis, Infect. Immun. 79 (2011) 2871–2879, https://doi.org/10.1128/IAI.01388-10.

[11] K.A. Fitzgerald, J.C. Kagan, Toll-like receptors and the control of immunity, Cell 180 (2020) 1044–1066, https://doi.org/10.1016/J.CELL.2020.02.041.

[12] B. Billack, Macrophage activation: role of toll-like receptors, nitric oxide, and nuclear factor kappa B, Am. J. Pharm. Educ. 70 (2006), https://doi.org/10.5688/AJ7005102.

[13] P.J. Murray, T.A. Wynn, Protective and pathogenic functions of macrophage subsets, Nat. Rev. Immunol. 11 (2011) 723–737, https://doi.org/10.1038/NRI3073.

[14] B. Greenwood, The contribution of vaccination to global health: past, present and future, Philos. Trans. R. Soc. Lond. Ser. B Biol. Sci. 369 (2014), https://doi.org/10.1098/RSTB.2013.0433.

[15] X.Y. Shen, F.M. Orson, T.R. Kosten, Vaccines for drug abuse, Clin. Pharmacol. Ther. 91 (2012) 60, https://doi.org/10.1038/CLPT.2011.281.

[16] M. Pravetoni, S.D. Comer, Development of vaccines to treat opioid use disorders and reduce incidence of overdose, Neuropharmacology 158 (2019) 107662, https://doi.org/10.1016/J.NEUROPHARM.2019.06.001.

[17] L.M. Plein, H.L. Rittner, Opioids and the Immune System – Friend or Foe, John Wiley and Sons Inc., 2018, https://doi.org/10.1111/bph.13750.

[18] P. Sacerdote, E. Limiroli, L.G.-M.C. Bioscience, undefined 2013, Experimental evidence for immunomodulatory effects of opioids, Ncbi.Nlm.Nih.GovP Sacerdote, E Limiroli, L GaspaniMadame Curie Biosci. Database [Internet], 2013•ncbi.Nlm.Nih.Gov (n.d.). https://www.ncbi.nlm.nih.gov/books/NBK6402/(accessed October 23, 2023).

[19] T.K. Eisenstein, The role of opioid receptors in immune system function, Front. Immunol. (2019), https://doi.org/10.3389/FIMMU.2019.02904.

[20] R. Zajaczkowska, W. Leppert, J. Mika, M. Kocot-Kępska, J. Woroń, A. Wrzosek, J. Wordliczek, Perioperative immunosuppression and risk of cancer progression: the impact of opioids on pain management, Pain Res. Manag. 2018 (2018), https://doi.org/10.1155/2018/9293704.

[21] J.A. Malik, J.N. Agrewala, Future perspectives of emerging novel drug targets and immunotherapies to control drug addiction 119 (2023) 110210, https://doi.org/10.1016/J.INTIMP.2023.110210.

[22] M.E. Pichichero, Protein carriers of conjugate vaccines: characteristics, development, and clinical trials, Hum. Vaccin. Immunother. 9 (2013) 2505–2523, https://doi.org/10.4161/HV.26109.

[23] V. Gradinati, F. Baruffaldi, S. Abbaraju, M. Laudenbach, R. Amin, B. Gilger, P. Velagaleti, M. Pravetoni, Polymer-mediated delivery of vaccines to treat opioid use disorders and to reduce opioid-induced toxicity, Vaccine 38 (2020) 4704–4712, https://doi.org/10.1016/J.VACCINE.2020.05.027.

[24] R. Pati, M. Shevtsov, A. Sonawane, Nanoparticle vaccines against infectious diseases, Front. Immunol. 9 (2018), https://doi.org/10.3389/FIMMU.2018.02224.

[25] M.J. Mitchell, M.M. Billingsley, R.M. Haley, M.E. Wechsler, N.A. Peppas, R. Langer, Engineering precision nanoparticles for drug delivery, Nat. Rev. Drug Discov. 20 (2021) 101–124, https://doi.org/10.1038/S41573-020-0090-8.

[26] R. Bezbaruah, V.P. Chavda, L. Nongrang, S. Alom, K. Deka, T. Kalita, F. Ali, B. Bhattacharjee, L. Vora, Nanoparticle-based delivery systems for vaccines, Vaccines 10 (2022), https://doi.org/10.3390/VACCINES10111946.

[27] D. Lozano, V. Larraga, M. Vallet-Regí, M. Manzano, An overview of the use of nanoparticles in vaccine development, Nanomater. (Basel, Switzerland) 13 (2023), https://doi.org/10.3390/NANO13121828.

[28] Y. Fan, J.J. Moon, Nanoparticle drug delivery systems designed to improve cancer vaccines and immunotherapy, Vaccines 3 (2015) 662–685, https://doi.org/10.3390/VACCINES3030662.

[29] M. Zhu, R. Wang, G. Nie, Applications of nanomaterials as vaccine adjuvants, Hum. Vaccin. Immunother. 10 (2014) 2761–2774, https://doi.org/10.4161/HV.29589.

[30] S. Nooraei, A. Sarkar Lotfabadi, M. Akbarzadehmoallemkolaei, N. Rezaei, Immunogenicity of different types of adjuvants and nano-adjuvants in veterinary vaccines, a comprehensive review, Vaccines 11 (2023), https://doi.org/10.3390/VACCINES11020453.

[31] L. Mao, Z. Chen, Y. Wang, C. Chen, Design and application of nanoparticles as vaccine adjuvants against human corona virus infection, J. Inorg. Biochem. 219 (2021), https://doi.org/10.1016/J.JINORGBIO.2021.111454.

[32] M.F. Bachmann, G.T. Jennings, Vaccine delivery: a matter of size, geometry, kinetics and molecular patterns, Nat. Rev. Immunol. 10 (2010) 787–796, https://doi.org/10.1038/NRI2868.

[33] J.A. Malik, G. Kaur, J.N. Agrewala, Revolutionizing medicine with toll-like receptors: a path to strengthening cellular immunity, Int. J. Biol. Macromol. (2023) 127252. doi:10.10 16/J.IJBIOMAC.2023.127252.

[34] S. Akira, K. Takeda, T. Kaisho, Toll-like receptors: critical proteins linking innate and acquired immunity, Nat. Immunol. 2 (2001) 675–680, https://doi.org/10.1038/90609.

[35] L. Oliveira-Nascimento, P. Massari, L.M. Wetzler, The role of TLR2 in infection and immunity, Front. Immunol. 3 (2012), https://doi.org/10.3389/FIMMU.2012.00079.

[36] A.S. Sameer, S. Nissar, Toll-like receptors (TLRs): structure, functions, signaling, and role of their polymorphisms in colorectal cancer susceptibility, Biomed. Res. Int. 2021 (2021), https://doi.org/10.1155/2021/1157023.

[37] T. Duan, Y. Du, C. Xing, H.Y. Wang, R.F. Wang, Toll-like receptor signaling and its role in cell-mediated immunity, Front. Immunol. 13 (2022), https://doi.org/10.3389/FIMMU.2022.812774.

[38] J.A. Malik, M.A. Zafar, T. Lamba, S. Nanda, M.A. Khan, J.N. Agrewala, The impact of aging-induced gut microbiome dysbiosis on dendritic cells and lung diseases, Gut Microbes 15 (2023), https://doi.org/10.1080/19490976.2023.2290643.

[39] J.A. Burns, D.S. Kroll, D.E. Feldman, C. Kure Liu, P. Manza, C.E. Wiers, N.D. Volkow, G.J. Wang, Molecular imaging of opioid and dopamine systems: insights into the pharmacogenetics of opioid use disorders, Front. Psychiatry 10 (2019). doi:10.3389/ FPSYT.2019.00626.

[40] R. Al-Hasani, M.R. Bruchas, Molecular mechanisms of opioid receptor-dependent signaling and behavior, Anesthesiology 115 (2011) 1363–1381, https://doi.org/10.1097/ALN.0b013e318238bba6.

[41] Y. Wang, X. Wang, L. Ye, J. Li, L. Song, N. Fulambarkar, W. Ho, Morphine suppresses IFN signaling pathway and enhances AIDS virus infection, PLoS One 7 (2012), https://doi.org/10.1371/journal.pone.0031167.

[42] E.A. Grego, A.C. Siddoway, M. Uz, L. Liu, J.C. Christiansen, K.A. Ross, S.M. Kelly, S. K. Mallapragada, M.J. Wannemuehler, B. Narasimhan, Polymeric nanoparticle-based vaccine adjuvants and delivery vehicles, Curr. Top. Microbiol. Immunol. 433 (2021) 29–76, https://doi.org/10.1007/82_2020_226.

[43] C. Feng, Y. Li, B.E. Ferdows, D.N. Patel, J. Ouyang, Z. Tang, N. Kong, E. Chen, W. Tao, Emerging vaccine nanotechnology: from defense against infection to sniping cancer, Acta Pharm. Sin. B 12 (2022) 2206–2223, https://doi.org/10.1016/J.APSB.2021.12.021.

[44] R. Tenchov, R. Bird, A.E. Curtze, Q. Zhou, Lipid nanoparticles—from liposomes to mRNA vaccine delivery, a landscape of research diversity and advancement, ACS Nano 15 (2021) 16982–17015, https://doi.org/10.1021/ACSNANO.1C04996.

[45] A.E. Gregory, R. Titball, D. Williamson, Vaccine delivery using nanoparticles, Front. Cell. Infect. Microbiol. 3 (2013), https://doi.org/10.3389/FCIMB.2013.00013.

[46] M. Kheirollahpour, M. Mehrabi, N.M. Dounighi, M. Mohammadi, A. Masoudi, Nanoparticles and vaccine development, Pharm. Nanotechnol. 8 (2020) 6–21, https://doi.org/10.2174/2211738507666191024162042.

[47] J.K. Patra, G. Das, L.F. Fraceto, E.V.R. Campos, M.D.P. Rodriguez-Torres, L. S. Acosta-Torres, L.A. Diaz-Torres, R. Grillo, M.K. Swamy, S. Sharma, S. Habtemariam, H.S. Shin, Nano based drug delivery systems: recent developments and future prospects, J. Nanobiotechnology 16 (2018), https://doi.org/10.1186/S12951-018-0392-8.

[48] L. Yang, W. Li, M. Kirberger, W. Liao, J. Ren, Design of nanomaterial based systems for novel vaccine development, Biomater. Sci. 4 (2016) 785–802, https://doi.org/10.1039/C5BM00507H.

[49] J. Wallis, D.P. Shenton, R.C. Carlisle, Novel approaches for the design, delivery and administration of vaccine technologies, Clin. Exp. Immunol. 196 (2019) 189–204, https://doi.org/10.1111/CEI.13287.

[50] D. Kumar Das, M.A. Zafar, S. Nanda, S. Singh, T. Lamba, H. Bashir, P. Singh, S.K. Maurya, S. Nadeem, S. Sehrawat, V. Bhalla, J.N. Agrewala, Targeting dendritic

cells with TLR-2 ligand-coated nanoparticles loaded with *Mycobacterium tuberculosis* epitope induce antituberculosis immunity, J. Biol. Chem. 298 (2022). doi:https://doi.org/10.1016/J.JBC.2022. 102596.
[51] S. Pahari, G. Kaur, M. Aqdas, S. Negi, D. Chatterjee, H. Bashir, S. Singh, J. N. Agrewala, Bolstering immunity through pattern recognition receptors: a unique approach to control tuberculosis, Front. Immunol. 8 (2017), https://doi.org/10.3389/FIMMU.2017.00906.
[52] S. Awate, L.A. Babiuk, G. Mutwiri, Mechanisms of action of adjuvants, Front. Immunol. 4 (2013), https://doi.org/10.3389/FIMMU.2013.00114.
[53] M. Zaman, I. Toth, Immunostimulation by synthetic lipopeptide-based vaccine candidates: structure-activity relationships, Front. Immunol. 4 (2013), https://doi.org/10.3389/FIMMU.2013.00318.
[54] D. Chatzikleanthous, D.T. O'Hagan, R. Adamo, Lipid-based nanoparticles for delivery of vaccine adjuvants and antigens: toward multicomponent vaccines, Mol. Pharm. 18 (2021) 2867–2888, https://doi.org/10.1021/ACS.MOLPHARMACEUT.1C00447.
[55] K. Kennerknecht, R. Noschka, F. Löffler, S. Wehrstedt, G.K. Pedersen, D. Mayer, M. Grieshober, D. Christensen, S. Stenger, Toll like-receptor agonist Pam3Cys modulates the immunogenicity of liposomes containing the tuberculosis vaccine candidate H56, Med. Microbiol. Immunol. 209 (2020) 163–176, https://doi.org/10.1007/S00430-020-00657-3.
[56] M. Komai-Koma, L. Jones, G.S. Ogg, D. Xu, F.Y. Liew, TLR2 is expressed on activated T cells as a costimulatory receptor, Proc. Natl. Acad. Sci. USA 101 (2004) 3029–3034, https://doi.org/10.1073/PNAS.0400171101.
[57] A.H. Rahman, D.K. Taylor, L.A. Turka, The contribution of direct TLR signaling to T cell responses, Immunol. Res. 45 (2009), https://doi.org/10.1007/S12026-009-8113-X.
[58] J.M. Reynolds, B.P. Pappu, J. Peng, G.J. Martinez, Y. Zhang, Y. Chung, L. Ma, X. O. Yang, R.I. Nurieva, Q. Tian, C. Dong, Toll-like receptor 2 signaling in CD4(+) T lymphocytes promotes T helper 17 responses and regulates the pathogenesis of auto-immune disease, Immunity 32 (2010) 692–702, https://doi.org/10.1016/J.IMMUNI.2010.04.010.
[59] B.C. Mercier, A. Cottalorda, C.-A. Coupet, J. Marvel, N. Bonnefoy-Bérard, TLR2 engagement on CD8 T cells enables generation of functional memory cells in response to a suboptimal TCR signal, J. Immunol. 182 (2009) 1860–1867, https://doi.org/10.4049/JIMMUNOL.0801167.
[60] C.N. Fries, E.J. Curvino, J.L. Chen, S.R. Permar, G.G. Fouda, J.H. Collier, Advances in nanomaterial vaccine strategies to address infectious diseases impacting global health, Nat. Nanotechnol. 16 (2021), https://doi.org/10.1038/S41565-020-0739-9.
[61] S.A. Mirtajaddini, M.F. Najafi, S.A.V. Yazdi, R.K. Oskuee, Preparation of chitosan nanoparticles as a capable carrier for antigen delivery and antibody production, Iran. J. Biotechnol. 19 (2021) 32–40, https://doi.org/10.30498/IJB.2021.247747.2871.
[62] A.N. Ilinskaya, M.A. Dobrovolskaia, Understanding the immunogenicity and antigenicity of nanomaterials: past, present and future, Toxicol. Appl. Pharmacol. 299 (2016) 70–77, https://doi.org/10.1016/J.TAAP.2016.01.005.
[63] S.C. Eisenbarth, Dendritic cell subsets in T cell programming: location dictates function, Nat. Rev. Immunol. 19 (2019) 89–103, https://doi.org/10.1038/S41577-018-0088-1.
[64] M. Ugur, S.N. Mueller, T cell and dendritic cell interactions in lymphoid organs: more than just being in the right place at the right time, Immunol. Rev. 289 (2019) 115–128, https://doi.org/10.1111/IMR.12753.
[65] P.K. Rai, S.B. Chodisetti, S.K. Maurya, S. Nadeem, W. Zeng, A.K. Janmeja, D. C. Jackson, J.N. Agrewala, A lipidated bi-epitope vaccine comprising of MHC-I and MHC-II binder peptides elicits protective CD4 T cell and CD8 T cell immunity against Mycobacterium tuberculosis, J. Transl. Med. 16 (2018), https://doi.org/10.1186/S12967-018-1653-X.
[66] U. Gowthaman, V. Singh, W. Zeng, S. Jain, K.F. Siddiqui, S.B. Chodisetti, R. K. Gurram, P. Parihar, P. Gupta, U.D. Gupta, D.C. Jackson, J.N. Agrewala, Promiscuous peptide of 16 kDa antigen linked to Pam2Cys protects against Mycobacterium tuberculosis by evoking enduring memory T-cell response, J. Infect. Dis. 204 (2011) 1328–1338, https://doi.org/10.1093/INFDIS/JIR548.
[67] K.F. Siddiqui, M. Amir, N. Khan, G. Rama Krishna, J.A. Sheikh, K. Rajagopal, J. N. Agrewala, Prime-boost vaccination strategy with bacillus Calmette-Guérin (BCG) and liposomized alpha-crystalline protein 1 reinvigorates BCG potency, Clin. Exp. Immunol. 181 (2015) 286–296, https://doi.org/10.1111/CEI.12634.
[68] M.M. Eid, Characterization of nanoparticles by FTIR and FTIR-microscopy, in: Handb. Consum. Nanoproducts, 2021, pp. 1–30, https://doi.org/10.1007/978-981-15-6453-6_89-1.
[69] Z. Alfian, H. Marpaung, M. Taufik, R. Harahap, C. Simanjuntak, Detection and identification of morphine in blood of male white rats (rattus norvegicus) by ultraviolet-visible spectrophotometry, J. Phys. Conf. Ser. 1116 (2018) 042004, https://doi.org/10.1088/1742-6596/1116/4/042004.
[70] Akbarzadeh A, Mehraby M, Zarbakhsh M, Farzaneh H. Design and synthesis of a morphine-6-succinyl-bovine serum albumin hapten for vaccine development. Biotechnol. Appl. Biochem. 1999 Oct;30(2):139-46. PMID: 10512793.
[71] KF Siddiqui, M Amir, RK Gurram, N Khan, A Arora, K Rajagopal, et al., Latency-associated protein Acr1 impairs dendritic cell maturation and functionality: a possible mechanism of immune evasion by *Mycobacterium tuberculosis*, J. Infect. Dis. 209 (9) (2014), https://doi.org/10.1093/infdis/jit595, 1436-45.

Copy of one or two specific publications/research papers of the applicant, relevant to the research work on which the award is claimed.

Int J Biol Macromol [IF 8.2] 14:2024:274. A novel strategy to elicit enduring anti-morphine immunity and relief from addiction by targetting Acr1 protein nano vaccine through TLR-2 to dendritic cells. Nanda S, Zafar MA, Lamba T, Malik JA, Khan MA, Bhardwaj P, Bisht B, Ghadi R, Kaur G, Bhalla V, Sehrawat S, Owais M, Jain S, **Agrewala JN***.

Cell Mol Life Sci. 79:2022:567 [IF: 9.2]. *Mycobacterium tuberculosis* exploits MPT64 to generate myeloid-derived suppressor cells to evade the immune system. Singh S, Maurya SK, Aqdas M, Bashir H, Arora A, Bhalla V, **Agrewala JN***.